UNIVERSITÀ DI PARMA

UNIVERSITA' DEGLI STUDI DI PARMA

DOTTORATO DI RICERCA IN
"SCIENZE CHIMICHE"
CICLO XXXI

SYNTHESIS OF MULTICHROMOPHORIC CALIX[4]ARENE-BASED SYSTEMS FOR THE INVESTIGATION OF ENERGY AND CHARGE FLOW

Coordinatore:
Prof. Roberto Corradini

Tutor:
Prof.ssa Laura Baldini

Dottoranda: Federica Faroldi

Anni 2015/2018

"…Sono debitore al mio mestiere anche di ciò che fa maturo l'uomo, il successo e l'insuccesso, riuscire e non riuscire, le due esperienze della vita adulta necessarie per crescere. Per il chimico che lavora in laboratorio ci vogliono tutte e due; il chimico militante le conosce entrambe: sbagliare e correggersi, incassare colpi e renderli, affrontare un problema e risolverlo oppure uscirne sconfitto e subito ricominciare la battaglia…"

Primo Levi

CONTENTS

ABSTRACT

The work presented in this thesis describes the synthesis and the spectroscopic characterization of chromophore-equipped calix[4]arenes designed for two different purposes: the development of bichromophoric model systems for the investigation of photoinduced energy and electron transfer processes, and the preparation of antenna ligands for the sensitization of lanthanoid ions. The calix[4]arene represents a versatile scaffold that can be functionalized with several chromophores and ligating units, can adopt different conformations, offering control over the distance and reciprocal orientation of the dyes, and is endowed of a residual flexibility that can be modulated according to the medium.

After an introductory chapter, the second chapter describes the synthesis of a bichromophoric dyad obtained by anchoring a Nile Red dye and a fullerene C_{60} on the upper rim of a *cone* calix[4]arene and the steady-state spectroscopic studies aimed at investigating the energy and charge transfer phenomena occurring after photoexcitation of Nile Red.

In the third chapter is reported the functionalization of a *cone* and a *1,3-alternate* calix[4]arene with two different BODIPY dyes specifically selected to study the occurrence of coherent phenomena in the energy transfer process. The use of different conformations of the scaffold allowed us to investigate the influence of the interchromophore distance on the transfer efficiency.

The fourth chapter deals with the exploration of synthetic pathways to obtain a small library of calix[4]arene-based antenna ligands for the photosensitization of lanthanoid ions. The library was designed with the aim of analyzing the role of different factors, such as the antenna structure, the distance between the antenna and the lanthanoid and the number of antennae, on the efficiency of the sensitization. Three different antennae, absorbing in the UV and visible region, were thus synthesized to be linked either at the upper or at the lower rim of three different calix[4]arene scaffolds. One of them is a redox-reversible antenna that can be exploited to investigate the potential of on-off switching of lanthanoid luminescence.

CHAPTER 1

INTRODUCTION

1.1 Photosynthesis: a source of inspiration

Photosynthesis is the process, carried out by living organisms, through which solar energy is transformed into chemical energy, which is then used for the development and sustenance of life on earth. In oxygenic photosynthesis, plants, algae, cyanobacteria and their relatives, convert carbon dioxide into carbohydrates, using water as the electron donor and consequently evolving molecular oxygen. Although photosynthetic organisms are of different species, they all share a similar photosynthetic unit containing peripheral pigment-protein complexes, also called light-harvesting antenna systems, surrounding a reaction center (RC). Sunlight is initially absorbed by the several pigments in the antenna complexes, whose number ranges from a few to about two hundreds, and the excitation energy is then transferred rapidly and efficiently, often over hundreds of Ångströms, to the reaction center where it initiates an electron transfer cascade chain for the production of chemical energy.[1] The close proximity between pigments, with an average distance of 10 Å, is responsible for strong interchromophore interactions, and thus for electronic excitation to be delocalized over several molecules, creating strongly-coupled excitons, which are present in combination with more localized excitations due to the presence of weakly coupled pigments. Common antenna chromophores include, other than chlorophylls, also carotenoids, xantophylls and phycobilins, open-chain tetrapyrrole bilins found in cyanobacteria. Often, pigments present on the periphery of the antenna complex absorb at shorter wavelengths than those at the core, creating an excitation energy gradient from the periphery to the center, as it happens with purple bacteria, probably the most studied and best characterized photosynthetic systems.[2] As an example, a schematic representation of the light-harvesting process in purple bacteria is reported in **Figure 1.2**. Two types of

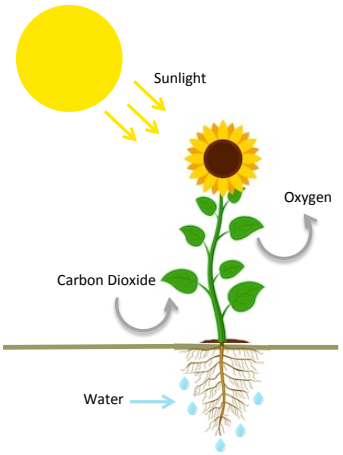

Figure 1.1. Pictorial representation of oxygenic photosynthesis.

light-harvesting complexes (LH1 and LH2) are present: LH1 surrounds directly the reaction center, while LH2 transfers energy to the reaction center through LH1. LH2 is composed by ring-like aggregates of bacteriochlorophylls and carotenoids, maintained in a fixed spatial relationship by the surrounding polypeptides. Two different sets of bacteriochlorophyll rings constitute the complex LH2, having absorption maxima at different wavelengths, 800 and 850 nm, and therefore named B800 and B850. The first energy transfer step takes place from B800 to B850, covering a distance of around 10 Å in few hundreds of femtoseconds. Then the energy collected by LH2 complex is transferred to LH1, travelling for an average distance of 20 Å in 3 to 5 ps. Finally, the last step requires about 35 ps for the energy to travel from LH1 to the reaction center, where charge separation occurs, followed by stabilization of the long-lived charge-separated state. An efficiency close to unity (95%) was found for the whole process, which overall consists of a cascade-like system of excited states, characterized by ultrafast energy migration from the periphery of the complex to the reaction center with minimal losses.

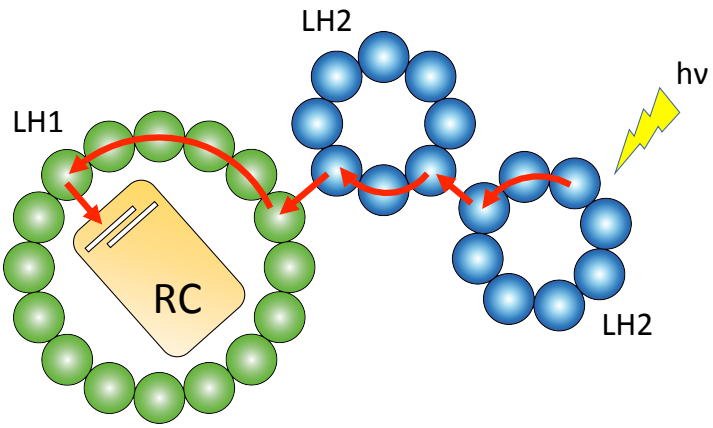

Figure 1.2. Schematic representation of the light-harvesting process in bacterial photosynthesis.

Until few decades ago all the transfer processes inside the photosynthetic unit were believed to occur following a Förster[3] mechanism, *i.e.*, according to semi-classical rules, the excitation energy was thought to be hopping from one molecule to the

other in a random walk. With the increasing availability of experimental data on more complex systems, the applicability of this theory began to be questioned.[4–6] In particular, Förster theory holds when the electronic coupling between donor and acceptor molecules is weak; instead, to deal with molecular aggregates, and hence delocalized excitons, extensions of the dipole-dipole Förster theory needed to be developed and the Generalized Förster Theory (GFT) was introduced to describe how delocalized states transfer excitation.[6–9] In photosynthetic antennae there are groups of chromophores strongly coupled, in which electronic excitation is no longer localized on one molecule, but is shared coherently among them. If these subsets of excitonically coupled molecules are weakly coupled to each other, the energy transfer can still be described as incoherent hopping and it can be treated in the framework of the generalized Förster approach. In light-harvesting systems coherences can also involve coherent dynamics of the energy transfer, resulting in a superposition of excitonic states.[10] The development of two-dimensional (2D) electronic spectroscopy, then, offered a new set of experimental information on the site energies and the electronic couplings on both aggregated chromophores and photosynthetic antennae.[11,12] 2D electronic spectra of the Fenna-Matthews-Olson complex, a water soluble pigment-protein complex found in green sulphur bacteria, revealed the presence of long-lived coherences among the electronic excited states of the chlorophylls linked to the antenna, yielding evidence for wavelike energy transfer through quantum coherence.[13,14] These quantum-coherent groups of molecules seem to efficiently direct the energy transfer through the most efficient pathway. More recently, such electronic coherences have also been observed in more complex systems, like the LH2 complex of higher plants.[15]

From all the investigations carried out on natural photosynthetic systems, it has emerged that the efficiency of the energy transfer steps, which take place in the antenna complexes, and the stabilization of the charge separated state in the reaction center, depend on the specific structural properties of these systems and on the interaction of the pigments with the environment, namely the surrounding protein. It

has emerged that the medium, besides keeping the chromophores at relatively fixed distance and orientation, can actually play a constructive role in excitonic transport. In particular, environmental interactions may modulate the electronic and vibrational properties of the chromophores and promote specific quantum mechanical effects enhancing the transfer probability.[16–18]

1.2 Artificial systems mimicking photosynthesis

As described above, photosynthesis represents the most effective way on earth to convert solar energy into fuel. Inspired by nature, several research groups in recent years developed synthetic multichromophoric systems capable of fast energy and electron transfer and slow charge recombination.[19–21] Besides the possibility of using these systems in functional working devices, in photovoltaics as well as in molecular electronics and photonics, they offer an excellent opportunity to study the mechanisms influencing the efficiency of energy transfer and charge separation.

Numerous classes of dyes have been used to design multichromophoric architectures for light-harvesting purposes and as mimics of the reaction centers, whereas fewer examples that combine the two steps of energy and charge transfer are reported. Artificial light harvesting structures are often based on dendritic molecular systems. These tree-like macromolecules, organized in a branching form from a central core, in which a large number of chromophores can be collocated in a restricted space, naturally resemble natural light-harvesting complexes. Dendrimers based on metal complexes,[22,23] porphyrins[24,25] and different organic molecules[26,27] were synthesized as antenna mimics. Also multi-porphyrin arrays,[24,28] based both on covalent and non-covalent interactions, raised a lot of interest as light-harvesting antennae and were actually used in the construction of solar cells.[29] Energy transfer has also been studied in simplified artificial dyads and triads based on naturally occurring chromophores, such as carotenoids,[30] and on different synthetic dyes, among which BODIPYs have been largely used both as energy donor and energy acceptor (**Figure 1.3**).[31–33]

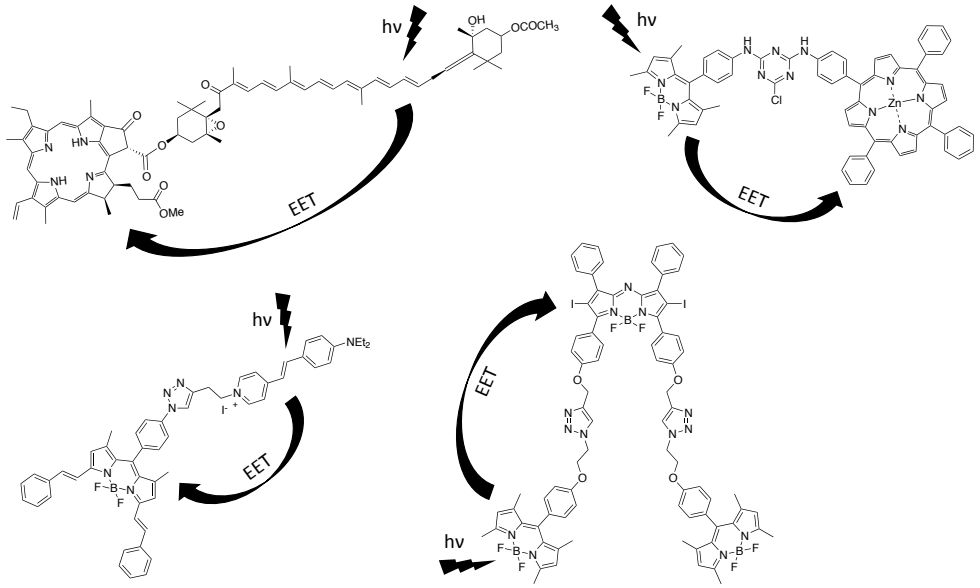

Figure 1.3. Examples of artificial dyads and triads for the study of energy transfer.

Several attempts at mimicking the natural reaction center are present throughout the literature, beginning with the simplest model based on an electron donor-electron acceptor dyad, in which the two components are organized in space in order to have control over their distance and interaction (**Figure 1.4**).[34–38]

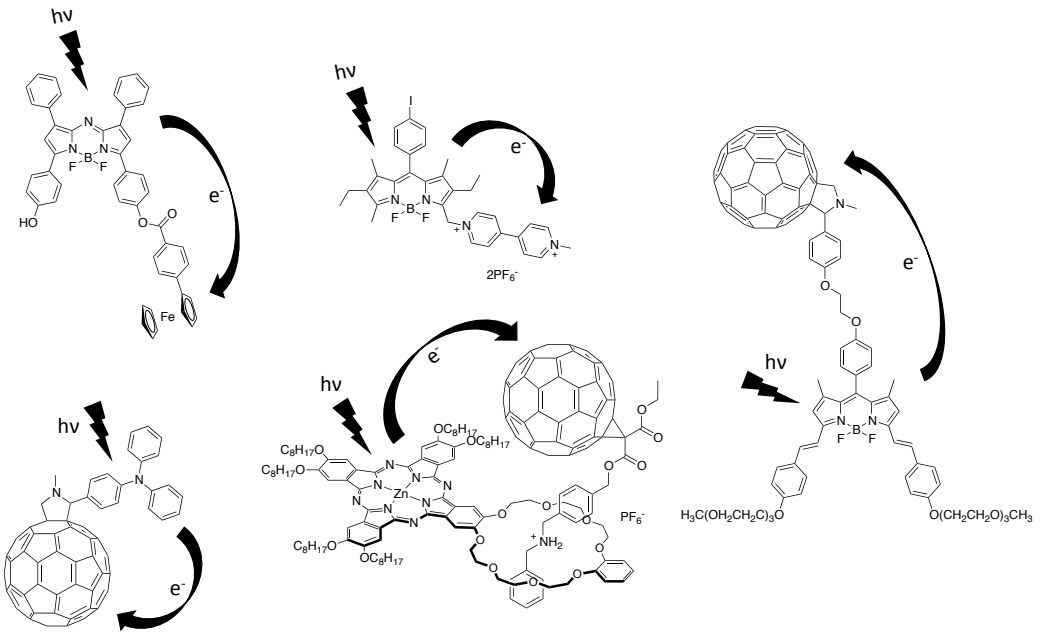

Figure 1.4. Examples of electron donor-acceptor dyads.

Nature overcame the problem of fast charge recombination by carrying out a series of short-range electron transfer steps that lead to a charge separation over a long distance.[39] As a consequence, systems with increasing complexity, consisting of three or more components and thus capable of more than one electron transfer step, have been developed. Fullerenes are probably the most used electron acceptors for these applications, mainly thanks to their high electron affinity and small reorganization energy in the electron transfer processes.[40–42] They have been coupled several times with porphyrins as electron donors,[43–49] due to their rich redox and photochemical properties, but the use of other dyes such as azaBODIPYs, naphthalene bisimide and carotenoids has also been explored. Some examples of triads for electron transfer are shown in **Figure 1.5**.[50–53]

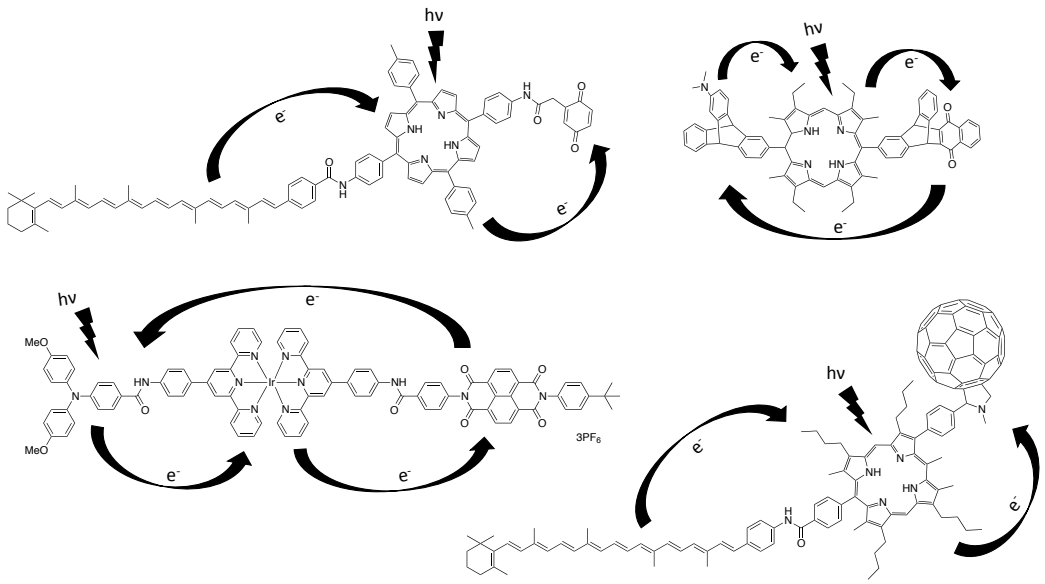

Figure 1.5. Examples of mimics of the natural reaction center.

Efforts of combining the two steps of electron and energy transfer led to the synthesis of very interesting structures in which covalent and supramolecular approaches are exploited to improve the performances of the systems (**Figure 1.6**).[54–57]

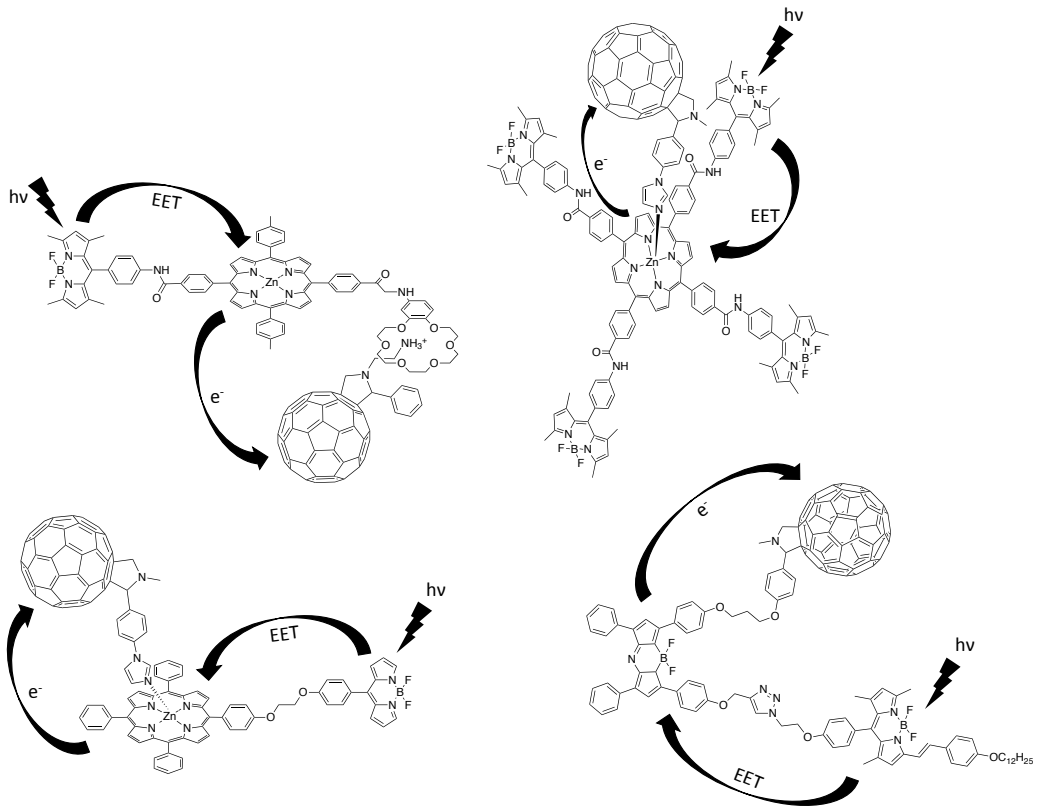

Figure 1.6. Examples of artificial systems combining the two steps of energy and electron transfer.

Very interestingly, recently for the first time, Engel et al.[58] reported the synthesis of three rigid heterodimers (**Figure 1.7**) able to reproduce the long-lived coherences observed in natural photosynthetic systems, opening the possibility for the study of these phenomena in small, tunable models.

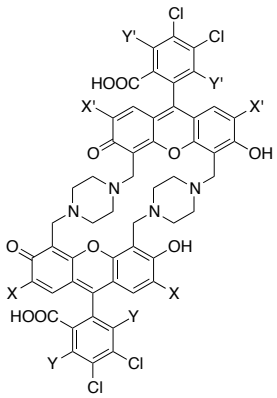

Figure 1.7. Heterodimers by Engel et al.[58] able to support long-lived coherences.

1.3 Calix[n]arenes

Calix[n]arenes[59–61] are cyclic oligomers obtained from the condensation of n units of para-substituted phenols and formaldehyde in basic conditions. Although the first report of the isolation of these structures dates back to 1941, we have to wait until 1978 for Gutsche to systematically optimize the synthetic procedures and to coin the term calixarene.[62] The name of these synthetic macrocycles was inspired by the shape of the cyclic tetramer that resembles a Greek vase called *calyx krater* (**Figure 1.8**). The suffix arene refers to the aromatic rings forming the annulus. As depicted in **Figure 1.8b**, it is possible to distinguish a lower rim, also known as narrow rim, characterized by the presence of the phenol hydroxyl groups, and an upper rim, also called wide rim, identified by the para-positions of the phenol units.

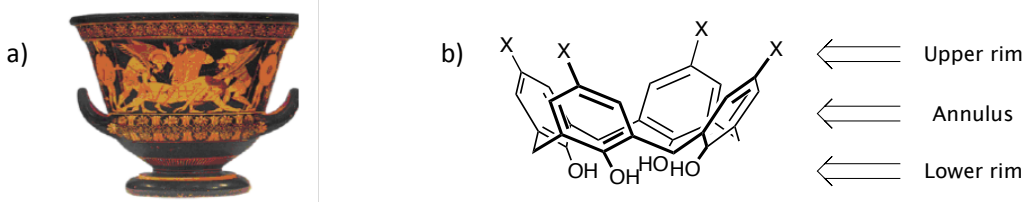

Figure 1.8. a) Example of a *calyx krater* from which the name calixarene is derived; b) generic structure of a calix[4]arene with indication of the upper and the lower rim.

Calixarenes with different valency, i.e. with a different number of phenol units (**Figure 1.9**), can be obtained by changing the solvent, the temperature, the base and the ratio of the reactants used in the condensation reaction. The even-numbered macrocycles (n = 4, 6, 8), nowadays commercially available, are the easiest to obtain even in kilogram scales using well-consolidated synthetic procedures.[63,64] The odd-numbered analogues (n = 5, 7, 9), on the contrary, can be prepared only in lower yields, through demanding procedures, especially in terms of purification protocols.

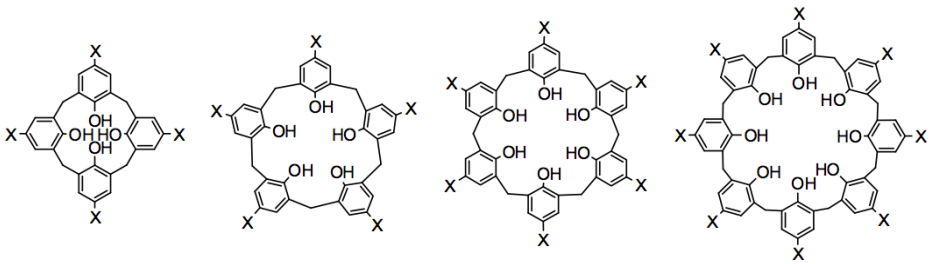

Figure 1.9. Calix[n]arenes with different valency (n = 4, 5, 6, 8).

A wide number of well-established procedures is known to exhaustively or selectively functionalize the lower and the upper rim and thus obtain a great variety of compounds.[65]

Calix[n]arenes with n > 4 show high conformational mobility in solution, and are generally present as a mixture of conformers with similar energy that rapidly interconvert from one to the other. For calix[4]arenes, on the contrary, different stable geometries can be identified.

1.3.1 Conformational behavior of the calix[4]arene

Tetrahydroxycalix[4]arenes, both at the solid state and in solution, are kept in the *cone* conformation, where all the phenolic rings are oriented in the same direction and a π-rich aromatic cavity is well defined, by the establishment of strong intramolecular hydrogen bonding between the proximal phenolic hydroxyls. By raising the

temperature, the rotation about the σ-bonds of the Ar-CH_2-Ar groups allows for a ring flipping, as shown in **Figure 1.10**.

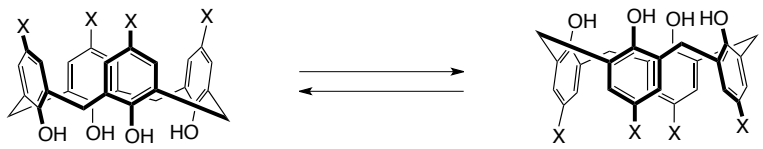

Figure 1.10. Ring flipping in a tetrahydroxycalix[4]arene.

When the phenolic oxygens are substituted with R groups, besides the already cited *cone* conformation, the calix[4]arene can exist in three other forms, identified as *partial cone* (often abbreviated as *paco*), *1,2-alternate* and *1,3-alternate* conformations and characterized by a different orientation of the phenolic units (**Figure 1.11**).[60] Tetramethoxy- and tetraethoxy derivatives, however, are conformationally mobile, with the aromatic rings free to rotate because there is no steric hindrance for methyl and ethyl groups to pass through the annulus. Only when bulky substituents, typically larger than ethyl groups, are introduced at the lower rim, the macrocycle can be locked into one of the four conformations.

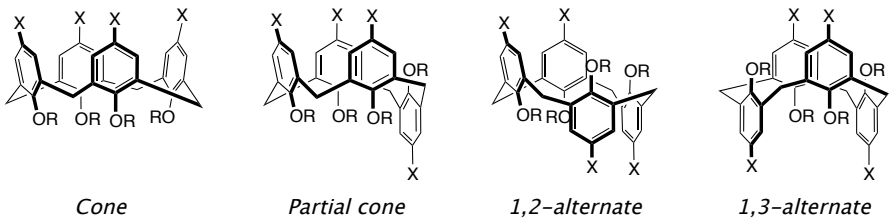

Figure 1.11. The four possible conformations adopted by the calix[4]arene (R > Et).

The conformation adopted by the calixarene can be easily identified by means of ^{1}H NMR spectroscopy. In the case of a *cone* calix[4]arene, in fact, the two protons of each methylene bridge experience a different magnetic environment: one is almost perpendicular to the aromatic rings and is named *equatorial*, the other is almost parallel and is referred to as *axial* (**Figure 1.12a**). These two protons are diastereotopic and, in ^{1}H NMR spectra, give rise to two doublets, coupled with a typical geminal coupling constant (*J*) of 13-16 Hz. The *equatorial* protons experience the shielding

cone of the aromatic nuclei and are thus upfield shifted compared to the *axial* protons. In the case of a *partial cone*, *1,2-alternate* or *1,3-alternate* calix[4]arene, on the other hand, the protons of the methylene bridge between two opposite rings (**Figure 1.12b**) are chemically equivalent and give rise to a singlet in the ^{1}H NMR spectrum.

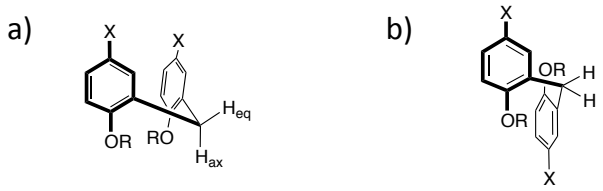

Figure 1.12. Disposition of the protons of the methylene bridge between two aromatic rings oriented a) in the same direction, b) in opposite direction.

Even if the tetraalkylated calix[4]arenes are blocked in the *cone* conformation by the steric hindrance of the substituents at the lower rim, the aromatic scaffold possesses a residual conformational mobility, thanks to the swinging of the aromatic rings around the carbon atoms of the bridge. As a consequence, the *cone* conformation of C_{4v} symmetry, with which these systems are usually represented, can indeed be considered as the transition state for the interconversion between two limiting *flattened cone* conformations, equally stable, having C_{2v} symmetry (**Figure 1.13**).[66] When four identical substituents are present at the upper rim of the *cone* calix[4]arene, the interconversion between these two limiting structures is fast on the NMR timescale, and thus the NMR spectrum reflects the C_{4v} symmetry of the scaffold, as an average between the two C_{2v} flattened conformations that possess the same energy.

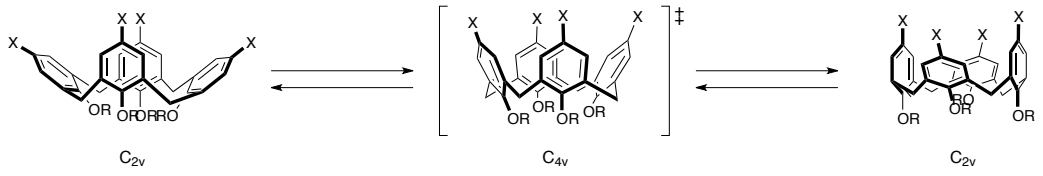

Figure 1.13. Residual conformational mobility of the *cone* calix[4]arene.

When, on the other hand, only two substituents are present on the 1,3-distal positions of the upper rim, the two flattened conformations no longer have the same energy and the ^{1}H NMR spectrum offers a picture of the more stable structure.[67] Typically, this is the one minimizing the steric repulsion between the substituents, that is the conformation with the substituted aromatic rings pointing outwards and therefore called *open flattened cone* (**a**, **Figure 1.14**). In case of attractive interactions between the substituents, such as hydrogen bonds or electrostatic interactions, however, the two substituted aromatic rings get closer and the calixarene adopts what has been defined as a *closed flattened cone* conformation (**b**, **Figure 1.14**).

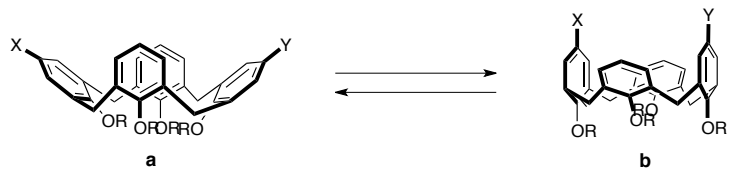

Figure 1.14. Open (**a**) and closed flattened cone (**b**) conformation of 1,3-substituted calix[4]arene.

The two different conformations can be distinguished by ^{1}H NMR spectroscopy through the observation of the reciprocal positions of the signals of the aromatic protons on the substituted and unsubstituted aromatic rings. In fact, the aromatic protons of the rings parallel to each other experience the shielding cone of the outward-oriented rings and therefore resonate at higher fields. The solvent, in case of attractive interactions between the distal upper rim substituents, can efficiently shift the equilibrium towards one or the other flattened cone conformation, as a function of its ability to favor or disfavor these interactions. The solvent polarity and ability to form hydrogen bonds are the properties usually considered to modulate the calix[4]arene *flattened cone* conformations.

1.4 State-of-the-art of chromophore-equipped calix[4]arenes

Several examples of chromophore-equipped systems and dyads based on the calixarene scaffold can be found within the literature for different applications. Among

these, calix[4]arenes functionalized with binding sites for specific guests and with a fluorophore reporting moiety have gained a lot of interest as fluorescent sensors and probes,[68,69] mainly because of the high selectivity they can achieve, combined with the high sensitivity of fluorescence detection. Very selective calixarene-based sensors towards toxic metal ions exploit photoinduced electron transfer (PET) and/or Förster Resonance Energy Transfer processes (FRET).[70–73] For instance, calixarenes **I**, **II** and **III**, reported in **Figure 1.15**, were developed by Dabestani and coworkers[74] for sensing of Cs^+: the binding of the cation to the crown inhibits the photoinduced electron transfer from the benzocrown to the cyanoanthracene fluorophore, which takes place in the absence of the ion, thus resulting in an enhancement of the fluorescence emission of cyanoanthracene.

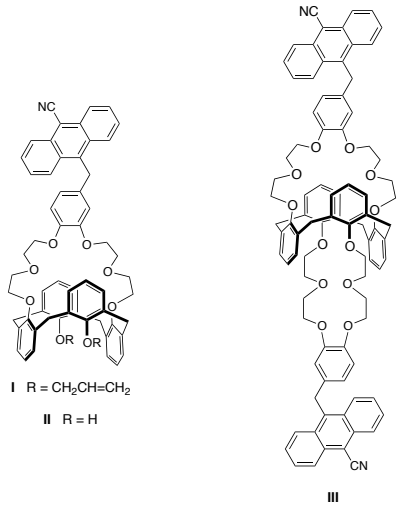

Figure 1.15. Example of Cs^+ PET sensors based on the calixarene scaffold.

Calix[4]arenes have also been widely employed as nonlinear optical (NLO) chromophores.[75–80] These systems, in which a calixarene in *cone* conformation is functionalized at the upper rim with suitable chromophores resulting in an extended π-conjugation, can be considered as an assembly of non-conjugated donor-acceptor units, held together by covalent interactions and oriented almost in the same direction. Examples of systems with improved second-order hyperpolarizability are reported in **Figure 1.16**.[76,80]

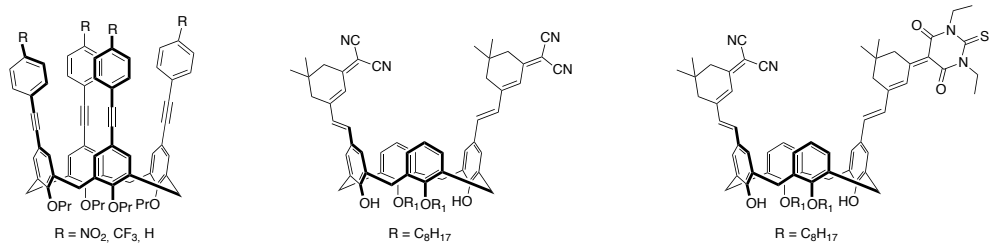

Figure 1.16. Examples of calix[4]arenes for NLO applications.

Significantly more limited is their use as model systems for the study of the processes at the basis of photosynthesis, *i.e.* photoinduced electron and energy transfer. In this field, two works are reported in which a zinc porphyrin is used as electron donor towards a trichloroquinone or a pyrromellitimide acceptor, linked at the upper rim of a *cone* and *1,3-alternate* calix[4]arene, respectively (**IV** and **V**, **Figure 1.17**).[81,82] In these systems the electron transfer was proved to happen with a *through-space* mechanism, with the calixarene being just a scaffold to juxtapose the two chromophores. On the other hand, dyad **VI** (**Figure 1.17**), analogous to **V**, but based on the scaffold in *cone* conformation, did not give rise to any electron transfer, due to the larger distance between the two photoactive units.

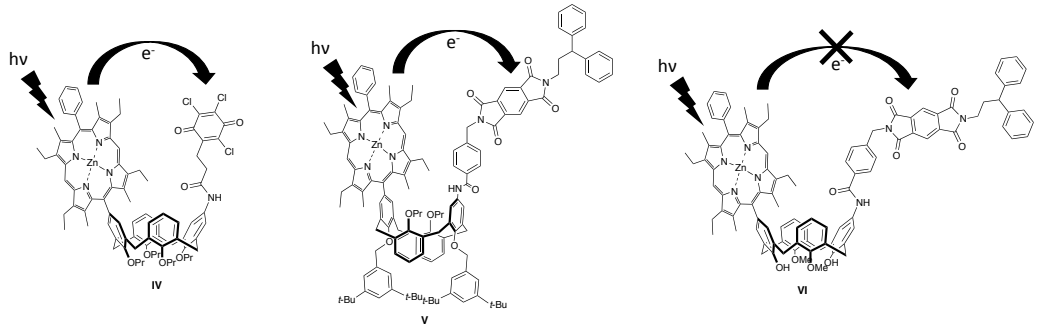

Figure 1.17. Examples of porphyrin-calix[4]arenes for the study of electron transfer.

An efficient energy transfer between two porphyrins anchored on a *cone* calix[4]arene, was reported by Pognon et al.:[83] an open and a closed conformer were synthesized (**VII** and **VIII**, **Figure 1.18**), but no significant difference in the energy transfer efficiencies was found.

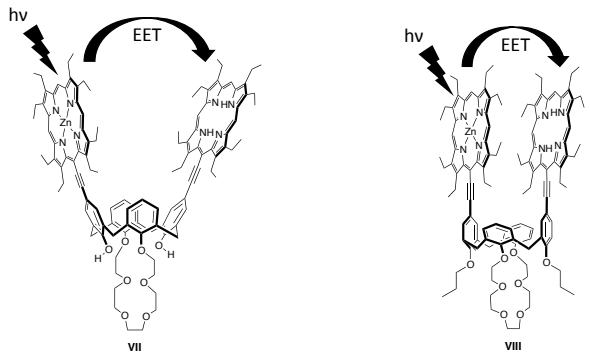

Figure 1.18. Biporphyrin-calix[4]arenes for the study of energy transfer.

Other works on bichromophoric calixarenes for energy and electron transfer are based on the perylene bisimide (PBI) chromophore.[84–86] A first example is given by a small family of PBI-calix[4]arenes (**IX**, **X**, **XI**, **Figure 1.19**) in which the formation of π-stacking interactions between the chromophores, modulated by the steric hindrance of the substituents and by the polarity of the solvent, causes different decay behaviors of the excited state.[87]

For the perylene-pyrene calix[4]arene **XII**,[85] shown in **Figure 1.19**, a strong charge-transfer interaction between the two dyes is indicated, but differently from calixarenes **IV** and **V**, the scaffold seems to effectively participate in the electron transfer process.

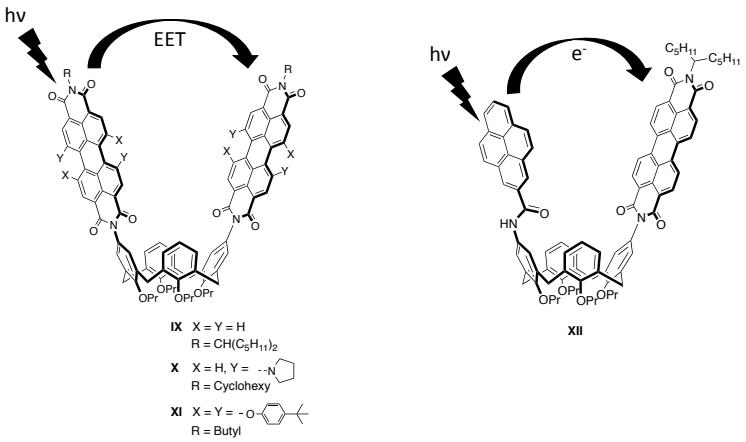

Figure 1.19. Examples of bichromophoric perylene bisimide-containing calixarenes for energy (on the left) and electron transfer (on the right).

Despite these few interesting works, the potential offered by calixarenes in this field has not been fully exploited. No systematic studies, in which number of, orientation, geometry and reciprocal distance between the dyes are rationally modified, have been carried out, to the best of our knowledge. In addition, there are no examples where light-harvesting and electron acceptor units are combined on a single calixarene scaffold. The study of electron and energy transfer processes on these macrocyclic compounds can be then considered at an early stage, but meaningful results can be envisaged through the design and characterization of new systems.

1.5 Aim of the work

Both in natural photosynthesis and in artificial devices, the nature and the efficiency of the energy and electron transfer processes are deeply influenced by energetic and structural parameters. Developing simple and manipulable model systems can allow for a deeper understanding of the factors that drive these processes and that determine their great efficiency. In particular, bichromophoric model units can be very helpful to study these phenomena, since their properties can be changed in a simple and controlled way. In fact, in these dyads, the electronic properties are determined by the choice of the dyes and the strength of the electronic coupling is determined by the distance and orientation of the chromophores. In this context, calixarenes represent suitable and versatile candidates for the anchoring of chromophoric units, offering easy functionalization of the scaffold, also with several chromophores, and the possibility of studying the role of the distance and reciprocal orientation of the dyes by changing the calixarene conformation and exploiting its residual flexibility.

Just recently, our research group started to explore this field, by developing a family of calix[4]arene-based bichromophores for the study of energy transfer.[88,89] Two couples of chromophores, Coumarin 343/7-nitrobenzo furazan (NBD) and NBD/hydroxy-Nile Red (NR), in which NBD acts as energy acceptor and energy donor, respectively, were linked at the 1,3-distal positions of a *cone* and a *partial cone* calix[4]arene, to obtain a small library of six heterobichromophoric systems (**Figure 1.20**) where the different

geometry of the scaffold allowed control of the interchromophore distance and relative orientation.

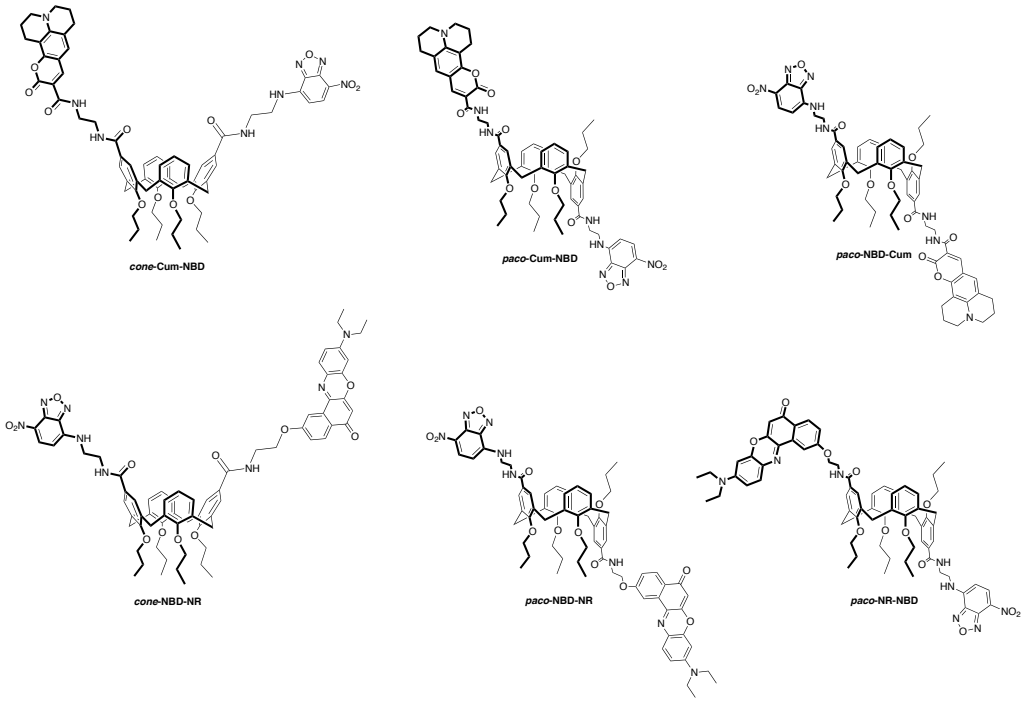

Figure 1.20. Family of calix[4]arene-based bichromophores developed by our research group.[88,89]

Interestingly, it was found that, in the case of the *cone* compounds, the interactions between the chromophores can be deeply influenced by the choice of the solvent, as a consequence of the particular conformation adopted by the calixarene in solution. In apolar solvents, in fact, an intramolecular hydrogen bond between the amide groups at the upper rim favors a *closed flattened cone* conformation, while polar solvents, preventing the formation of this interaction, stabilize the *open flattened cone* structure where the distance between the dyes is larger. The efficiencies of the energy transfer were found to be high (> 90%) for all the investigated systems independently of the solvent, but it was proved that the kinetics of the process were affected by the medium as a consequence of the different inter-chromophore distance. These interesting results, together with the simple architecture of these systems, open the possibility of broadening the study to more complex structures. For this reason, this

recent study carried out in our research group represents the starting point of the work presented in chapters 2 and 3 of this thesis, which focuses on the development of two types of bichromophoric calixarene-based systems as models for the study of energy and charge transfer processes of higher complexity.

In particular, chapter 2 describes the synthesis and basic spectroscopic characterization of a Nile Red-fullerene C_{60} dyad, as electron donor-acceptor system. Nile Red has been used as final energy acceptor in the above-described family of bichromophoric calix[4]arenes developed by our research group, and, if coupled with a proper electron acceptor, could allow for a structure in which energy transfer is followed by electron transfer. In chapter 3, the quantum-coherent mechanism of energy transfer is taken into account. With the aim to investigate by 2D electronic spectroscopy if long-lived coherences can occur in small flexible systems, two calix[4]arenes functionalized with BODIPY dyes, in *cone* and *1,3-alternate* conformations, were developed.

Finally, chapter 4 describes the work carried out at Curtin University, in Perth, during a period of six months. In this case, the energy transfer phenomenon is exploited to increase the emission of lanthanoid ions that are characterized by very interesting luminescence properties also in the NIR, but suffer from low molar absorptivity. The synthesis of calix[4]arenes functionalized with a lanthanide binding site and with antenna chromophores for the sensitization of lanthanoid ions is reported, together with the spectroscopic behavior of the complexes of Tb^{3+}, Eu^{3+} and Yb^{3+} with one of the synthesized ligands.

1.6 References

(1) Blankenship, R. E. *Molecular Mechanism of Photsynthesis, 2nd E*; John Wiley & Sons, 2014.

(2) Hu, X.; Damjanovic, A.; Ritz, T.; Schulten, K. Architecture and Mechanism of the Light-Harvesting Apparatus of Purple Bacteria. *Proc. Natl. Acad. Sci. USA* **1998**, *95*, 5953–5941.

(3) Forster, T. Energiewanderung Und Fluoreszenz. *Naturwissenschaften* **1946**, *33* (6), 166–175.

(4) Braslavsky, S. E.; Fron, E.; Rodríguez, H. B.; Román, E. S.; Scholes, G. D.; Schweitzer, G.; Valeur, B.; Wirz, J. Pitfalls and Limitations in the Practical Use of Förster's Theory of Resonance Energy Transfer. *Photochem. Photobiol. Sci.* **2008**, *7* (12), 1444–1448.

(5) Beljonne, D.; Curutchet, C.; Scholes, G. D.; Silbert, R. J. Beyond Forster Resonance Energy Transfer in Biological and Nanoscale Systems. *J. Phys. Chem. B* **2005**, *113* (19), 14795–14806.

(6) Scholes, G. D.; Jordanides, X. J.; Fleming, G. R. Adapting the Förster Theory of Energy Transfer for Modeling Dynamics in Aggregated Molecular Assemblies. *J. Phys. Chem. B* **2001**, *105* (8), 1640–1651.

(7) Jang, S.; Newton, M. D.; Silbey, R. J. Multichromophoric Förster Resonance Energy Transfer. *Phys. Rev. Lett.* **2004**, *92* (21), 21–24.

(8) Scholes, G. D.; Fleming, G. R. On the Mechanism of Light Harvesting in Photosynthetic Purple Bacteria: B800 to B850 Energy Transfer. *J. Phys. Chem. B* **2000**, *104* (8), 1854–1868.

(9) Jang, S.; Newton, M. D.; Silbey, R. J. Multichromophoric Förster Resonance Energy Transfer from B800 to B850 in the Light Harvesting Complex 2: Evidence for Subtle Energetic Optimization by Purple Bacteria. *J. Phys. Chem. B* **2007**, *111* (24), 6807–6814.

(10) Collini, E. Spectroscopic Signatures of Quantum-Coherent Energy Transfer. *Chem. Soc. Rev.* **2013**, *42* (12), 4932–4947.

(11) Collini, E.; Scholes, G. D. Coherent Intrachain Energy Migration in a Conjugated Polymer at Room Temperature. *Science (80-.).* **2009**, *323* (5912), 369–373.

(12) Collini, E.; Wong, C. Y.; Wilk, K. E.; Curmi, P. M. G.; Brumer, P.; Scholes, G. D. Coherently Wired Light-Harvesting in Photosynthetic Marine Algae at Ambient Temperature. *Nature* **2010**, *463* (7281), 644–647.

(13) Engel, G. S.; Calhoun, T. R.; Read, E. L.; Ahn, T. K.; Mančal, T.; Cheng, Y. C.; Blankenship, R. E.; Fleming, G. R. Evidence for Wavelike Energy Transfer through Quantum Coherence in Photosynthetic Systems. *Nature* **2007**, *446* (7137), 782–786.

(14) Panitchayangkoon, G.; Hayes, D.; Fransted, K. A.; Caram, J. R.; Harel, E.; Wen, J.; Blankenship, R. E.; Engel, G. S. Long-Lived Quantum Coherence in Photosynthetic Complexes at Physiological Temperature. *Proc. Natl. Acad. Sci.* **2010**, *107* (29), 12766–

12770.

(15) Calhoun, T. R.; Ginsberg, N. S.; Schlau-Cohen, G. S.; Cheng, Y.-C.; Ballottari, M.; R. Bassi; Fleming, G. R. Quantum Coherence Enabled Cetermination of the Energy Landscape in Light-Harvesting Complex II. *J. Phys. Chem. B* **2009**, *113*, 16291–16295.

(16) Ishizaki, A.; Calhoun, T. R.; Schlau-Cohen, G. S.; Fleming, G. R. Quantum Coherence and Its Interplay with Protein Environments in Photosynthetic Electronic Energy Transfer. *Phys. Chem. Chem. Phys.* **2010**, *12* (27), 7319–7337.

(17) León-Montiel, R. D. J.; Kassal, I.; Torres, J. P. Importance of Excitation and Trapping Conditions in Photosynthetic Environment-Assisted Energy Transport. *J. Phys. Chem. B* **2014**, *118* (36), 10588–10594.

(18) Shabani, A.; Mohseni, M.; Rabitz, H.; Lloyd, S. Numerical Evidence for Robustness of Environment-Assisted Quantum Transport. *Phys. Rev. E - Stat. Nonlinear, Soft Matter Phys.* **2014**, *89* (4), 1–7.

(19) Balzani, V.; Credi, A.; Venturi, M. *Photochemical Conversion of Solar Energy*; 2008; Vol. 1.

(20) El-Khouly, M. E.; El-Mohsnawy, E.; Fukuzumi, S. Solar Energy Conversion: From Natural to Artificial Photosynthesis. *J. Photochem. Photobiol. C Photochem. Rev.* **2017**, *31*, 36–83.

(21) Gust, D.; Moore, T. A.; Moore, A. L. Mimicking Photosynthetic Solar Energy Transduction. *Acc. Chem. Res.* **2001**, *34* (1), 40–48.

(22) Zhou, X.; Tyson, D. S.; Castellano, F. N. First Generation Light-Harvesting Dendrimers with a [Ru(Bpy)3]2+ Core and Aryl Ether Ligands Functionalized with Coumarin 450. *Angew. Chemie - Int. Ed.* **2000**, *39* (23), 4301–4305.

(23) Balzani, V.; Ceroni, P.; Juris, A.; Venturi, M.; Campagna, S.; Puntoriero, F.; Serroni, S.; Ciamician, C. G.; Inorganica, C.; Analitica, C. Dendrimers Based on Photoactive Metal Complexes. Recent Advances. *Coord. Chem. Rev.* **2001**, *219–221*, 545–572.

(24) Choi, M. S.; Yamazaki, T.; Yamazaki, I.; Aida, T. Bioinspired Molecular Design of Light-Harvesting Multiporphyrin Arrays. *Angew. Chemie - Int. Ed.* **2003**, *43* (2), 150–158.

(25) You, C.-C.; Dobrawa, R.; Saha-Möller, C. R.; Würthner, F. Metallosupramolecular Dye Assemblies BT - Supermolecular Dye Chemistry; Würthner, F., Ed.; Springer Berlin Heidelberg: Berlin, Heidelberg, 2005; pp 39–82.

(26) Adronov, A.; Gilat, S. L.; Fréchet, J. M. J.; Ohta, K.; Neuwahl, F. V. R.; Fleming, G. R. Light

Harvesting and Energy Transfer in Laser-Dye-Labeled Poly(Aryl Ether) Dendrimers. *J. Am. Chem. Soc.* **2000**, *122* (6), 1175–1185.

(27) Ahn, T. S.; Thompson, A. L.; Bharathi, P.; Müller, A.; Bardeen, C. J. Light-Harvesting in Carbonyl-Terminated Phenylacetylene Dendrimers: The Role of Delocalized Excited States and the Scaling of Light-Harvesting Efficiency with Dendrimer Sizet. *J. Phys. Chem. B* **2006**, *110* (40), 19810–19819.

(28) Aratani, N.; Kim, D.; Osuka, A. Discrete Cyclic Porphyrin Arrays as Artificial. *Acc. Chem. Res.* **2009**, *42* (12), 1922–1934.

(29) Panda, M. K.; Ladomenou, K.; Coutsolelos, A. G. Porphyrins in Bio-Inspired Transformations : Light-Harvesting to Solar Cell. *Coord. Chem. Rev.* **2012**, *256* (21–22), 2601–2627.

(30) Pellnor, M.; Melo, E.; Sundstro, V. Polarity-Tuned Energy Transfer Efficiency in Artificial Light-Harvesting Antennae Containing Carbonyl Carotenoids Peridinin and Fucoxanthin. *J. Phys. Chem. C* **2007**, *111*, 467–476.

(31) Guo, S.; Ma, L.; Zhao, J.; Küçüköz, B.; Karatay, A.; Hayvali, M.; Yaglioglu, H. G.; Elmali, A. BODIPY Triads Triplet Photosensitizers Enhanced with Intramolecular Resonance Energy Transfer (RET): Broadband Visible Light Absorption and Application in Photooxidation. *Chem. Sci.* **2014**, *5* (2), 489–500.

(32) Lazarides, T.; Charalambidis, G.; Vuillamy, A.; Réglier, M.; Klontzas, E.; Froudakis, G.; Kuhri, S.; Guldi, D. M.; Coutsolelos, A. G. Promising Fast Energy Transfer System via an Easy Synthesis: Bodipy-Porphyrin Dyads Connected via a Cyanuric Chloride Bridge, Their Synthesis, and Electrochemical and Photophysical Investigations. *Inorg. Chem.* **2011**, *50* (18), 8926–8936.

(33) Di Donato, M.; Iagatti, A.; Lapini, A.; Foggi, P.; Cicchi, S.; Lascialfari, L.; Fedeli, S.; Caprasecca, S.; Mennucci, B. Combined Experimental and Theoretical Study of Efficient and Ultrafast Energy Transfer in a Molecular Dyad. *J. Phys. Chem. C* **2014**, *118* (41), 23476–23486.

(34) Frath, D.; Yarnell, J. E.; Ulrich, G.; Castellano, F. N.; Ziessel, R. Ultrafast Photoinduced Electron Transfer in Viologen-Linked BODIPY Dyes. *ChemPhysChem* **2013**, *14* (14), 3348–3354.

(35) Amin, A. N.; El-Khouly, M. E.; Subbaiyan, N. K.; Zandler, M. E.; Supur, M.; Fukuzumi, S.; D'Souza, F. Syntheses, Electrochemistry, and Photodynamics of Ferrocene-

Azadipyrromethane Donor-Acceptor Dyads and Triads. *J. Phys. Chem. A* **2011**, *115* (35), 9810–9819.

(36) Guldi, D. M.; Feng, L.; Radhakrishnan, S. G.; Nikawa, H.; Mizorogi, N.; Tsuchiya, T.; Akasaka, T.; Nagase, S.; Ángeles, M. Photoinduced Charge Transfer and Electrochemical Properties of Triphenylamine Ih-Sc3N@C80 Donor-Acceptor Conjugates. *J. Am. Chem. Soc.* **2009**, *131*, 7727–7734.

(37) Liu, J.-Y.; El-Khouly, M. E.; Fukuzumi, S.; Ng, D. K. P. Photoinduced Electron Transfer in a Distyryl BODIPY-Fullerene Dyad. *Chem. An Asian J.* **2011**, *6* (1), 174–179.

(38) Guldi, D. M.; Ramey, J.; Martínez-Díaz, M. V.; Escosura, D.; Torres, T. Reversible Zinc Phthalocyanine Fullerene Ensembles. *Chem. Commun.* **2002**, 2774–2775.

(39) Balzani, V.; Credi, A.; Venturi, M. Photochemical Conversion of Solar Energy. *ChemSusChem* **2008**, *1* (1–2), 26–58.

(40) Lee, S. H.; Larsen, A. G.; Ohkubo, K.; Cai, Z. L.; Reimers, J. R.; Fukuzumi, S.; Crossley, M. J. Long-Lived Long-Distance Photochemically Induced Spin-Polarized Charge Separation in β,B'-Pyrrolic Fused Ferrocene-Porphyrin-Fullerene Systems. *Chem. Sci.* **2012**, *3* (1), 257–269.

(41) Rudolf, M.; Kirner, S. V.; Guldi, D. M. A Multicomponent Molecular Approach to Artificial Photosynthesis-the Role of Fullerenes and Endohedral Metallofullerenes. *Chem. Soc. Rev.* **2016**, *45* (3), 612–630.

(42) Wróbel, D.; Graja, A. Photoinduced Electron Transfer Processes in Fullerene-Organic Chromophore Systems. *Coord. Chem. Rev.* **2011**, *255* (21–22), 2555–2577.

(43) Imahori, H.; Tkachenko, N. V.; Vehmahen, V.; Tamaki, K.; Lemmetyinen, H.; Sakata, Y.; Fukuzumi, S. An Extremely Small Reorganization Energy of Electron Transfer in Porphyrin-Fullerene Dyad. *J. Phys. Chem. A* **2001**, *105* (10), 1750–1756.

(44) Guldi, D. M. Fullerene-Porphyrin Architectures; Photosynthetic Antenna and Reaction Center Models. *Chem. Soc. Rev.* **2002**, *31* (1), 22–36.

(45) Choi, M. S.; Aida, T.; Luo, H.; Araki, Y.; Ito, O. Fullerene-Terminated Dendritic Multiporphyrin Arrays: "Dendrimer Effects" on Photoinduced Charge Separation. *Angew. Chemie - Int. Ed.* **2003**, *42* (34), 4060–4063.

(46) Stangel, C.; Plass, F.; Charisiadis, A.; Giannoudis, E.; Chararalambidis, G.; Karikis, K.; Rotas, G.; Zervaki, G. E.; Lathiotakis, N. N.; Tagmatarchis, N.; et al. Interfacing Tetrapyridyl-C60 with Porphyrin Dimers via π-Conjugated Bridges: Artificial

Photosynthetic Systems with Ultrafast Charge Separation. *Phys. Chem. Chem. Phys.* **2018**, *20* (33), 21269–21279.

(47) Imahori, H. Porphyrin – Fullerene Linked Systems as Artificial Photosynthetic Mimics. *Org. Biomol. Chem.* **2004**, *2*, 1425–1433.

(48) Ito, O.; D'Souza, F. Recent Advances in Photoinduced Electron Transfer Processes of Fullerene-Based Molecular Assemblies and Nanocomposites. *Molecules* **2012**, *17* (5), 5816–5835.

(49) D'Souza, F.; Sandanayaka, A. S. D.; Ito, O. SWNT-Based Supramolecular Nanoarchitectures with Photosensitizing Donor and Acceptor Molecules. *J. Phys. Chem. Lett.* **2010**, *1* (17), 2586–2593.

(50) Gust, D.; Moore, T. A.; Moore, A. L. Molecular Mimicry of Photosynthetic Energy and Electron Transfer. *Acc. Chem. Res.* **1993**, *26* (4), 198–205.

(51) Liddell, P. A.; Kuciauskas, D.; Sumida, J. P.; Nash, B.; Nguyen, D.; Moore, A. L.; Moore, T. A.; Gust, D. Photoinduced Charge Separation and Charge Recombination to a Triplet State in a Carotene-Porphyrin-Fullerene Triad. *J. Am. Chem. Soc.* **1997**, *119* (6), 1400–1405.

(52) Flamigni, L.; Baranoff, E.; Collin, J. P.; Sauvage, J. P. A Triad Based on an Iridium(III) Bisterpyridine Complex Leading to a Charge-Separated State with a 120-Us Lifetime at Room Temperature. *Chem. - A Eur. J.* **2006**, *12* (25), 6592–6606.

(53) Wasielewski, M. R.; Niemczyk, M. P.; Svec, W. A.; Pewitt, E. B. High-Quantum-Yield Long-Lived Charge Separation in a Photosynthetic Reaction Center Model. *J. Am. Chem. Soc.* **1985**, *107* (19), 5562–5563.

(54) Shi, W. J.; El-Khouly, M. E.; Ohkubo, K.; Fukuzumi, S.; Ng, D. K. P. Photosynthetic Antenna-Reaction Center Mimicry with a Covalently Linked Monostyryl Boron-Dipyrromethene-Aza-Boron-Dipyrromethene-C60 Triad. *Chem. - A Eur. J.* **2013**, *19* (34), 11332–11341.

(55) Maligaspe, E.; Tkachenko, N. V; Subbaiyan, N. K.; Chitta, R.; Zandler, M. E.; Lemmetyinen, H.; Souza, F. D. Photosynthetic Antenna-Reaction Center Mimicry: Sequential Energy- and Electron Transfer in a Self-Assembled Supramolecular Triad Composed of Boron Dipyrrin, Zinc Porphyrin and Fullerene. *J. Phys. Chem. A* **2009**, *113*, 8478–8489.

(56) D'Souza, F. ; Smith, P. M.; Zandler, M. E.; Mccarty, A. L.; Itou, M.; Araki, Y.; Ito, O.

Energy Transfer Followed by Electron Transfer in a Supramolecular Triad Composed of Boron Dipyrrin, Zinc Porphyrin and Fullerene: A Model for the Photosynthetic Antenna-Reaction Center Complex. *J. Am. Chem. Soc.* **2004**, *126*, 7898–7907.

(57) Maligaspe, E.; Kumpulainen, T.; Subbaiyan, N. K.; Zandler, M. E.; Lemmetyinen, H.; Tkachenko, N. V.; D'S. Electronic Energy Harvesting Multi BODIPY-Zinc Porphyrin Dyads Accommodating Fullerene as Photosynthetic Composite of Antenna-Reaction Center. *Phys. Chem. Chem. Phys.* **2010**, *12*, 7434–7444.

(58) Hayes, D.; Griffin, G. B.; Engel, G. S. Engineering Coherence Among Excited States in Synthetic Heterodimer Systems. *Science (80-.).* **2013**, *340*, 1431–1434.

(59) Gutsche, C. D. *Calixarenes Revisited*; Monographs in Supramolecular Chemistry; The Royal Society of Chemistry, 1998.

(60) Gutsche, C. D. *Calixarenes*; Monographs in Supramolecular Chemistry; The Royal Society of Chemistry, 2008.

(61) Casnati, A. Calixarenes and Cations: A Time-Lapse Photography of the Big-Bang. *Chem. Commun.* **2013**, *49* (61), 6827–6830.

(62) Gutsche, C. D.; Muthukrishnan, R. Calixarenes. Analysis of the Product Mixtures Produced by the Base-Catalyzed Condensation of Formaldehyde with Para-Substituted Phenols. *J. Org. Chem.* **1978**, *43* (25), 4905–4906.

(63) *Calixarene in the Nanoworld*; Vicens, J., Harrowfield, J. M., Eds.; Springer, 2007.

(64) Neri, P.; Sessler, J.; Wang, M. *Calixarenes and Beyond*; Springer, 2016.

(65) *Calixarenes 2001*; Asfari, Z., Böhmer, V., Harrowfield, J., Vicens, J., Eds.; KLUWER ACADEMIC PUBLISHERS, 2001.

(66) Arduini, A.; Fabbi, M.; Mantovani, M.; Mirone, L.; Pochini, A.; Secchi, A.; Ungaro, R. Calix[4]Arenss Blocked in a Rigid Cone Conformation by Selective Functionalization at the Lower Rim. *J. Org. Chem.* **1995**, *60* (5), 1454–1457.

(67) Lazzarotto, M.; Sansone, F.; Baldini, L.; Casnati, A.; Cozzini, P.; Ungaro, R. Synthesis and Properties of Upper Rim C-Linked Peptidocalix[4]Arenes. *Eur. J.Org. Chem.* **2001**, No. 3, 595–602.

(68) Kim, J. S.; Quang, D. T. Calixarene-Derived Fluorescent Probes. *Chem. Rev.* **2007**, *107* (9), 3780–3799.

(69) Leray, I.; Valeur, B. Calixarene-Based Fluorescent Molecular Sensors for Toxic Metals. *Eur. J. Inorg. Chem.* **2009**, No. 24, 3525–3535.

(70) Erdemir, S.; Kocyigit, O.; Karakurt, S. A New Perylene Bisimide-Armed Calix[4]-Aza-Crown as "Turn on" Fluorescent Sensor for Hg^{2+} Ion and Its Application to Living Cells. *Sensors Actuators, B Chem.* **2015**, *220*, 381–388.

(71) Pham, X. Q.; Jonusauskaite, L.; Depauw, A.; Kumar, N.; Lefevre, J. P.; Perrier, A.; Ha-Thi, M. H.; Leray, I. New Water-Soluble Fluorescent Sensors Based on Calix[4]Arene Biscrown-6 for Selective Detection of Cesium. *J. Photochem. Photobiol. A Chem.* **2018**, *364* (April), 355–362.

(72) Souchon, V.; Leray, I.; Valeur, B. Selective Detection of Cesium by a Water-Soluble Fluorescent Molecular Sensor Based on a Calix[4]Arene-Bis(Crown-6-Ether). *Chem. Commun.* **2006**, No. 40, 4224–4226.

(73) Castellano, R. K.; Craig, S. L.; Nuckolls, C.; Rebek, J. Detection and Mechanistic Studies of Multicomponent Assembly by Fluorescence Resonance Energy Transfer. *J. Am. Chem. Soc.* **2000**, *122* (33), 7876–7882.

(74) Ji, H. F.; Dabestani, R.; Brown, G. M.; Sachleben, R. A. A New Highly Selective Calix[4]Crown-6 Fluorescent Caesium Probe. *Chem. Commun.* **2000**, *1* (10), 833–834.

(75) Kenis, P. J. A.; Noordman, O. F. J.; Houbrechts, S.; Van Hummel, G. J.; Harkema, S.; Van Veggel, F. C. J. M.; Clays, K.; Engbersen, J. F. J.; Persoons, A.; Van Hulst, N. F.; et al. Second-Order Nonlinear Optical Properties of the Four Tetranitrotetrapropoxycalix[4]Arene Conformers. *J. Am. Chem. Soc.* **1998**, *120* (31), 7875–7883.

(76) Bai, Z.; Zhang, C. Z.; Lu, G. Y.; Liu, F. Synthesis of Calix[4]Arene Derivatives with NLO Properties. *Chinese J. Chem.* **2006**, *24*, 124–128.

(77) Alemi, A. A.; Shaabani, B.; Dilmaghani, K. A.; Ganjali, S. T. Synthesis and Characterization of Two New P-Tert-Butylcalix[4]-Arene Schiff Bases. *Molecules* **2001**, *7* (1), 417–423.

(78) Hennrich, G.; Murillo, M. T.; Prados, P.; Song, K.; Asselberghs, I.; Clays, K.; Persoons, A.; Benet-Buchholz, J.; De Mendoza, J. Tetraalkynyl Calix[4]Arenes with Advanced NLO Properties. *Chem. Commun.* **2005**, No. 21, 2747–2749.

(79) Kart, H. H.; Bayrakdar, A.; Elcin, S.; Deligoz, H.; Karabacak, M. Synthesis and Investigation of the Properties of Novel Azocalix[4]Arenes. *Spectrochim. Acta - Part A Mol. Biomol. Spectrosc.* **2015**, *146*, 151–162.

(80) Hennrich, G.; Murillo, M. T.; Prados, P.; Al-Saraierh, H.; El-Dali, A.; Thompson, D. W.;

Collins, J.; Georghiou, P. E.; Teshome, A.; Asselberghs, I.; et al. Alkynyl Expanded Donor-Acceptor Calixarenes: Geometry and Second-Order Nonlinear Optical Properties. *Chem. - A Eur. J.* **2007**, *13* (27), 7753–7761.

(81) Arimura, T.; Ide, S.; Suga, Y.; Tachiya, M. Syntheses and Characterizations of a New Calixarene-Porphyrin Conjugate as Electron Transfer System. *J. Oleo Sci.* **2007**, *56* (3), 149–153.

(82) Arimura, T.; Ide, S.; Suga, Y.; Nishioka, T.; Murata, S.; Tachiya, M.; Nagamura, T.; Inoue, H. Electron Transfer Through-Space or Through-Bonds? A Novel System That Permits a Direct Evaluation. *J. Am. Chem. Soc.* **2001**, *123*, 10744–10745.

(83) Pognon, G.; Wytko, J. A.; Harvey, P. D.; Weiss, J. Evidence for Dual Pathway in Through-Space Singlet Energy Transfers in Flexible Cofacial Bisporphyrin Dyads. *Chem. - A Eur. J.* **2009**, *15* (2), 524–535.

(84) Hippius, C.; van Stokkum, I. H. M.; Zangrando, E.; Williams, R. M. Ground- and Excited-State Pinched Cone Equilibria in Calix [4] Arenes Bearing Two Perylene Bisimide Dyes. *J. Phys. Chem. C* **2008**, *112*, 14626–14638.

(85) Van AnH, N.; Schlosser, F.; Groeneveld, M. M.; van Stokkum, I. H. M.; Wurthner, F.; Williams, R. M. Photoinduced Interactions in a Pyrene-Calix[4]Arene-Perylene Bisimide Dye System: Probing Ground-State Conformations with Excited-State Dynamics of Charge Separation. *J. Phys. Chem. C* **2009**, *113*, 18358–18368.

(86) Hippius, C.; Schlosser, F.; Vysotsky, M. O.; Bohmer, V.; Wurthner, F. Energy Transfer in Calixarene-Based Cofacial-Positioned Perylene Bisimide Arrays. *J. Am. Chem. Soc.* **2006**, *128*, 3870–3871.

(87) Hippius, C.; van Stokkum, I. H. M.; Zangrando, E.; Williams, R. M. Ground- and Excited State Pinched Cone Equilibria in Calix[4]Arenes Bearing Two Perylene Bisimide Dyes. *J. Phys. Chem. C* **2008**, *112*, 14626–14638.

(88) Tosi, I. Model Systems for Artificial Photosynthesis: Calix[4]Arenes Functionalized with Chromophoric Units for Energy and Charge Transfer, Doctorate in Chemical Sciences - Cycle XXVII. Università di Parma, 2014.

(89) Tosi, I.; Segado Centellas, M.; Campioli, E.; Iagatti, A.; Lapini, A.; Sissa, C.; Baldini, L.; Cappelli, C.; Di Donato, M.; Sansone, F.; et al. Excitation Dynamics in Hetero-Bichromophoric Calixarene Systems. *ChemPhysChem* **2016**, *17* (11), 1686–1706.

CHAPTER 2

ELECTRON VS. ENERGY TRANSFER IN A BICHROMOPHORIC CALIX[4]ARENE-BASED SYSTEM

2.1 Introduction

Energy and electron transfer processes are universal in physical, biological, organic and inorganic chemical systems. For our purpose, more relevant is their implication in photosynthetic organisms. In these systems sunlight is harvested by the antenna complexes and the excitation energy is transferred, often over hundreds of Ångströms, to a reaction center where it initiates an electron transfer cascade chain for the production of chemical energy. The nature and the efficiency of these energy and electron transfer processes are influenced by energetic and structural parameters. For these reasons developing simple and manipulable model systems can allow for a deeper understanding of the factors that drive these processes and that determine their great efficiency. In particular, bichromophoric model units can be very helpful to study these phenomena, since their properties can be changed in a simple and controlled way.

2.1.1 Energy transfer

The energy, travelling towards the reaction center inside the photosynthetic unit, can be transferred following two different mechanisms. The first energy transfer process is based on the hopping mechanism, which follows semi-classical rules and in which the energy hops from one molecule to the other in a random walk; the second process is based instead on the formation of excitons that can travel through the system in a coherent, wavelike fashion. This chapter will only focus on the first mechanism; the quantum coherence phenomenon will be dealt with in Chapter 3.

Excitation energy transfer from a donor molecule (D) to an acceptor one (A) may be described as

$$D^* + A \rightarrow D + A^*$$

where the asterisk represents electronic excitation. This means that the de-excitation of D is associated with the excitation of A, or that at some initial time the electronic excitation may be unambiguously associated with D and at some later time is

unambiguously associated with A.[1] The energy transfer processes can then be divided into *radiative* and *radiationless*. The first one, termed trivial because of the simplicity of the physical processes involved, is not of particular interest and is typically avoided, for example by using very low concentrations in the measurements of fluorescence spectra. It is basically constituted by two steps: first the donor decays by emitting photons that are subsequently reabsorbed by the acceptor:

$$D^* \rightarrow D + h\nu_D$$

$$A + h\nu_D \rightarrow A^*$$

For the radiative transfer to happen no interaction between the partners is needed and the process is usually observed when the distance between D and A is larger than the wavelength of the corresponding photon.

The radiationless energy transfer, on the contrary, does not involve the emission and reabsorption of any real photon. This occurs when the D-A distance is much shorter than the wavelength of the corresponding photon, in other words in the so-called near field. Differently from the radiative process, the radiationless energy transfer requires some interaction between the two species and it can result from different interaction mechanisms. Coulombic interactions consist of long-range (up to 80-100 Å) dipole-dipole interactions (Förster's mechanism), and short-range multipolar interactions; interactions due to intermolecular orbital overlap, which include electron exchange (Dexter's mechanism) and charge resonance interactions, are only short-range (< 10 Å). Besides the nature of the interaction, its magnitude is equally important and a distinction between strong and weak coupling can be made. In the *strong coupling* regime, the intermolecular interaction is much larger than the interaction between the electronic and nuclear motions within the individual molecules and the transfer of excitation energy is faster than the nuclear vibrations and the vibrational relaxation ($\sim 10^{-12}$ s). The excitation energy is not localized on one of the molecules but is delocalized over the two components and the transfer of excitation is a coherent process that can be described in the frame of the exciton theory. In the *weak coupling* regime, the vibrational relaxation of the donor and of the bath is much faster than the

timescale of energy transfer (internal conversion is usually as fast as 10^{-12} s versus ~10^{-9} s for energy transfer) and the coupling between donor and acceptor is much weaker than the coupling with the bath, condition that ensures that the transfer is incoherent and no delocalized electronic states between D and A exist. In the weak coupling regime, energy transfer can be described using the perturbation theory, as originally proposed by Förster in the late thirties.[1]

2.1.2 Förster resonance energy transfer

Radiationless transfer of excitation energy can occur if the emission spectrum of the donor overlaps the absorption spectrum of the acceptor, so that several vibronic transitions in the donor have practically the same energy as the corresponding transitions in the acceptor. Such transitions are coupled or, in other words, in *resonance*;[2] from there the term RET (Resonance Energy Transfer) to describe this type of processes. Thanks to Förster's great contribution on this matter, RET is often called FRET which stands for Förster Resonance Energy Transfer.

The rate of the energy transfer process in Förster theory is described as follows

$$k_{RET} = \frac{8.79 \cdot 10^{23}}{n^4} \frac{\kappa^2}{R_{DA}^6} \frac{\phi_D}{\tau_D} J \qquad (1)$$

and is related to the quantum yield of the donor in the absence of the acceptor (ϕ_D), to the fluorescence lifetime of the donor in the absence of the acceptor (τ_D), to the inverse sixth power of the distance between the donor and the acceptor (R_{DA}), to the inverse fourth power of the refractive index of the medium (n), to the factor κ^2, which depends on the relative orientation in space of the transition dipoles of the donor and of the acceptor (the value 2/3 is usually employed, except when conditions hinder rotational diffusion) and finally to the overlap integral J. J is expressed as

$$J = \int d\tilde{\nu} \frac{\bar{F}_D(\tilde{\nu}) \varepsilon_A(\tilde{\nu})}{\tilde{\nu}^4} \qquad \text{or} \qquad J = \int \bar{F}_D(\lambda) \varepsilon_A(\lambda) \lambda^4 d\lambda \qquad (2)$$

and is connected to the overlap between the fluorescence spectrum of the donor normalized to unit area ($\bar{F}_D(\tilde{\nu})$) and the absorption spectrum of the acceptor ($\varepsilon_A(\tilde{\nu})$) expressed as molar extinction coefficient (**Figure 2.1**).

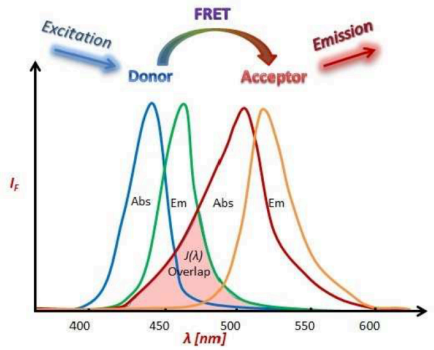

Figure 2.1. Graphical representation of FRET through the overlap between the emission spectrum of the donor and the absorption spectrum of the acceptor.

From a classical point of view, the process can be explained by associating to D^* an oscillating electric dipole which can exchange energy with another dipole with a similar resonance frequency.[3] The process is illustrated in **Figure 2.2,** in which the oscillating electric dipole of D^* is able to drive into resonance the initially non-oscillating electrical receiver A, leading to the creation of A^* through a dipole-dipole energy transfer mechanism.

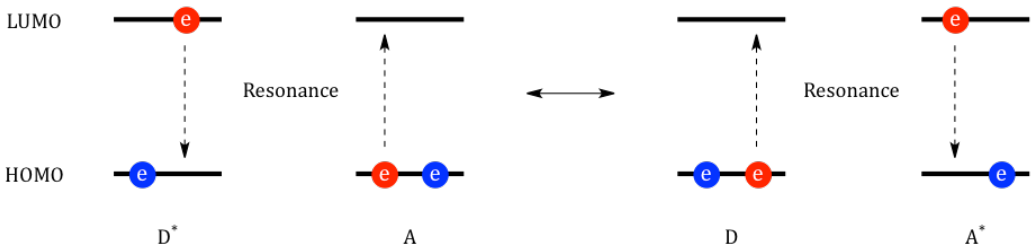

Figure 2.2. Dipole-dipole mechanism of electronic energy transfer.

Going back to the rate of the transfer, the quantities ϕ_D, τ_D and J can be easily obtained through the analysis of the donor emission and of the acceptor absorption; the distance between the oscillating dipoles, instead, is not directly accessible. This is the reason why Förster introduced the distance R_0, which was called from then on Förster radius. R_0 is defined as the distance in which FRET is 50% efficient,[3] that is the distance at which the transfer rate (k_{RET}) is equal to the decay rate of the donor in the

absence of the acceptor ($1/\tau_D$). The Förster radius can be easily estimated from κ^2, ϕ_D and J and the rate of the transfer can be expressed as follows

$$k_{RET} = \frac{1}{\tau_D}\left(\frac{R_0}{R_{DA}}\right)^6 \qquad (3)$$

If the transfer rate is much faster than the decay rate, the energy transfer will be efficient. On the contrary, if the transfer rate is slower than the decay rate only little transfer will occur and the RET will be inefficient.

The *efficiency of the transfer* (E) is defined as:

$$E = \frac{k_{RET}}{\tau_D^{-1} + k_{RET}} \qquad (4)$$

which, after substituting k_{RET} from (3), can be rearranged as

$$E = \frac{R_0^6}{R_0^6 + R_{DA}^6} \qquad (5)$$

This equation shows that the efficiency is strongly dependent on the distance: it quickly increases to 100% when the distance decreases below R_0 and, conversely, quickly decreases to zero when the distance is bigger than R_0.

Different methods for the determination of the *transfer efficiency* have been developed, based on the measure of four different phenomena:

- Decrease in donor fluorescence: the transfer from the donor to the acceptor causes the quantum yield of the donor to decrease. The *transfer efficiency* is given by

$$E = 1 - \frac{\phi_{D(A)}}{\phi_D} \qquad (6)$$

  where $\phi_{D(A)}$ is the fluorescence quantum yield of the donor in the presence of the acceptor and ϕ_D the fluorescence quantum yield of the isolated donor.

Analogously,

- Decrease of the donor lifetime: starting from equation (4) and defining the lifetime of the donor in the presence of the acceptor, $\tau_{D(A)}$, so that

$$\tau_{D(A)}^{-1} = \tau_D^{-1} + k_{RET} \qquad (7)$$

  the *transfer efficiency* is given by

$$E = 1 - \frac{\tau_{D(A)}}{\tau_D} \qquad (8)$$

- Enhancement of the acceptor fluorescence: the fluorescence intensity of the acceptor is enhanced in the presence of transfer. The *transfer efficiency* can be written as

$$E = \left[1 - \frac{F_{D(A)}(\lambda_A^{em})}{F_A(\lambda_A^{em})}\right] \frac{\varepsilon_A(\lambda_D^{exc})}{\varepsilon_D(\lambda_D^{exc})} \qquad (9)$$

  where $\varepsilon_D(\lambda_D^{exc})$ and $\varepsilon_A(\lambda_D^{exc})$ are the molar extinction coefficients of the donor and the acceptor, respectively, at the excitation wavelength of the donor, $F_A(\lambda_A^{em})$ and $F_{AD}(\lambda_A^{em})$ the fluorescence intensities of the isolated acceptor and of the acceptor in the presence of the donor, respectively, at the emission wavelength of the acceptor.

- Comparison between the absorption spectrum and excitation spectrum (through observation of the acceptor fluorescence): in the case of quantitative transfer (E = 100%) the two spectra are identical, after normalization at the same height. For any other value of E, the excitation band corresponding to the donor is relatively lower than its absorption band. The *transfer efficiency* is then calculated as follows

$$E = \frac{A_A(\lambda_A)}{A_D(\lambda_D)} \left[\frac{I_A(\lambda_D, \lambda_A^{em})}{I_A(\lambda_A, \lambda_A^{em})} - \frac{A_A(\lambda_D)}{A_A(A)}\right] \qquad (10)$$

  where $A_A(\lambda_A)$ and $A_D(\lambda_D)$ are the maximum absorbance of the acceptor and donor respectively, $A_A(\lambda_D)$ the absorbance of the acceptor at the wavelength of maximum absorption of the donor, $I_A(\lambda_D, \lambda_A^{em})$ and $I_A(\lambda_A, \lambda_A^{em})$ the intensities of the excitation spectrum at the donor and acceptor maximum wavelength, respectively.

2.1.3 Electron transfer

The electron transfer process occurs when an electron relocates from one molecular entity to another, or between two localized sites in the same molecular entity. It consists of a spontaneous transition from a metastable initial state to a stable final state, where the initial state can be prepared either by charge injection or by photoabsorption. In the first case, the process can be described as

$$D^- A \rightarrow D A^-$$

which indicates that in the reactant state there is an excess electron localized at the donor that moves to the acceptor forming the product state. In the second case, the reaction involves an excited electron, which can come from direct photoexcitation or *via* excitation energy transfer, and can be depicted as

$$D^* A \rightarrow D^+ A^-$$

This type of electron transfer is called Photoinduced Electron Transfer (PET) and it is the one we will be dealing with in this chapter.

In order for PET to occur, two main requirements need to be fulfilled: first, the reactants must be in close contact, to promote the overlap between their electronic orbitals, and, secondly, the LUMO of the donor must be higher in energy than the LUMO of the acceptor, and the same must be true for their HOMOs. In fact, if the last condition is not respected and the HOMO of the acceptor is higher in energy than the HOMO of the donor, a back electron transfer between the HOMOs could occur, thus resulting in energy transfer and charge recombination (**Figure 2.3**). These two phenomena, electron transfer and energy transfer, both lead to the quenching of the donor fluorescence, but they can be discriminated by looking at the acceptor emission. In fact in the case of the occurrence of energy transfer, the acceptor fluorescence is increased.[4]

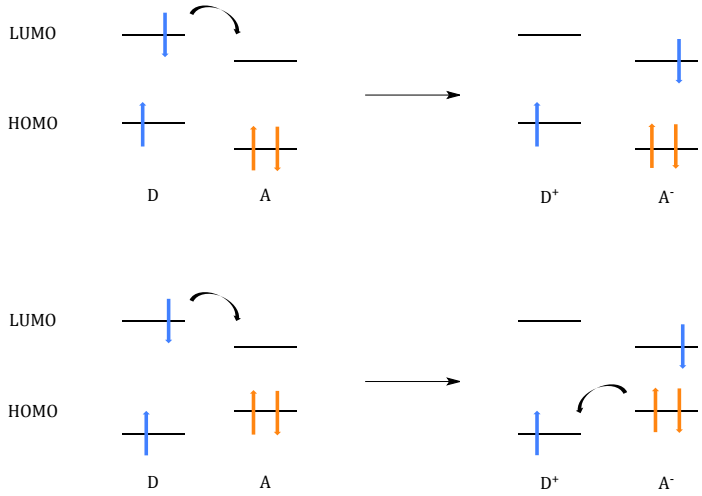

Figure 2.3. Donor and acceptor electronic configuration leading to electron transfer (at the top) and to charge recombination (at the bottom).

In general, the electron donor and acceptor can belong to the same molecule or to two distinct molecules: in the first case the process is called *intramolecular* or unimolecular electron transfer, in the second case it is called *intermolecular* or bimolecular. This thesis deals with the study of electron and energy transfer between chromophores belonging to the same molecule.

2.1.4 Intramolecular electron transfer

The change in the electronic charge distribution due to the electron transfer process causes a change of the equilibrium configuration of the nuclei and of the surrounding solvent. The process can be described through the potential energy surface (PES) reported in **Figure 2.4,** in which the potential energy of the reactants (U_R) and the potential energy of the products (U_P) versus a single reaction coordinate are reported. If we neglect the electronic coupling that leads to electron transfer, the two PES will intersect; the so-called diabatic representation is given by the full curves. When the electronic coupling is not neglected, the interaction between donor and acceptor causes a splitting of the two surfaces in the vicinity of the intersection (see U_+ and U_-).

This splitting amounts to twice the interaction energy between reactants and products ($2|V_{RP}|$) and in this case we talk about adiabatic representation.

In classical term, the electron transfer can occur only at the configuration where the reactant and product curves intersect (q^*), overcoming a barrier potential (transition state).[5]

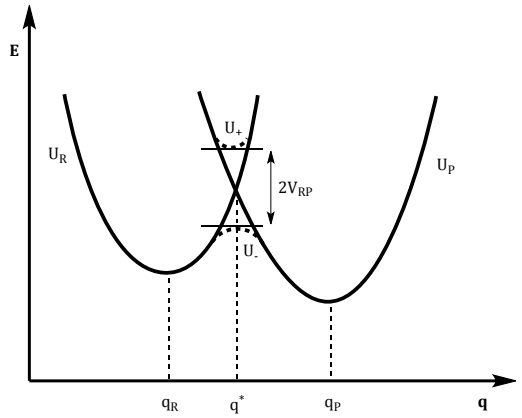

Figure 2.4. Potential energy surface (PES) for reactants and products. Full curves: diabatic representation; dashed curves: adiabatic representation.

The expression for the rate constant of the electron transfer is given by

$$k_{ET} = Ae^{-\frac{E_a}{k_B T}} \qquad (11)$$

where E_a is the activation energy and k_B is the Boltzmann constant. Marcus defined the rate in terms of experimentally accessible quantities,[6] in particular he expressed the activation energy as a function of two quantities, ΔE and E_λ, as shown in **Figure 2.5**, which are the energy difference between reactants and products at their equilibrium positions and the reorganization energy, respectively.

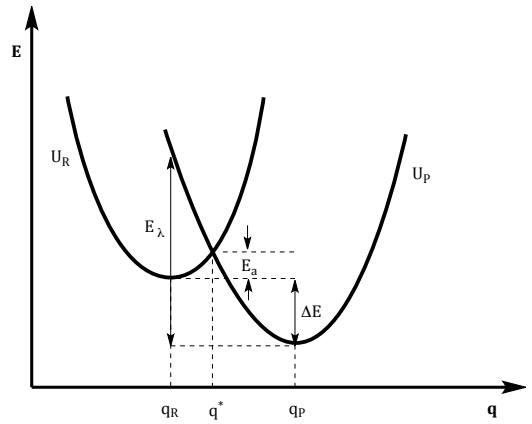

Figure 2.5. Graphic representation of the activation energy (E_a), the driving force (ΔE) and the reorganization energy (E_λ).

ΔE is also defined as the driving force[5] of the electron transfer reaction and E_λ corresponds to the energy gain due to the molecular rearrangement from the reactants' to the products' equilibrium configuration after a "vertical" electron transfer. The rate for the transfer can then be rewritten as

$$k_{ET} = Ae^{-\frac{(\Delta E + E_\lambda)^2}{4E_\lambda k_B T}} \qquad (12)$$

Spontaneous electron transfer generally takes place with thermal activation, which pushes the reactants over the activation barrier. At low temperature, however, the electron transfer can occur via tunneling and, in this case, quantum mechanical considerations of the vibrational coordinates[6,7] need to be taken into account.

When the transfer proceeds directly from the donor to the acceptor, even if they are connected through a bridging unit, the process is called *through-space* transfer. This is possible only for distances between donor and acceptor smaller than 20 Å, since a finite overlap between the molecular orbitals of donor and acceptor is needed. When, on the other hand, the bridging unit connecting the two chromophores is involved in the transfer, and thus the reaction proceeds across the spacer, the process is called *through-bond* or *bridge-assisted.* In this case, the process can occur following two different mechanisms, showed in **Figure 2.6**. According to the *superexchange* mechanism, the LUMOs of donor and acceptor are off-resonant with respect to the

bridge levels, so the most important function of the spacer is to provide a means for delocalization of the donor state wave function across the whole bridge. The second mechanism is called *sequential* or *hopping* transfer; in this case the LUMOs of donor and acceptor are almost resonant with respect to the bridge levels and the charge jumps from one orbital to the other, locating itself on a precise LUMO for a finite time. The global rate of the process depends on the number of steps constituting the electronic pathway.[8]

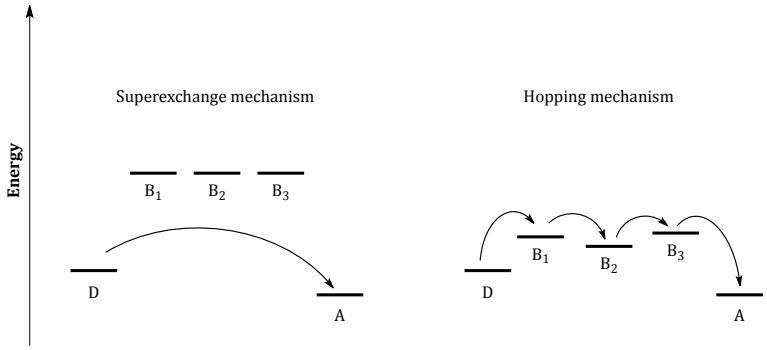

Figure 2.6. Schematic comparison of the superexchange and hopping mechanism of through-bond electron transfer for a D-bridge-A system.

2.2 Aim of the chapter

This chapter is focused on the synthesis of a simple bichromophoric model system for the study of the electron transfer process. The dyad was designed within the frame of a wider project that aims at the development of multichromophoric calix[4]arene systems able to perform, subsequently and intramolecularly, an energy and an electron transfer step. Previously, in our research group, in fact, 7-nitrobenz-2-oxa-1,3-diazol-4-yl (NBD) and Nile Red (NR) chromophores were linked to the upper rim of a *cone* and a *partial cone* calix[4]arene to obtain structures able to efficiently perform energy transfer from NBD to Nile Red.[9] Interestingly, it was found that the distance and the interactions between the chromophores could be regulated by the choice of the solvent. With the goal of obtaining a more complex structure in which energy transfer from NBD to NR could be followed by electron transfer from NR to a suitable

electron acceptor, a simple model dyad based on the calixarene scaffold was therefore designed to specifically study the electron transfer step. Nile Red, chosen as the energy acceptor in the previously studied bichromophores, is a highly fluorescent dye that has been previously studied as electron donor towards TiO_2 colloidal nanoparticles.[10] As pointed out in 2.1.3 in order to have electron transfer, the donor and acceptor chromophores must possess the right orbital configuration. As electron acceptor, therefore, our choice fell on fullerene C_{60}. Fullerenes, widely used as electron acceptor molecules, possess high electron affinity and are characterized by small reorganization energy in the electron transfer processes.[11,12] When coupled with an electron donor, they tend to accelerate forward electron transfer and slow down backward electron transfer, offering unique opportunities for stabilizing charged entities.[13–15] Calculations reported in 16 by McGehee *et al*. show that the energy of the frontier orbitals of Nile Red and fullerene C_{60} are ideally organized to promote the electron migration and avoid the charge recombination. On the other hand, previous studies demonstrated the competition between electron and energy transfer in donor-C_{60} dyads, with one process being favored over the other depending on experimental conditions and orientation of the donor with respect to the fullerene.[17,18]

With this in mind, we anchored Nile Red and C_{60} to a calix[4]arene in *cone* conformation, in order to assure the spatial vicinity of the chromophores and thus the overlap of the respective molecular orbitals (**Figure 1.7**). The residual mobility of the calixarene in solution and the flexibility of the two spacers linking the two dyes to the scaffold can be exploited to slightly change the interchromophoric distance and to allow for the establishment of attractive interactions between the dyes. In addition, a previous study on a pyromellitimide-porphyrin-calix[4]arene confirmed the role of the calixarene as versatile scaffold to bring the chromophores together, without being involved in the electron transfer (through-space transfer).[19]

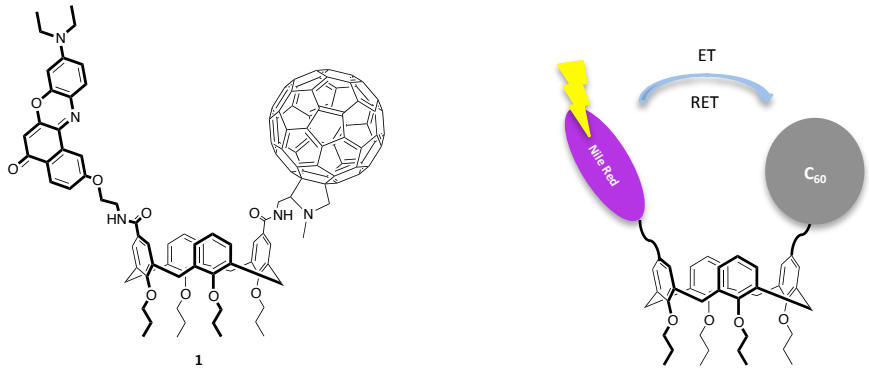

Figure 1.7. Target calix[4]arene-based dyad (on the left) and schematic representation of the transfer between the two chromophores (on the right).

2.3 Results and discussion

2.3.1 Synthesis

Hydroxy Nile Red (**NR-OH**) was synthesized starting from the commercially available 3-diethylaminophenol, which was reacted with $NaNO_2$ in aqueous HCl to obtain 5-diethylamino-2-nitrosophenol hydrochloride **13**. The subsequent reaction of **13** with 1,6-dihydroxynaphthalene gave **NR-OH** in 68% yield (**Scheme 2.1**).

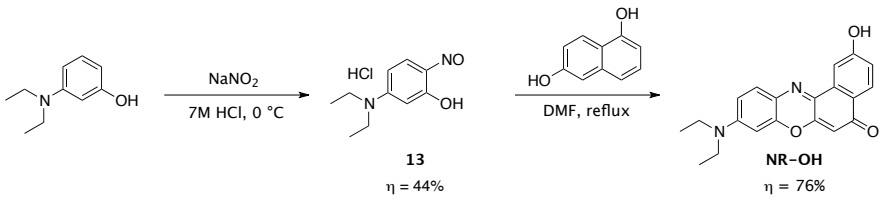

Scheme 2.1. Reaction pathway for the synthesis of **NR-OH**.

1,2-dibromoethane was then introduced on **NR-OH** and the bromide substituted with an azido group, which was in turn reduced to amine through the Staudinger reaction using triphenylphosphine and water (**Scheme 2.2**) obtaining **NR-NH_2**.

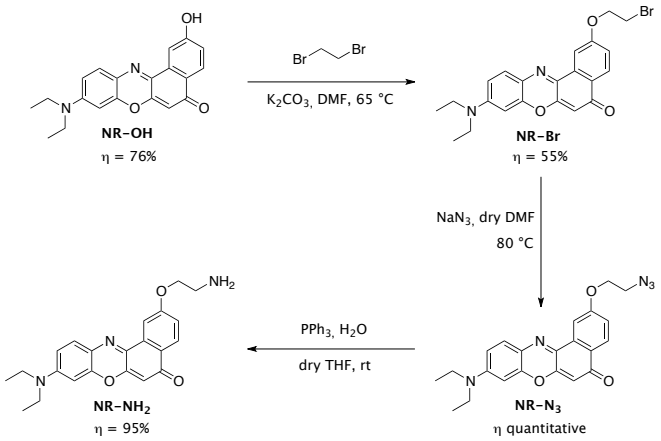

Scheme 2.2. Reaction pathway for the synthesis of **NR-NH$_2$**.

The synthesis of the bichromophoric system **1** (**Scheme 2.3**) started with diacid calixarene **4**, which had been synthesized from tetrahydroxy calixarene according to literature procedures.[20] Compound **4** was transformed in the corresponding acyl chloride **5** and immediately reacted with an equimolar mixture of **NR-NH$_2$** and 2,2-diethoxyethanamine obtaining the difunctionalized calixarene **6**. This statistical approach, on the one hand, allows the introduction of two moieties in a single step, on the other, it makes the purification more difficult, due to the presence of at least three different products. After column chromatography, compound **6** was isolated pure in 47% yield. The acetal protecting group was then removed from **6** using 1M HCl in 1,4-dioxane and the small amount of reagent, still present when the reaction was quenched, was removed by column chromatography. Finally, fullerene C_{60} was linked to the calixarene through the well-known Prato reaction using sarcosine in toluene under reflux. The reaction was quenched after only three hours to avoid multiple functionalization of the fullerene and the crude was purified by column chromatography and preparative TLC plates to afford the product as a dark purple solid in 23% yield.

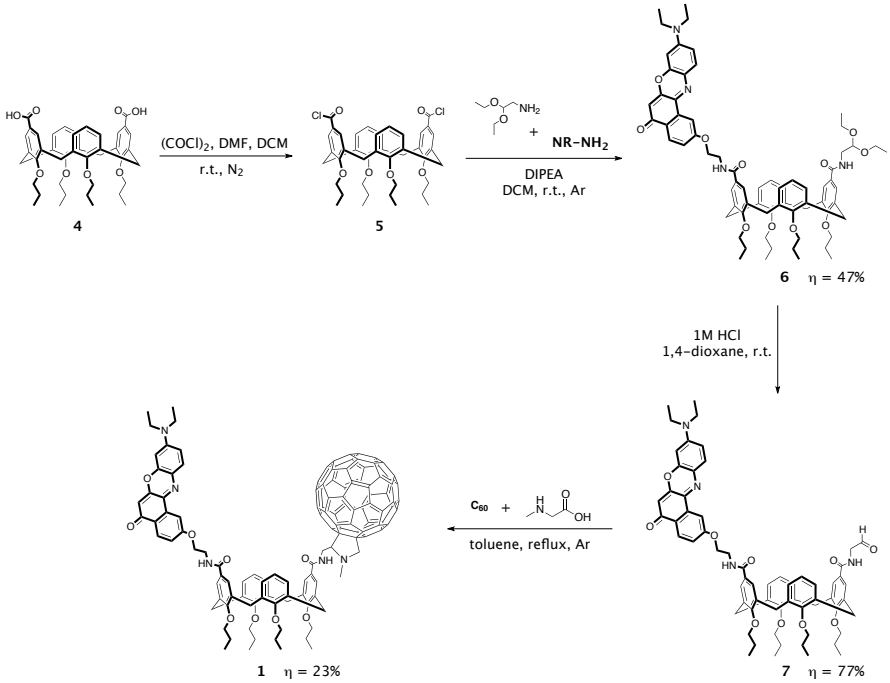

Scheme 2.3. Synthetic pathway for the synthesis of calixarene **1**.

Calixarenes **6**, **7** and **1** were fully characterized by 1D and 2D ^{1}H and ^{13}C NMR and ESI mass spectrometry. All the peaks in the ^{1}H NMR spectrum of **1** (Figure 8) have been assigned thanks to ROESY experiment. The ^{1}H NMR, in fact, clearly reflects the asymmetric nature of the molecule, giving rise to different signals for each of the protons of methylene groups l, m and o (**Figure 2.8**), which are diastereotopic, and for the aromatic protons of the substituted rings of the calixarene.

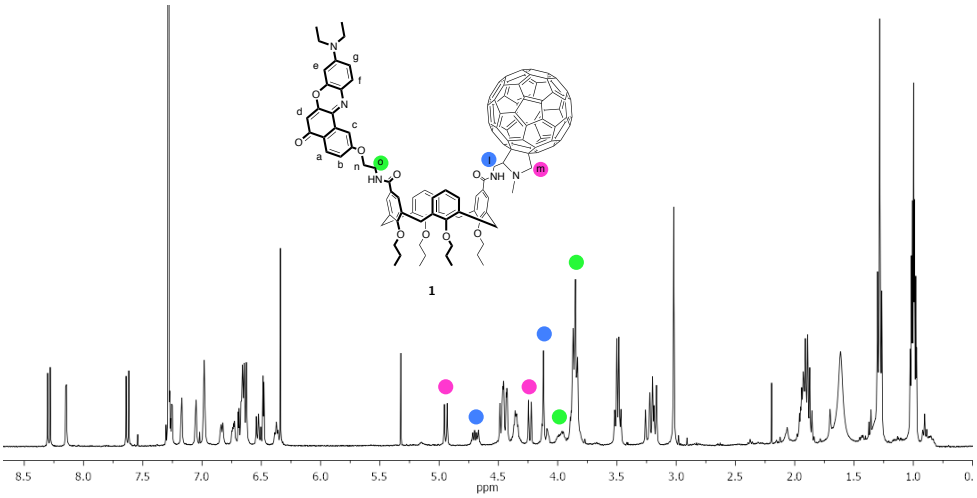

Figure 2.8. ^{1}H NMR spectrum (400 MHz, $CDCl_3$) of compound **1**.

Regarding the conformation adopted by the calixarene in solution, from the ^{1}H NMR in $CDCl_3$ it seems that the preferred conformation is the *open flattened cone*. As explained in section 1.3.1, thanks to its residual conformational mobility in solution, the *cone* calix[4]arene functionalized on the distal aromatic rings can adopt two limiting flattened conformation, the open and the closed one, that can be distinguished by the resonance of the aromatic protons. The rings parallel to each other, in fact, experience the shielding cone of the outward-oriented rings, and as a result resonate at higher fields. In this case the resonance of the aromatic protons (singlets at 7.17, 7.05 and 6.98 ppm for the protons ortho to the amide group, multiplet between 6.57-6.49 ppm and triplet at 6.53 ppm for the protons on the unsubstituted aromatic rings) implies the absence of an intramolecular hydrogen bond between the NH and CO of the amide moieties on the distal aromatic rings, differently from what it was found previously in similar molecules,[21,22] and of π-stacking interaction between the chromophores. The conformation of **1**, therefore, is simply determined by the reduction of the steric repulsion between the bulky substituents at the upper rim of the calixarene. The spectrum of **1** registered in toluene-d_8 shows no peculiar differences from the one in $CDCl_3$. The conformational behavior of **1** could only be investigated in $CDCl_3$ and toluene-d_8 due to the poor solubility of the compound in all the other organic solvents.

In order to have a complete spectroscopic characterization and investigate the possible influence of the calixarene scaffold on the energy and electron transfer processes, the two monochromophoric compounds (**2** and **3**) were synthesized (**Scheme 2.4** and **Scheme 2.5**). Both the derivatives were obtained starting from 5-hydroxycarbonyl-25,26,27,28-tetrapropoxycalix[4]arene **9**, which was in turn derived from 5-formyl-25,26,27,28-tetrapropoxycalix[4]arene **8**[23] For the synthesis of **2** (**Scheme 2.4**), the oxidation reaction of **8** was carried out with sodium chlorite and sulfamic acid, as reported in the literature.[20] The reaction mixture, however, resulted unexpectedly complex and the ^{1}H NMR spectrum showed many signals, difficult to assign, due to the presence of different species. This behavior has been attributed to the chlorination of one of the non-substituted phenol rings of the calixarene. The chlorinating agent might be the hypochlorous acid generated during the reaction[24] and not fully neutralized by sulfamic acid. Working with a large excess of the sulfamic scavenger and lowering the temperature during the slow addition of the chlorite did not improve the results. Unable to isolate compound **9** from the chlorinated subproducts through the classical purification techniques, because of their structural similarity, we performed the next reactions on the crude mixture, with the aim to purify the final compound after the attachment of the Nile Red chromophore. Thus, the mixture of calixarenes containing **9** was activated as acyl chloride and then reacted with **NR-NH$_2$**. Several spots were present on the TLC of the crude, but this time it was possible to isolate the desired compound, albeit in a modest yield due to the long and complex purification.

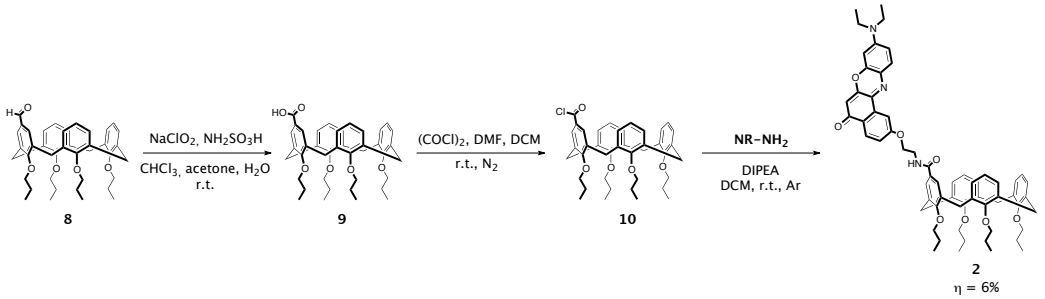

Scheme 2.4. Synthesis of **2**.

To avoid the problems encountered in the purification of **9**, when we started the synthesis of calixarene **3** (**Scheme 2.5**), the oxidation reaction was carried out using hydrogen peroxide as scavenger for the hypochlorous acid formed in the presence of sodium chlorite as oxidant.[25] With this procedure, the reaction time increased greatly, but monoacid calixarene **9** was obtained pure after a quick column separation. 2,2-ethoxyethanamine was then introduced on calixarene **9**, previously activated as acyl chloride, then the acetal protecting group was removed and fullerene C_{60} was attached through the Prato reaction, to give the final product **3** as a light brown powder in 13% yield (**Scheme 2.5**).

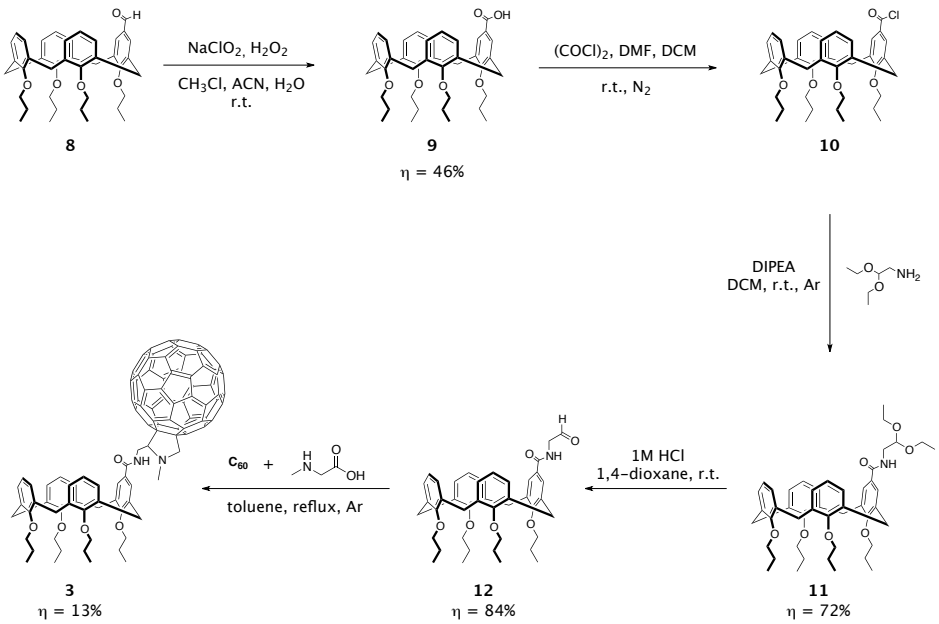

Scheme 2.5. Reaction pathway for the synthesis of **3**.

2.3.2 Spectroscopic studies

2.3.2.1 Steady-state absorption and fluorescence

Bichromophoric calixarene **1** was studied by absorption and steady-state fluorescence spectroscopy, together with monochromophoric systems **2** and **3**, which were used as references for the correct analysis of the data gathered on **1**. Fluorescence and absorption spectra were collected only in chloroform and toluene due to the poor solubility of the fullerene-containing compounds in all the other organic solvents. The absorption and emission spectra of the donor-acceptor system **1** (**Figure 2.9**) clearly match the spectroscopic features of the donor **2** and of the acceptor **3**.

Comparing the spectral characteristics of **1** and **2** in the two solvents, the solvatochromic nature of Nile Red is evident, both in absorption and in emission, with a red-shift of 25 nm going from toluene to chloroform (**Figure 2.9** and **Figure 2.10**).

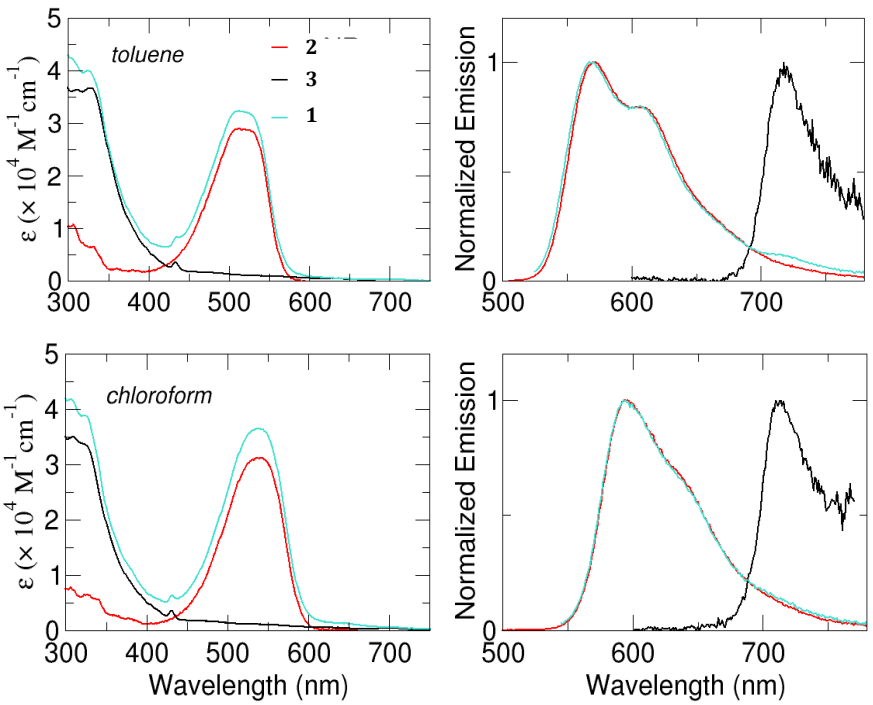

Figure 2.9. Absorption (on the left) and emission (on the right) spectra of **2**, **3** and **1** in toluene (on the top) and in chloroform (on the bottom).

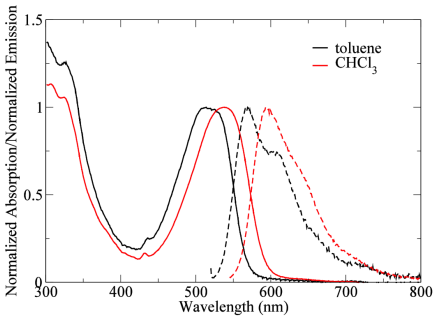

Figure 2.10. Normalized absorption (continuous line) and emission (dotted line) spectra of **1** in toluene and $CHCl_3$.

The main spectroscopic properties of the three systems are summarized in **Table 2.1**. The fluorescence quantum yield of **3** could not be measured due to the low emission of the fullerene.

Table 2.1. Main spectroscopic properties of **1**, **2** and **3** in toluene and chloroform. Fluorescence quantum yields were measured at 23 °C using fluorescein in 0.1 M NaOH as standard (Φ = 90%).

Solvent	Compound	λ_{abs}^{max} (nm)	λ_{em}^{max} (nm)	ε (10^4 M^{-1} cm^{-1}) @ λ_{abs}^{max}	Φ [λ_{exc} (nm)]
Toluene	**2**	513	570	2.9	84 [530]
	3	-	718	-	<< 1
	1	514	567	3.2	1.9 [515]
$CHCl_3$	**2**	538	596	3.1	78 [540]
	3	-	710	-	<< 1
	1	538	593	3.6	2.7 [540]

2.3.2.2 Energy and electron transfer studies

To evaluate the occurrence of energy transfer within **1** from Nile Red to fullerene C_{60} and, in case of positive feedback, to calculate the efficiency of the process, the spectral overlap between the donor (**2**) and the acceptor (**3**) species was considered.

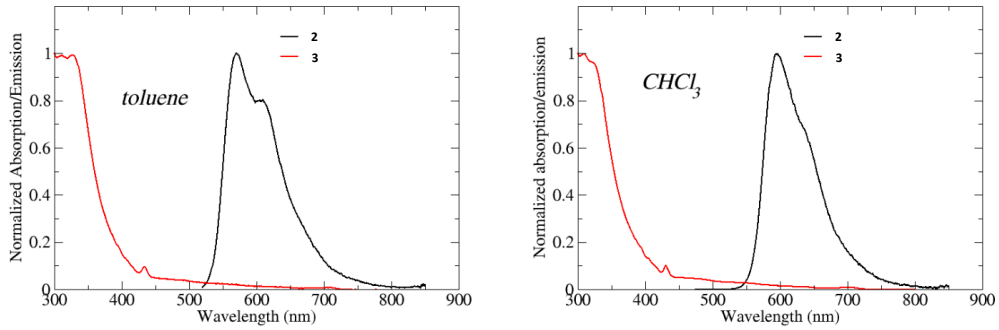

Figure 2.11. Spectral overlap between emission of **2** and absorption of **3.**

At first sight, the overlap between the emission spectrum of **2** and the absorption spectrum of **3** seems very small (**Figure 2.11**). Numerical values of the overlap integrals, reported in **Table 2.2**, on the other hand, are unexpectedly high, or at least comparable to those calculated for similar systems[22] which gave rise to highly efficient energy transfer. The calculated Förster radii R_0 are 25 Å in toluene and 30 Å in chloroform, respectively. Considering that the distance between the two chromophores should be lower than 20 Å, as found for similar systems,[22] an efficient energy transfer is expected.

Table 2.2. Estimation of the overlap integrals *J* between **2** and **3** and Forster radius R_0.

Solvent	***J*** **(M^{-1} cm^3 $(nm)^4$)**	**R_0 (Å)**
Toluene	$2.180 \cdot 10^{13}$	25
$CHCl_3$	$7.562 \cdot 10^{13}$	30

To calculate the efficiency of the energy transfer, two methods were used. The first one is based on the increase of the acceptor fluorescence, according to equation (9). **Figure 2.12** displays the deconvolution of the fluorescence spectrum of **1** in toluene as the sum of the normalized spectra of **2** and **3** and shows that the best fit is obtained for an increase of the acceptor emission of 23 times, yielding an efficiency of 79%. The same calculation in chloroform gives an efficiency of 74%.

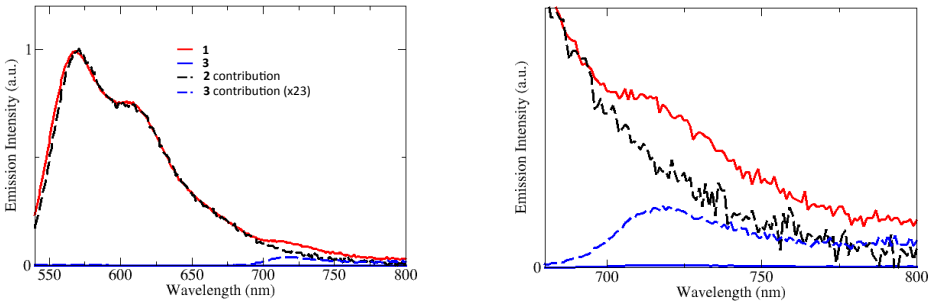

Figure 2.12. Deconvolution of the emission spectrum in toluene of **1** as the sum of **2** and **3** (on the left); enlargement of the emission region of the acceptor (on the right).

The second method is based on the quenching of the donor emission. Using equation (6) in fact, it is possible to obtain the efficiency of the process by estimating the decrease of the donor emission when linked to the acceptor.

As it can be seen in **Figure 2.13**, a huge decrease of the donor emission in toluene is observed.

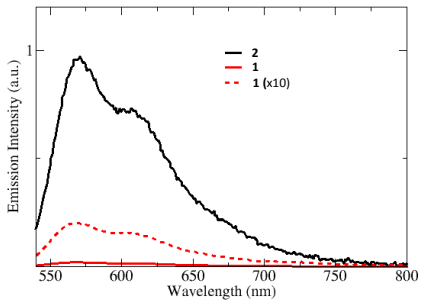

Figure 2.13. Fluorescence spectrum in toluene of compounds **1** and **2**, showing the quenching of the emission of the donor.

The efficiencies calculated with this method in the two solvents (**Table 2.3**) result to be 98% and 95% in toluene and chloroform, respectively.

Table 2.3. Estimation of the energy transfer efficiencies from quenching of the donor emission. Φ_D is the quantum yield of the isolated donor; $\Phi_{D(A)}$ is the quantum yield of the donor in the presence of the acceptor.

Solvent	Φ_D%	λ_{exc} (nm)	$\Phi_{D(A)}$%	Efficiency %
Toluene	84	530	1.9	98
$CHCl_3$	78	540	3.5	95

If, on the one hand, the increase of the acceptor emission when linked to the donor is only attributed to an energy transfer process, on the other hand the quenching of the donor emission could be due either to an energy transfer or to an electron transfer process, or to the coexistence of both mechanisms. Thus, if the energy transfer was the only process at stake, the efficiencies found with the two methods shown above would coincide. Experimentally, however, the values obtained with the second method are considerably higher than the ones determined with the first one (98% vs 79% in toluene and 95% vs 74% in chloroform) and so electron transfer could occur together with energy transfer.

2.4 Concluding remarks

This chapter deals with the synthesis of *cone* calix[4]arene **1** functionalized with Nile Red and fullerene C_{60} to evaluate the occurrence of electron transfer. The two dyes were chosen based on their orbital configuration that favors the electron migration from Nile Red to the fullerene and avoids the back transfer. In addition, the spectral overlap between the emission spectrum of the donor and the absorption spectrum of the acceptor is rather small. The molecule was initially studied by steady-state spectroscopy, together with the two monochromophoric compounds **2** and **3** used as references. A huge quenching of the donor fluorescence was observed, together with an increase in the acceptor fluorescence. If on the one hand the quenching of the donor emission could be attributed to both phenomena, only the energy transfer process is responsible for the increase of the acceptor emission. The efficiencies of the energy transfer calculated with the two methods are different, with the one calculated

through the quenching of the donor fluorescence being significantly higher than the one calculated through the increase of the acceptor emission. One possible explanation is that the energy and electron transfer phenomena are coexisting in the synthesized dyad. Transient absorption spectroscopy and spectroelectrochemical studies are ongoing to investigate the formation of the Nile Red cation and thus confirm the occurrence of electron transfer.

2.5 Experimental section

General information. All moisture sensitive reactions were carried out under a nitrogen or argon atmosphere, using previously oven-dried glassware. All dry solvents were prepared according to standard procedures, distilled before use and stored over 3 or 4 Å molecular sieves. All other reagents were commercial samples and used without further purification. Analytical TLC were performed using prepared plates of silica gel (Merck 60 F-254 on aluminum) and then, according to the functional groups present on the molecules, revealed with UV light or using staining reagents: $FeCl_3$ (1% in H_2O/CH_3OH 1:1) and Brady's reagent. Merck silica gel 60 was used for flash chromatography (40-63 μm) and for preparative TLC plates (10-12 μm).

^1H NMR and ^{13}C NMR spectra were recorded on Bruker AV300 and Bruker AV400 spectrometers (observation of ^1H nucleus at 300 MHz and 400 MHz, respectively, and of ^{13}C nucleus at 75 MHz and 100 MHz, respectively) and partially deuterated solvents were used as internal standards to calculate the chemical shifts (δ values in ppm). All ^{13}C NMR spectra were performed with proton decoupling. Electrospray ionization (ESI) mass analysis were performed with a Waters single-quadrupole spectrometer in positive mode using MeOH or CH_3CN as solvents. Melting points were determined on an Electrothermal apparatus in closed capillaries. UV-vis absorption spectra were recorded on a Perkin Elmer Lambda 650 spectrometer. Steady-state fluorescence spectra and fluorescence decays were carried out on a Fluoromax-3 Horiba Jobin Yvon spectrofluorometer. Fluorescence decays were measured in a TCSPC (time-correlated single-photon counting) configuration, under excitation from selected nanoLED or

laser-diode sources; fluorescence lifetimes were obtained from the reconvolution fit analysis of the decay profiles; the quality of the fits was judged by the reduced χ^2 value (fits are retained for $\chi^2 < 1.1$).

5,17-dihydroxycarbonyl-25,26,27,28-tetrapropoxycalix[4]arene **4**,[20] 5-formyl-25,26,27,28-tetrapropoxycalix[4]arene **8**,[23] **NR-OH,**[26] **NR-Br**,[27] **NR-N_3**[27] were synthesized according to literature procedures.

2-(2-aminoethoxy)-9-diethylamino-5*H*-benzo[α]phenoxazin-5-one (NR-NH_2):

A mixture of **NR-N_3** (512 mg, 1.27 mmol) and triphenylphosphine (466 mg, 1.78 mmol) in dry THF (15 mL) was stirred at room temperature for 1 hour, then 10 drops of H_2O were added. After 24 hours the reaction was quenched by evaporation of the solvent at reduced pressure. The purple residue was purified by column chromatography (DCM/MeOH 9:1) to give the pure product in 94% yield (454 mg, 1.20 mmol).

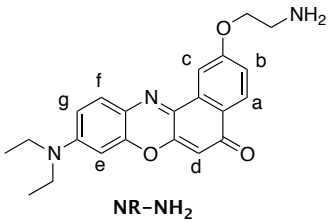

NR–NH_2

^{1}H NMR (400 MHz, $CDCl_3$) δ (ppm): 8.23 (d, *J* = 8.7 Hz, 1H, H_a), 8.08 (d, *J* = 2.6 Hz, 1H, H_c), 7.61 (d, *J* = 9.1 Hz, 1H, H_f), 7.19 (dd, *J* = 8.7, 2.6 Hz, 1H, H_b), 6.67 (dd, *J* = 9.1, 2.7 Hz, 1H, H_g), 6.47 (d, *J* = 2.7 Hz, 1H, H_e), 6.31 (s, 1H, H_d), 4.22 (t, *J* = 5.2 Hz, 2H, OCH_2), 3.48 (q, *J* = 7.1 Hz, 4H, NCH_2), 3.17 (t, *J* = 5.2 Hz, 2H, CH_2NH_2), 1.27 (t, *J* = 7.1 Hz, 6H, CH_3). The compound showed the same physico-chemical properties as those reported in the literature.[28]

5-hydroxycarbonyl-25,26,27,28-tetrapropoxycalix[4]arene (9):

To a solution of 5-formyl-25,26,27,28-tetrapropoxycalix[4]arene **8** (390 mg, 0.63 mmol) in a 1:1 mixture of chloroform and acetonitrile (8 mL), a 30% solution of hydrogen peroxide (117 µL, 1.26 mmol) and sodium phosphate monobasic buffer (2 mL, pH = 4,3) were added. A solution of sodium chlorite (80 mg, 0.88 mmol) in water

(4 mL) was then added dropwise. After stirring the mixture overnight at room temperature, hydrogen peroxide (117 µL, 1.26 mmol) and sodium chlorite (80 mg, 0.88 mmol) were added together with 30 µL of 32% HCl to lower the pH, and the mixture was stirred overnight. The reaction was quenched by evaporating the organic solvents and then adding 1M HCl to the residue. The yellow precipitate was filtered off and then purified by column chromatography (hexane/AcOEt 7:3) to give the pure product in 46% yield (187 mg, 0.29 mmol). ^{1}H NMR (400 MHz, $CDCl_3$) δ (ppm): 7.34 (s, 1H, 2H, ArHCO), 6.85-6.40 (m, 9H, ArH), 4.50 (d, *J* = 13.6, 2H, ArC*H*H_{ax}Ar), 4.47 (d, *J* = 13.6, 2H, ArC*H*H_{ax}Ar), 4.08-3.55 (m, 8H, OCH_2), 4.24 (d, *J* = 13.6, 2H, ArC*H*H_{eq}Ar), 3.18 (d, *J* = 13.6, 2H, ArC*H*H_{ax}Ar), 2.00-1.89 (m, 8H, OCH_2CH_2), 1.08-0.96 (m, 12H, CH_3). The compound showed the same physico-chemical properties as those reported in the literature.[29]

Compound 6:

To a solution of **4** (242 mg, 0.36 mmol) in dry DCM (35 mL), oxalyl chloride (931 µL, 10.68 mmol) was added, together with few drops of dry DMF. The mixture was stirred for 5 hours at room temperature under nitrogen atmosphere and the solvent removed at reduced pressure. The diacyl chloride **5** thus obtained was immediately added to a stirred solution of **NR-NH_2** (148 mg, 0.39 mmol), 2,2-diethoxyethanamine (57 µL, 0.39 mmol) and DIPEA (0.84 mL, 4.81 mmol) in dry DCM (30 mL) and the purple mixture stirred overnight at room temperature under nitrogen. The reaction was quenched with 1M HCl (35 mL) and the organic layer separated. The aqueous phase was extracted with DCM and the combined organic layers were washed twice with deionized water and concentrated under pressure. The residue was purified by column chromatography (DCM/MeOH 9:1) to give the desired compound as a purple solid in 47% yield (196 mg, 0.17 mmol).

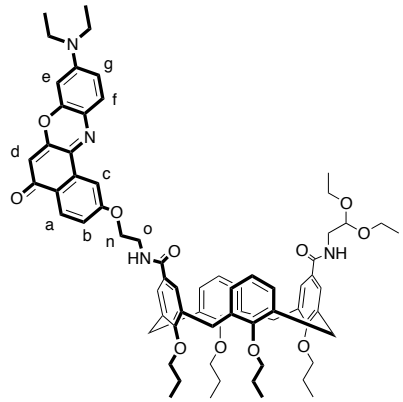

6

^{1}H NMR (400 MHz, $CDCl_3$) δ (ppm): 8.28 (d, *J* = 8.7 Hz, 1H, H_a), 8.14 (d, *J* = 2.6 Hz, 1H, H_c), 7.65 (d, *J* = 9.1 Hz, 1H, H_f), 7.25 (dd, *J* = 8.8, 2.6 Hz, 1H, H_b), 7.12 (s, 2H, ArH), 7.11 (s, 2H, ArH) 6.69 (dd, *J* = 9.1, 2.7 Hz, 1H, H_g), 6.61-6.56 (m, 6H, ArH), 6.49 (d, *J* = 2.7 Hz, 1H, H_e), 6.40 (t, *J* = 6.0 Hz, 1H, N*H*CH_2CH_2O), 6.34 (s, 1H, H_d), 6.12 (t, *J* = 5.8 Hz, 1H, N*H*CH_2CH), 4.62 (t, *J* = 5.5 Hz, 1H, C*H*$(OCH_2CH_3)_2$), 4.48 (d, *J* = 13.4 Hz, 2H, ArC*H*H_{ax}Ar), 4.46 (d, *J* = 13.4 Hz, 2H, ArC*H*H_{ax}Ar), 4.36 (t, *J* = 5.1 Hz, 2H, H_n), 3.94-3.82 (m, 10H, O$CH_2CH_2CH_3$ and H_o), 3.80-3.72 (m, 2H, OC*H*HCH_3), 3.65-3.56 (m, 2H, OCH*H*CH_3), 3.55-3.47 (m, 6H, NCH_2CH_3 and NHCH_2CH), 3.21 (d, *J* = 13.4 Hz, 2H, ArC*H*H_{eq}Ar), 3.20 (d, *J* = 13.4 Hz, 2H, ArC*H*H_{eq}Ar), 2.00-1.85 (m, 8H, $OCH_2CH_2CH_3$), 1.33-1.23 (m, 12H, $CH(OCH_2CH_3)_2$ and NCH_2CH_3), 1.06-0.94 (m, 12H, $OCH_2CH_2CH_3$). ^{13}C NMR (100 MHz, $CDCl_3$) δ (ppm): 190.7; 183.2; 167.9; 161.3; 159.7; 156.1; 150.78; 146.9; 140.1; 135.7;, 134.3;, 134.2; 131.2;, 128.7; 128.4; 128.3; 128.1;, 127.9;, 127.7; 127.2;, 127.0;, 126.9; 124.8; 122.6; 122.4; 118.2; 109.6; 106.9; 105.3; 100.9; 100.78; 96.3; 76.7; 72.4; 67.3; 62.8; 55.2; 45.1; 42.2; 39.4; 32.2; 30.9; 29.7; 29.34; 23.1; 22.7; 15.5; 14.1; 12.6; 10.3; 10.24; 10.15. ESI-MS: m/z calcd for $C_{70}H_{82}N_4O_{11}Na$ [(**6**+Na)$^+$] 1177.6, found 1178.2 (100%); calcd for $C_{70}H_{82}N_4O_{11}K$ [(**6**+K)$^+$] 1193.7, found 1194.3 (40%).

Compound 7:

After dissolving compound **6** (150 mg, 0.13 mmol) in 1,4-dioxane (20 mL), 1M HCl (20 mL) was added and the mixture allowed to stir at room temperature. After 4 hours DCM (30 mL) and H_2O (15 mL) were added to the flask and the two phases separated. The aqueous layer was extracted twice with DCM and the organic phases reunited and

washed twice with water (2x60 mL) to neutral pH, then concentrated under reduced pressure. The residue was purified by column chromatography (DCM/acetone 85:15) to afford the compound as a purple solid (108 mg, 0.10 mmol, 77% yield).

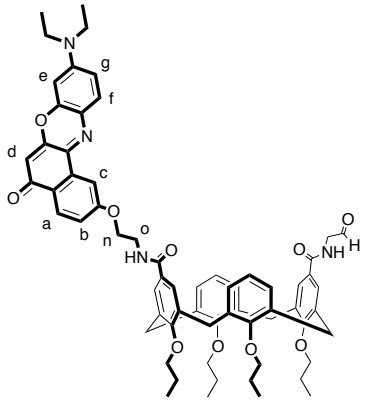

7

^{1}H NMR (400 MHz, $CDCl_3$) δ (ppm): 9.66 (s, 1H, CHO), 8.27 (d, *J* = 8.7 Hz, 1H, H_a), 8.12 (s, 1H, H_c), 7.65 (d, *J* = 9.1 Hz, 1H, H_f), 7.22 (d, *J* = 8.9 Hz, 1H, H_b), 7.01 (s, 2H, ArH), 6.96 (s, 2H, ArH), 6.81-6.67 (m, 8H, H_g and 6xArH and N*H*CH_2CH), 6.49 (s, 1H, H_e), 6.34 (br s, N*H*CH_2CH_2O and H_d), 4.48 (d, *J* = 13.4 Hz, 2H, ArC*H*H_{ax}Ar), 4.46 (d, *J* = 13.4 Hz, 2H, ArC*H*H_{ax}Ar), 4.32 (t, *J* = 5.1 Hz, 2H, H_n), 4.20 (d, *J* = 4.9 Hz, 2H, CH_2CHO), 3.95-3.78 (m, 10H, OC$H_2CH_2CH_3$ and H_o), 3.50 (q, *J* = 6.9 Hz, 4H, NCH_2CH_3), 3.23 (d, *J* = 13.4 Hz, 2H, ArC*H*H_{eq}Ar), 3.20 (d, *J* = 13.4 Hz, 2H, ArC*H*H_{eq}Ar), 2.00-1.85 (m, 8H, $OCH_2CH_2CH_3$), 1.29 (t, *J* = 6.6 Hz, 6H, NCH_2CH_3), 1.07-0.95 (m, 12H, $OCH_2CH_2CH_3$). ^{13}C NMR (100 MHz, $CDCl_3$) δ (ppm): 197.7, 183.2, 168.2, 168.0, 161.3, 159.6, 159.5, 156.5, 152.1, 150.8, 146.9, 139.8, 135.3, 134.8, 134.1, 131.2, 128.6, 127.97, 127.86, 127.6, 127.1, 126.9, 125.9, 124.8, 122.6, 118.2, 109.6, 106.8, 105.3, 96.3, 67.3, 50.5, 45.1, 39.3, 31.9, 30.9, 29.7, 29.4, 23.3, 23.2, 22.7, 14.1, 12.6, 10.4, 10.2. ESI-MS: m/z calcd for $C_{66}H_{72}N_4O_{10}Na$ [(**7**+Na)$^+$] 1103.5, found 1103.5 (100%); calcd for $C_{66}H_{72}N_4O_{10}K$ [(**7**+K)$^+$] 1119.6, found 1120.9 (30%).

Compound 1:

To a solution of **7** (102 mg, 0.094 mmol) in dry toluene (20 mL), N-methylglycine (17 mg, 0.19 mmol) and fullerene C_{60} (68 mg, 0.094 mmol) were added and the mixture

heated to reflux for 3 hours, after which the solvent was evaporated under vacuum. The residue was dissolved in DCM and washed twice with water, then the DCM evaporated at reduced pressure. The product was purified by column chromatography (DCM/MeOH 98:2) and then preparative TLC plates (DCM/MeOH 98:2) to give a purple solid in 23% yield (40 mg, 0.022 mmol).

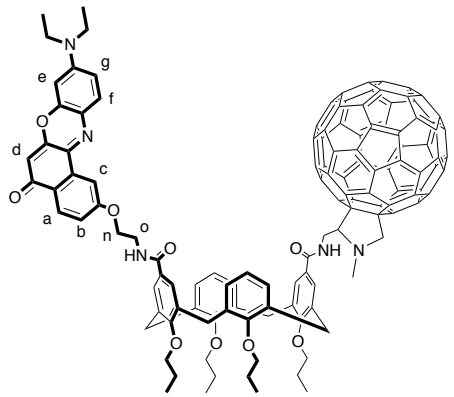

1

Mp: > 300 °C. ^{1}H NMR (400 MHz, $CDCl_3$) δ (ppm): 8.29 (d, *J* = 8.7 Hz, 1H, H_a), 8.15 (d, *J* = 2.6 Hz, 1H, H_c), 7.63 (d, *J* = 9.1 Hz, 1H, H_f), 7.25 (d, *J* = 2.6 Hz, 1H, H_b), 7.17 (s, 1H, ArHCO), 7.05 (s, 1H, ArHCO), 6.98 (s, 2H, ArHCO) 6.82 (br s, 1H, N*H*CH_2CH), 6.73 (br s, 1H, ArH), 6.57-6.49 (m, 5H, 4xArH and H_g), 6.53 (t, *J* = 7.4 Hz, 1H, ArH), 6.48 (d, *J* = 2.7 Hz, 1H, H_e), 6.37 (t, *J* = 5.5 Hz, 1H, N*H*CH_2CH_2), 6.34 (s, 1H, H_d), 4.94 (d, *J* = 9.5 Hz, 1H, CH_3NC*H*H), 4.69 (d, *J* = 12.8, 6.7 Hz, 1H, NHC*H*H), 4.52-4.40 (m, 4H, ArC*H*H_{ax}Ar), 4.39-4.30 (m, 2H, H_n), 4.23 (d, *J* = 9.5 Hz, 1H, CH_3NCH*H*), 4.12 (br s, 1H, NHC*H*H), 4.09 (br s, 1H, $NHCH_2$C*H*), 3.96 (br s, 1H, H_o), 3.90-3.79 (m, 9H, OCH_2 and $H_{o'}$), 3.49 (q, *J* = 7.1 Hz, 4H, NC*H*$_2$$CH_3$), 3.29-3.12 (m, 4H, ArC*H*H_{eq}Ar), 3.02 (s, 3H, NCH_3), 1.97-1.84 (m, 8H, OCH_2C*H*$_2$$CH_3$), 1.28 (t, *J* = 7.0 Hz, 6H, NCH_2C*H*$_3$), 1.04-0.96 (m, 12H, OCH_2CH_2C*H*$_3$). ^{13}C NMR (100 MHz, $CDCl_3$) δ (ppm): 183.2, 167.2, 161.4, 159.5, 156.5, 155.9, 154.3, 153.3, 152.7, 150.8, 147.3, 146.3, 146.2, 146.1, 145.9, 145.6, 145.5, 145.4, 145.26, 145.25, 145.20, 145.1, 144.64, 144.60, 144.4, 144.3, 143.1, 142.6, 142.5, 142.15, 142.10, 142.07, 141.9, 141.7, 141.6, 140.2, 140.1, 139.9, 139.8, 136.0, 135.7, 135.4, 135.3, 135.1, 134.7, 134.1, 131.2, 128.7, 128.5, 128.1, 127.8, 127.4, 127.3, 127.2, 126.9, 126.6, 125.9, 124.8, 122.5, 122.3, 118.3, 109.6, 106.9, 105.3, 96.3, 73.9, 70.0, 69.4,

67.5, 45.1, 39.5, 39.4, 37.5, 31.1, 31.0, 29.7, 23.3, 23.2, 23.1, 12.6, 10.39, 10.36, 10.2, 7.1. ESI-MS: m/z calcd for $C_{128}H_{78}N_5O_9$ [(**1**+H)$^+$] 1828.6, found 1830.2 (40%); calcd for $C_{128}H_{79}N_5O_9$ [(**1**+2H)$^{2+}$] 914.8, found 915.6 (100%).

Compound 2:

To a solution of **9** (0.21 g, 0.33 mmol) in dry DCM (20 mL) oxalyl chloride (0.87 mL, 9.90 mmol) was added together with few drops of dry DMF. The mixture was stirred for 4 hours at room temperature under nitrogen atmosphere and the solvent removed at reduced pressure. Compound **10** thus obtained was immediately added to a stirred solution of **NR-NH$_2$** (0.13 g, 0.35 mmol) and DIPEA (0.22 mL, 1.28 mmol) in dry DCM (20 mL) and the purple mixture stirred overnight at room temperature under nitrogen. The reaction was quenched with water (30 mL) and the organic layer separated. The aqueous phase was extracted with DCM (2x20 mL) and the organic layers were reunited, washed twice with water and concentrated under pressure. The residue was purified by column chromatography (hexane/AcOEt 1:1) and then preparative TLC plates (DCM/AcOEt 98:2) to give the desired compound as a purple solid in 6% yield (17.6 mg, 0.018 mmol).

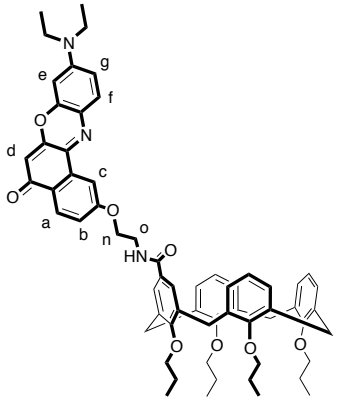

2

Mp: 102-103 °C.^{1}H NMR (400 MHz, $CDCl_3$) δ (ppm): 8.31 (d, *J* = 8.7 Hz, 1H, H_a), 8.15 (d, *J* = 2.6 Hz, 1H H_c), 7.66 (d, *J* = 9.0 Hz, 1H, H_f), 7.24 (dd, *J* = 8.8, 2.5 Hz, 1H, H_b), 6.85-6.67 (m, 10H, 9xArH and H_g), 6.50 (d, *J* = 2.7 Hz, 1H, H_e), 6.35 (s, 1H, H_d), 6.34 (s, 2H, ArH), 6.03 (t, *J* = 6.0 Hz, 1H, NH), 4.46 (d, *J* = 13.6 Hz, 2H, ArC*H*H_{ax}Ar), 4.43 (d, *J* = 13.6 Hz, 2H,

ArC*H*H_{ax}Ar), 4.33 (t, *J* = 5.0 Hz, 2H, OC*H*$_2$$CH_2$NH), 3.92-3.74 (m, 10H, OC*H*$_2$$CH_2$$CH_3$ and C*H*$_2$NH), 3.50 (q, *J* = 7.1 Hz, 4H, NC*H*$_2$$CH_3$), 3.18 (d, *J* = 13.6 Hz, 2H, ArC*H*H_{eq}Ar), 3.15 (d, *J* = 13.6 Hz, 2H, ArC*H*H_{eq}Ar), 2.06-1.87 (m, 8H, OCH_2C*H*$_2$$CH_3$), 1.29 (t, *J* = 7.0 Hz, 6H, NCH_2C*H*$_3$), 0.98-0.89 (m, 6H, OCH_2CH_2C*H*$_3$), 0.96 (t, *J* = 7.2 Hz, 6H, OCH_2CH_2C*H*$_3$). ^{13}C NMR (100 MHz, Acetone-d_6) δ (ppm): 182.6, 167.7, 162.5, 157.5, 160.3, 157.3, 152.9, 152.0, 147.7, 140.3, 136.2, 136.1, 135.9, 135.3, 135.0, 131.9, 129.3, 125.2, 129.3, 129.0, 128.3, 122.9, 122.8, 118.4, 110.7, 108.1, 105.5, 97.1, 77.4, 77.6, 68.0, 45.7, 40.1, 31.6, 24.1, 12.9, 10.7. ESI-MS: m/z calcd for $C_{66}H_{73}N_4O_{10}$ [(**7**+H)$^+$] 996.5, found 997.0 (55%); calcd for $C_{66}H_{72}N_4O_{10}Na$ [(**7**+Na)$^+$] 1018.5, found 1019.1 (100%); calcd for $C_{66}H_{72}N_4O_{10}K$ [(**7**+K)$^+$] 1034.6, found 1035.9 (30%).

5-(2,2-diethoxyethyl)carbamoyl-25,26,27,28-tetrapropoxycalix[4]arene (11):

To a solution of **9** (187 mg, 0.29 mmol) in dry DCM (30 mL), oxalyl chloride (385 µL, 4.41 mmol) was added, together with few drops of dry DMF. The mixture was stirred for 3 hours at room temperature under nitrogen atmosphere and the solvent removed at reduced pressure. The acyl chloride thus obtained was redissolved in dry DCM (25 mL) and 2,2-diethoxyethanamine (64 µL, 0.44 mmol) and DIPEA (0.31 mL, 1.76 mmol) were added. The mixture was allowed to stir overnight under nitrogen. The reaction was quenched with 1M HCl (30 mL) and the organic layer separated. The aqueous phase was extracted with DCM and the organic layers were reunited, washed twice with water and concentrated under pressure. The residue was purified by column chromatography (hexane/AcOEt 8:2) to give the desired compound in 72% yield (158 mg, 0.21 mmol). ^{1}H NMR (400 MHz, $CDCl_3$) δ (ppm): 6.89 (s, 2H, ArHCO), 6.79 (d, *J* = 7.4 Hz, 4H, ArH), 6.70 (t, *J* = 7.2 Hz, 2H, ArH), 6.44 (s, 3H, ArH), 5.86 (t, *J* = 5.8 Hz, 1H, NH), 4.57 (t, *J* = 5.4 Hz, 1H, C*H*$(OCH_2CH_3)_2$), 4.50 (d, *J* = 13.5 Hz, 2H, ArC*H*H_{ax}Ar) 4.48 (d, *J* = 13.5 Hz, 2H, ArC*H*H_{ax}Ar), 4.01-3.79 (m, 8H, OCH_2), 3.79-3.69 (m, 2H, OC*H*HCH_3), 3.64-3.55 (m, 2H, OC*H*HCH_3), 3.51 (t, *J* = 5.6 Hz, 2H, NHC*H*$_2$), 3.21 (d, J = 13.5 Hz, 2H, ArC*H*H_{eq}Ar), 318 (d, *J* = 13.5 Hz, 2H, ArC*H*H_{eq}Ar), 2.01-1.86 (m, 8H, OCH_2C*H*$_2$), 1.28 (t, *J* = 7.1 Hz, 6H, OCH_2C*H*$_3$), 1.06 (t, *J* = 7.4, Hz, 6H, OCH_2CH_2C*H*$_3$), 1.00 (t, *J* = 7.5 Hz, 6H, OCH_2CH_2C*H*$_3$). ^{13}C NMR (100 MHz, $CDCl_3$) δ (ppm): 167.6, 159.2, 156.9, 156.2, 135.8,

135.1, 135.0, 134.6, 128.6, 128.4, 128.0, 127.7, 126.7, 122.1, 121.8, 100.9, 62.9, 42.3, 31.05, 31.02, 23.3, 23.1, 15.4, 10.5, 10.4, 10.1. ESI-MS: m/z calcd for $C_{47}H_{61}NO_7Na$ [(**11**+Na)$^+$] 774.4, found 774.5 (100%); calcd for $C_{47}H_{61}NO_7K$ [(**11**+K)$^+$] 790.5, found 790.5 (20%).

5-(2-oxoethyl)carbamoyl-25,26,27,28-tetrapropoxycalix[4]arene (12):

After dissolving compound **11** (15 mg, 0.21 mmol) in 1,4-dioxane (30 mL), 1M HCl (20 mL) was added and the mixture allowed to stir at room temperature for 21 hours. After reaction completion the solvent was partly evaporated under reduced pressure, then DCM (30 mL) and H_2O (15 mL) were added to the flask and the two phases separated. The aqueous layer was extracted with DCM and the organic phases reunited and washed twice with water (2x60 mL) to neutral pH, then concentrated under reduced pressure. The residue was purified by column chromatography (Hexane/AcOEt 7:3) to afford the compound as a whitish solid (115 mg, 0.17 mmol, 81% yield). ^{1}H NMR (400 MHz, $CDCl_3$) δ (ppm): 9.74 (s, 1H, CHO), 6.98 (s, 2H, ArHCO), 6.75-6.63 (m, 6H, ArH), 6.53 (d, *J* = 7.5 Hz, 2H, ArH), 6.41 (t, *J* = 7.5 Hz, 1H, ArH), 6.36 (br s, 1H, NH), 4.49 (d, *J* = 13.5, 2H, ArC*H*H$_{ax}$Ar), 4.46 (d, *J* = 13.5, 2H, ArC*H*H$_{ax}$Ar), 4.31 (d, *J* = 4.7 Hz, 2H, NHC*H*$_2$), 3.93-3.78 (m, 8H, OCH$_2$), 3.21 (d, *J* = 13.5, 2H, ArC*H*H$_{eq}$Ar), 4.19 (d, *J* = 13.5, 2H, ArC*H*H$_{eq}$Ar), 1.98-1.87 (m, 8H, OCH$_2$C*H*$_2$), 1.07-0.95 (m, 12H, CH$_3$). ^{13}C NMR (100 MHz, $CDCl_3$) δ (ppm): 196.5, 167.7, 159.8, 156.7, 156.4, 135.5, 134.9, 134.7, 128.6, 128.3, 127.9, 127.0, 122.2, 122.1, 121.7, 50.7, 31.04, 31.00, 23.33, 23.31, 23.2, 10.42, 10.40, 10.2. ESI-MS: m/z calcd for $C_{43}H_{51}NO_6Na$ [(**12**+Na)$^+$] 700.4, found 701.0 (100%); calcd for $C_{43}H_{51}NO_6K$ [(**12**+K)$^+$] 716.5, found 717.3 (40%).

Compound 3:

To a solution of **12** (120 mg, 0.18 mmol) in dry toluene (20 mL), N-methylglycine (32 mg, 0.25 mmol) and fullerene C_{60} (128 mg, 0.18 mmol) were added and the mixture heated to reflux for 3 hours, after which the solvent was evaporated under vacuum. The residue was dissolved in DCM and washed twice with water, then the DCM was evaporated at reduced pressure. The solid was purified by preparative TLC plates

(DCM) to give a brownish solid in 13% yield (32 mg, 0.022 mmol). Mp: > 300 °C. ^{1}H NMR (400 MHz, $CDCl_3$) δ (ppm): 7.02 (s, 2H, ArHCO), 6.81 (br s, 1H, NH), 6.70-6.46 (m, 9H, ArH), 4.98 (d, *J* = 9.5 Hz, 1H, CH_3NCHH), 4.81 (dd, *J* = 14.6, 6.9 Hz, 1H, NHC*H*H), 4.51-4.41 (m, 4H, ArCHH_{ax}Ar), 4.26 (d, *J* = 9.5 Hz, 1H, CH_3NCHH), 4.21 (br s, 1H, $NHCH_2CH$), 4.13 (d, *J* = 14.8 Hz, 1H, NHCH*H*), 3.91-3.80 (m, 8H, OCH_2), 3.22-3.14 (m, 4H, ArCHH_{eq}Ar), 3.01 (s, 3H, NCH_3), 1.97-1.86 (m, 8H, OCH_2CH_2), 1.06-0.94 (m, 12H, CH_3). ESI-MS: m/z calcd for $C_{105}H_{57}N_2O_5$ [(**3**+H)$^+$] 1425.4, found 1425.8.

2.6 References

(1) Turro, N. J. Energy Transfer Processes. *Pure appl. chem.* **1977**, *49*, 405–429.

(2) Valeur, B. *Molecular Fluorescence: Principles and Applications.*; Wiley-VCH, 2001.

(3) Forster, T. Energiewanderung Und Fluoreszenz. *Naturwissenschaften* **1946**, *33* (6), 166–175.

(4) May, V.; Kühn, O.; Kuhn, O.; Schulten, K.; Inc, J. W. & S. *Charge and Energy Transfer Dynamics in Molecular Systems*; Wiley-VCH, 2004.

(5) Marcus, R. A.; Sutin, N. Electron Transfers in Chemistry and Biology. *Biochim. Biophys. Acta - Rev. Bioenerg.* **1985**, *811* (3), 265–322.

(6) Marcus, R. A. Electron Transfer Reactions. *Rev. Mod. Phys.* **1993**, *65* (3), 1–37.

(7) Barbara, P. F.; Meyer, T. J.; Ratner, M. A. Contemporary Issues in Electron Transfer Research. *J. Phys. Chem.* **1996**, *100* (31), 13148–13168.

(8) Gilbert, M.; Albinsson, B. Photoinduced Charge and Energy Transfer in Molecular Wires. *Chem. Soc. Rev.* **2015**, *44* (4), 845–862.

(9) Tosi, I. Model Systems for Artificial Photosynthesis: Calix[4]Arenes Functionalized with Chromophoric Units for Energy and Charge Transfer, Doctorate in Chemical Sciences - Cycle XXVII. Università di Parma, 2014.

(10) Anandan, S.; Yoon, M. Photoinduced Electron Transfer Studies of Nile Red in the Presence of TiO2colloidal Nanoparticles. *Spectrochim. Acta - Part A Mol. Biomol. Spectrosc.* **2004**, *60* (4), 885–888.

(11) Umeyama, T.; Imahori, H. Carbon Nanotube-Modified Electrodes for Solar Energy Conversion. *Energy Environ. Sci.* **2008**, *1* (1), 120–133.

(12) Imahori, H.; Tkachenko, N. V.; Vehmanen, V.; Tamaki, K.; Lemmetyinen, H.; Sakata, Y.;

Fukuzumi, S. An Extremely Small Reorganization Energy of Electron Transfer in Porphyrin−Fullerene Dyad. *J. Phys. Chem. A* **2001**, *105* (10), 1750–1756.

(13) Fukuzumi, S.; Imahori, H. Biomimetic Electron-Transfer Chemistry of Porphyrins and Metalloporphyrins. In *Electron Transfer in Chemistry*; Wiley-Blackwell, 2008; pp 927–975.

(14) D'Souza, F.; Kadish, K. M. FRONT MATTER. In *Handbook of Carbon Nano Materials*; pp i–xxiii.

(15) Guldi, D. M. Fullerene-Porphyrin Architectures; Photosynthetic Antenna and Reaction Center Models. *Chem. Soc. Rev.* **2002**, *31* (1), 22–36.

(16) Liu, Y. X.; Summers, M. A.; Scully, S. R.; McGehee, M. D. Resonance Energy Transfer from Organic Chromophores to Fullerene Molecules. *J. Appl. Phys.* **2006**, *99* (9), 1–4.

(17) Van Hal, P. A.; Meskers, S. C. J.; Janssen, R. A. J. Photoinduced Energy and Electron Transfer in Oligo(p-Phenylene Vinylene)-Fullerene Dyads. *Appl. Phys. A Mater. Sci. Process.* **2004**, *79* (1), 41–46.

(18) Martini, I. B.; Ma, B.; Da Ros, T.; Helgeson, R.; Wudl, F.; Schwartz, B. J. Ultrafast Competition between Energy and Charge Transfer in a Functionalized Electron Donor/Fullerene Derivative. *Chem. Phys. Lett.* **2000**, *327* (5–6), 253–262.

(19) Arimura, T.; Ide, S.; Suga, Y.; Nishioka, T.; Murata, S.; Tachiya, M.; Nagamura, T.; Inoue, H. Electron Transfer Through-Space or Through-Bonds? A Novel System That Permits a Direct Evaluation. *J. Am. Chem. Soc.* **2001**, *123*, 10744–10745.

(20) Arduini, A.; Fabbi, M.; Mantovani, M.; Mirone, L.; Pochini, A.; Secchi, A.; Ungaro, R. Calix[4]Arenss Blocked in a Rigid Cone Conformation by Selective Functionalization at the Lower Rim. *J. Org. Chem.* **1995**, *60* (5), 1454–1457.

(21) Lazzarotto, M.; Sansone, F.; Baldini, L.; Casnati, A.; Cozzini, P.; Ungaro, R. Synthesis and Properties of Upper Rim C-Linked Peptidocalix[4]Arenes. *European J. Org. Chem.* **2001**, No. 3, 595–602.

(22) Tosi, I.; Segado Centellas, M.; Campioli, E.; Iagatti, A.; Lapini, A.; Sissa, C.; Baldini, L.; Cappelli, C.; Di Donato, M.; Sansone, F.; et al. Excitation Dynamics in Hetero-Bichromophoric Calixarene Systems. *ChemPhysChem* **2016**, *17* (11), 1686–1706.

(23) Casnati, A.; Sartori, A.; Pirondini, L.; Bonetti, F.; Pelizzi, N.; Sansone, F.; Ugozzoli, F.; Ungaro, R. Calix[4]Arene Anion Receptors Bearing 2,2,2-Trifluoroethanol Groups at the Upper Rim. *Supramol. Chem.* **2006**, *18* (3), 199–218.

(24) Nwaukwa, S. O.; Keehn, P. M. Ring Chlorination of Benzenoid Compounds Using Calcium Hypochlorite [Ca(OCl)2]. *Synth. Commun.* **1989**, *19* (5–6), 799–804.

(25) Dalcanale, E.; Montanari, F. Selective Oxidation of Aldehydes to Carboxylic Acids with Sodium Chlorite-Hydrogen Peroxide. *J. Org. Chem.* **1986**, *51* (4), 567–569.

(26) Lee, H.; Choi, M. G.; Yu, H. Y.; Ahn, S.; Chang, S. K. Selective Mercuration of 2-Hydroxy Nile Red and Its Application towards Chemodosimetric Hg2+-Selective Signaling. *Bull. Korean Chem. Soc.* **2010**, *31* (12), 3539–3542.

(27) Ghini, G.; Lascialfari, L.; Vinattieri, C.; Cicchi, S.; Brandi, A.; Berti, D.; Betti, F.; Baglioni, P.; Mannini, M. Towards a General Organogelator: Combining a Versatile Scaffold and an Efficient Linking Process. *Soft Matter* **2009**, *5* (9), 1863.

(28) Sherman, D. B.; Pitner, J. B.; Ambroise, A.; Thomas, K. J. Synthesis of Thiol-Reactive, Long-Wavelength Fluorescent Phenoxazine Derivatives for Biosensor Applications. *Bioconjug. Chem.* **2006**, *17* (2), 387–392.

(29) Herbert, S. A.; Arnott, G. E. Synthesis of Inherently Chiral Calix[4]Arenes: Stereocontrol through Ligand Choice. *Org. Lett.* **2010**, *12* (20), 4600–4603.

CHAPTER 3

QUANTUM COHERENCE ENERGY TRANSFER IN CALIX[4]ARENE-BASED DYADS

3.1 Introduction

3.1.1 Quantum coherence energy transfer (QCET)

Early in the 30's, Erwin Schrödinger debated that classical physics alone fails in interpreting life and suggested, instead, that quantum mechanical laws are indeed necessary.[1] For years, though, quantum principles, like quantum tunneling, entanglement and coherence, have been neglected in the analysis of biological systems, and the general thought was that the biochemical mechanisms at the base of living organisms had nothing to do with quantum mechanics. Only recently, however, thanks to technological advances, direct observations of quantum effects in biological systems have been reported.[2] For example, recent works claim that quantum coherence is somehow involved in bird navigation,[3,4] the so-called "avian compass", and in the sense of smell.[5,6] Thanks to the development of two-dimensional (2D) electronic spectroscopy,[7] in 2007, Fleming and coworkers showed clear evidence of wavelike energy transfer through quantum coherence in the Fenna-Matthews-Olson (FMO) protein of the green sulphur bacterium Chlorobium Tepidium at 77 K.[8] Later, the same electronic coherence was shown to be operating in bacterial complexes also at ambient temperature.[9,10]

Besides the direct observation of these effects in nature, it is important to understand how quantum mechanics influences biological systems by improving their functions and, more importantly, if these mechanisms can be exploited in the development of artificial devices mimicking natural processes.[2,11] In this sense, the best example is represented by photosynthesis and light harvesting systems. It has been reported that, in the photosynthetic unit, antenna proteins are not constrained by classical probability laws, but are able to harvest and transfer energy according to quantum mechanical probability, thus overcoming the classical view of how far and how fast excitation energy can migrate.[12] In fact, experimentally detected coherences are long-lived in time, sufficient to efficiently funneling the energy flow,[9] and long-range in space, extended over several pigments across the whole light harvesting complex. The fact that these coherences persist on time scales comparable to those of typical

energy transfer may suggest that coherent dynamics are actually boosting the functions of the photosynthetic complex. So, for such systems, Förster theory alone is no longer sufficient to describe the energy transfer mechanism, but quantum coherences need to be taken into account. Förster theory holds true when the electronic coupling between the chromophores is weak, and in this case, the energy hops from one molecule to the other in an incoherent way, following what was defined as a random walk (**Figure 3.1**, top). As the electronic coupling increases, the strong coupling regime is reached and the energy transfer acquires quantum-coherent character. In this case, the electronic states of donor and acceptor mix strongly to produce new states, called excitons, in which the excitation energy is delocalized over several molecules and moves coherently, like a wave (**Figure 3.1**, bottom). An intermediate coupling regime also exists, and in this case the energy can be transferred in a coherent or incoherent way among partially delocalized electronic states.

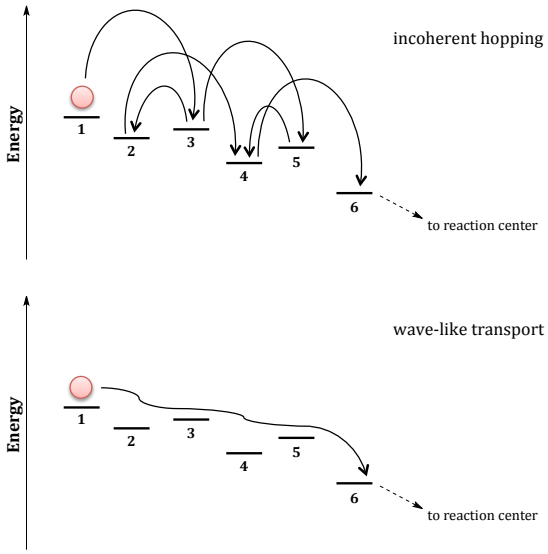

Figure 3.1. Schematic representation of classical (at the top) and quantum coherent (on the bottom) energy transfer.

In 2013 Engel and coworkers[13] developed small synthetic molecules, in which two different chromophores are linked to a rigid spacer that constrains their relative orientation and demonstrated that, in these systems, persistent electronic coherences can be observed (**Figure 3.2**).

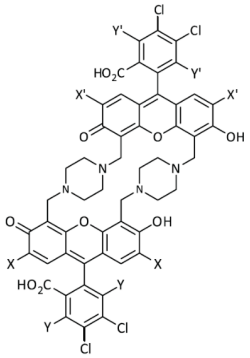

Figure 3.2. Heterodimers by Engel et al.[13] able to reproduce the long-lived quantum coherent phenomenon.

Later, the emergence of quantum coherences in simple molecular systems has been investigated in a family of perylene bisimide dimers, with well-defined distance and orientation between the chromophores,[14] and also in supramolecular arrays of porphyrins.[15]

Thus, in order to get a deeper understanding of the dynamics of coherent phenomena and allow for the design of optimized artificial light-harvesters, simplified and manipulable model systems represent valuable tools. In these molecules the relationship between structure and electronic properties is indeed more easily identifiable, and the role of the solvent and of the flexibility of the scaffold to which the chromophores are linked can be understood. In this context, our research group recently exploited the versatility of the *cone* calix[4]arene to investigate the occurrence of coherent phenomena also in flexible systems (**Figure 3.3**).[16] The two selected chromophores, that were anchored to the upper rim of the calixarene, belong to the family of 4,4-difluoro-4-bora-3a,4a-diaza-s-indacene (BODIPY) dyes, a good

example of biomimetic light-harvesters thanks to their structural analogy to the half-porphyrin moiety. They satisfy all the requirements to successfully study quantum coherence energy transfer, that is they possess absorption maxima very close in energy, a necessary condition to induce strong coupling effects, and narrow absorption and fluorescence bands, which allow the discrimination of their spectral features in the bichromophoric systems. In addition, their absorption bands fall in the red region of the visible spectrum, because, in order to be able to follow the dynamic of the transfer by 2D-electronic spectroscopy, they must absorb over 550 nm for experimental set up reasons.

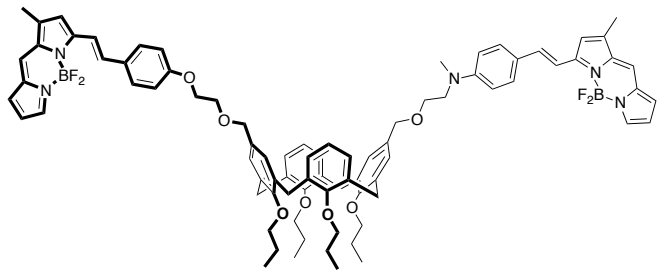

Figure 3.3. Calix[4]arene-BODIPY system for QCET previously synthesized in the research group.[16]

The spectroscopic characterization performed up to now did not evidence any significant coherent phenomena, probably because of the flexibility of the spacers linking the dyes to the scaffold. The absence of attractive interactions between the dyes, in fact, allowed the system to adopt an open flattened cone conformation that, together with the flexibility of the spacers, placed the dyes too far from each other, thus preventing the establishment of strong interchromophore interactions.

3.1.2 BODIPY dyes

BODIPYs, abbreviation for boron-dipyrromethenes, are very versatile fluorophores whose popularity greatly increased in the last twenty years. They have been widely used for biological labeling as well as tunable laser dyes, to the point that biologists and biochemists started to recognize them as photostable substitutes for fluorescein

and as a consequence the number of patents and papers regarding the synthesis and application of BODIPYs increased dramatically.[17,18]

BODIPYs tend to be strongly UV-visible absorbing molecules with sharp fluorescence profile and quantum yields approaching unity, depending on the attached substituents. They are characterized by thermal and photochemical stability, chemical robustness, negligible triplet-state formation, good solubility and relative insensitivity to polarity and pH of the environment.[19] Another interesting feature of this class of chromophores is that small modifications on their structure allow for an efficient tuning of their spectroscopic characteristics.

The BODIPY's structure is commonly described as a borodiazaindacene by analogy with the tricyclic ring *s*-indacene, and the numbering of the substituents follows the same rules as the all-carbon compound (**Figure 3.4**). By analogy with porphyrinic systems, on the other hand, the 8-position is often referred to as the *meso* position.

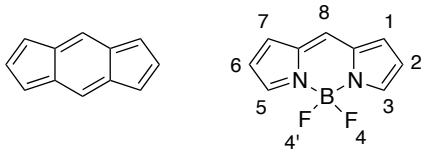

Figure 3.4. Numbering scheme for the BODIPY core (on the right) derived from *s*-indacene (on the left).

From a synthetic point of view (**Scheme 3.1**), the unstable dipyrromethene core (**II**) is formed through the well-known pyrrole condensation reaction used for the synthesis of certain types of porphyrins, in which a highly electrophilic carbonyl compound is used to form the methene bridge between two pyrrole units. **II** is then immediately reacted with boron trifluoride diethyletherate in the presence of a base, usually a tertiary amine, to complete the synthesis of the dye. In this way, several *symmetric* BODIPYs, differing for the substituent on the *meso* position and on the pyrrole rings, can be synthesized from readily available pyrroles.

The carbonyl compounds used in the dipyrromethene core construction can be of different nature. Acid-catalyzed condensation of a pyrrole derivative with an aldehyde

leads to the formation of a dipyrromethane compound (**I**), which is then transformed in the dipyrromethene using oxidizing agents like DDQ (2,3-dichloro-5,6-dicyano-1,4-benzoquinone) and p-chloranil. The required oxidation step, however, leads to the formation of byproducts that need to be removed after complexation with the boron. For preparing *meso*-substitued BODIPYs, the most straightforward procedure involves the use of acylium equivalents, such as acyl chlorides, acid anhydrides and orthoesters. Recently, a cyclic anhydride has been employed, leading to the formation of a BODIPY bearing a free carboxylic acid that can be exploited for further functionalization. A third approach, developed by Burgess and Wu,[20] is based on the preparation of dipyrromethene (**II**) by condensation of two units of the same pyrrole functionalized with a formyl group, in the presence of an excess of phosphoryl chloride.

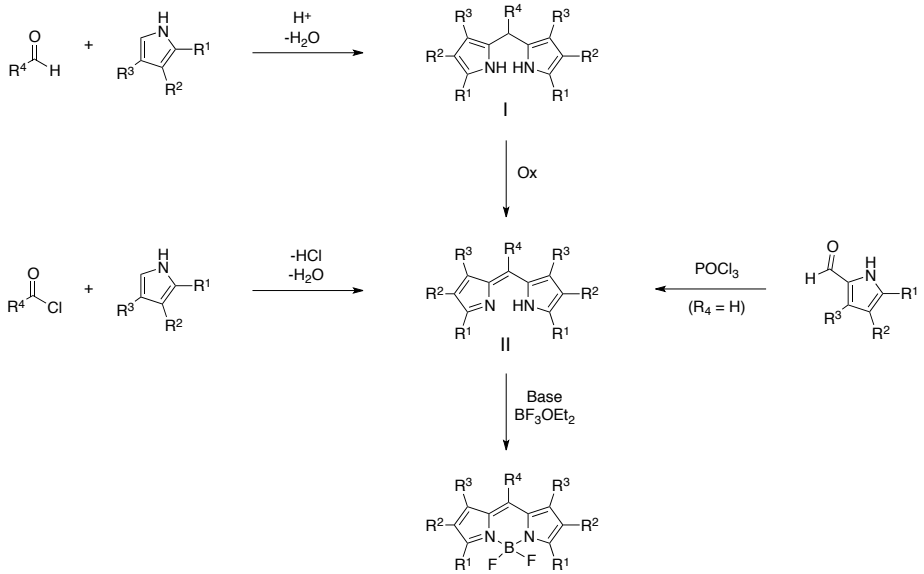

Scheme 3.1. Reaction scheme for the synthesis of symmetric BODIPYs.

Asymmetric BODIPYs can be obtained by condensation of a carbonyl-containing pyrrole with another pyrrole not substituted at the 2-position (**Scheme 3.2**).

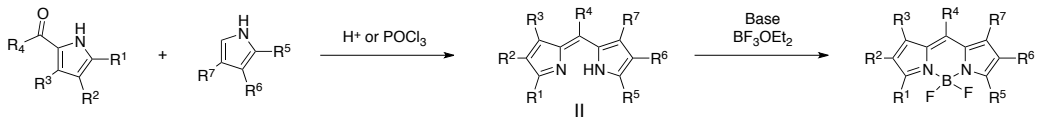

Scheme 3.2. Reaction scheme for the synthesis of asymmetric BODIPYs.

After the synthesis of the BODIPY core, several modifications can be introduced in a second time on its periphery. The BODIPY core, in fact, is robust enough to withstand a wide variety of chemical transformations. Examples of core modification by electrophilic substitution, nucleophilic substitution of leaving groups, metal-catalyzed cross-coupling and Knoevenagel condensation are reported.[17,19] Functionalization at the meso position has no relevant consequences on the spectroscopic properties of the core. On the contrary, modifications on the pyrrolic ring or on the boron center can alter absorption and emission spectra considerably. Expansion of the conjugated π-system on the BODIPY framework can be obtained by linking conjugated units to one or both pyrrole fragments. One efficient way to do so is to exploit the slight acidity of the methyl groups of 3,5-disubstituted BODIPYs. These methyl groups, in fact, can be deprotonated in mild conditions and reacted with aromatic aldehydes to give compounds with increased conjugation, which results in bathochromic shifts of both fluorescence and absorption maxima.

3.2 Aim of the chapter

This chapter describes the synthesis and the steady-state spectroscopic characterization of two bichromophoric calix[4]arene-based systems designed for the study of quantum coherent energy transfer. Starting from the calix[4]arene-BODIPY dyad previously developed in the research group (**Figure 3.3**, section 3.1.1),[16] the two systems reported here are designed to improve the performances of the bichromophore, by keeping the dyes closer to each other, thanks to the exploitation of a rigid alkynyl group as a spacer between the scaffold and the chromophores (**1** and **2**, **Figure 3.5**). The two chosen chromophores are very similar to the BODIPYs of the previous dyad, since they fulfill the energetic requirements to study coherent energy

transfer, but are linked to the calixarene from an additional phenyl ring present on the *meso* position of the BODIPY. As described in section 3.1.2, in fact, modifications on the *meso* position of the BODIPY core do not cause significant alteration in the spectroscopic characteristics of the dye.

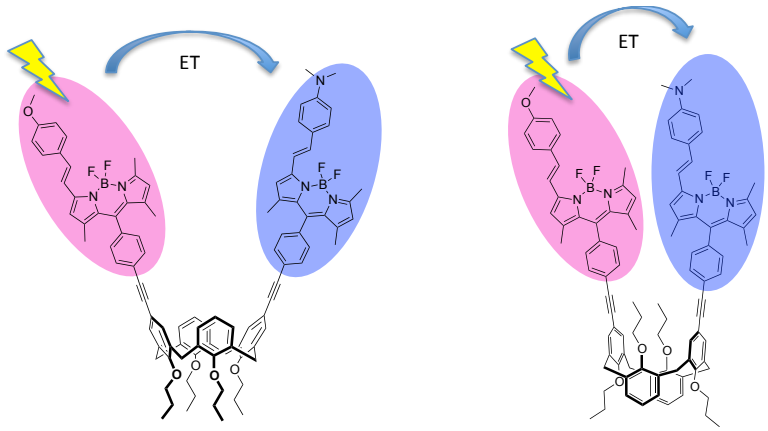

1 **2**

Figure 3.5. Bichromophoric calix[4]arene-based systems for the study of QCET.

Dyads **1** and **2** differ for the geometry of the calixarenic scaffold. The first compound is in the *cone* structure and is characterized by the residual flexibility of the calixarene (see section 1.3.1), which will presumably result in an *open flattened cone* conformation of the scaffold, but can also allow the dyes to get closer to each other in case of attractive interactions. On the contrary, the *1,3-alternate* conformation of the scaffold in the second structure keeps the opposite aromatic rings almost parallel to each other, and therefore place the two dyes at a closer distance.[21] Preliminary molecular modeling calculations performed on the two structures (**Figure 3.6**) clearly highlight the different distance between the dyes in the two conformations, with the *1,3-alternate* being the one placing the BODIPYs at closer distance.

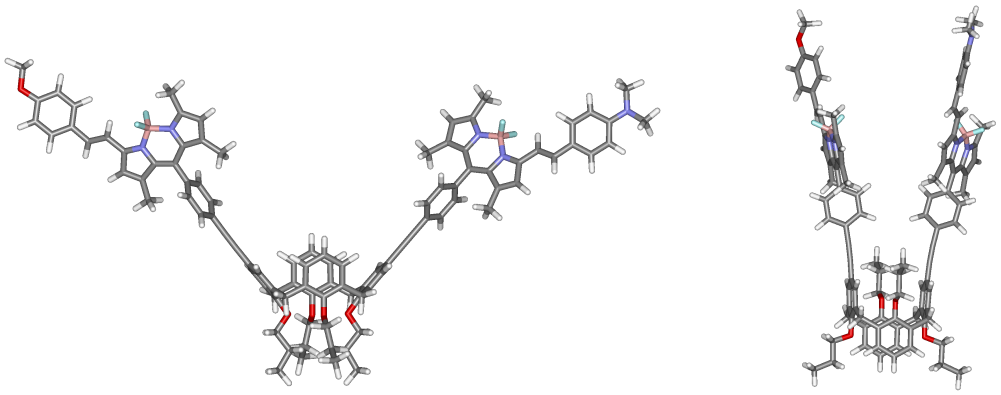

Figure 3.6. Energy-minimized structures (Spartan '16, MMFF) of calixarenes **1** and **2**.

3.3 Results and discussion

3.3.1 Synthesis

The two BODIPYs that were chosen for the study of QCET belong to the family of 3-styryl BODIPYs, typically obtained by the Knoevenagel condensation between 3-methylpyrroles and benzaldehydes (**Scheme 3.3**). This reaction is usually carried out in basic conditions or in buffer and requires the removal of water using a Dean-Stark apparatus or molecular sieves.

One interesting feature of 3-styryl BODIPYs is that their spectroscopic properties, in terms of absorption and emission wavelengths, can be easily tuned by changing the aldehyde used in the Knoevenagel condensation. In particular, a red-shift of the dye absorption and fluorescence occurs when an electron-donating substituent is present on the *para* position of the phenyl ring, as a consequence of the extendend π-conjugation.[22,23] To further functionalize the structure, a particular acylium equivalent (e.g. acyl chloride) can be used in the construction of the dipyrromethene core. In particular, the use of a functionalized benzoyl chloride allows the introduction of other interesting moieties on the phenyl ring that can be exploited to anchor the dyes to a different structure.

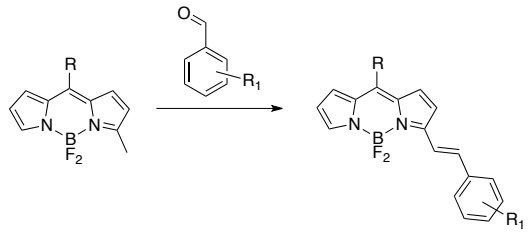

Scheme 3.3. Generic reaction for the synthesis of 3-styryl BODIPYs.

In our case the introduction of an iodide on the BODIPYs was required by the Sonogashira coupling that was used to bind the chromophores to the opportunely functionalized calixarenes (**Figure 3.7**).

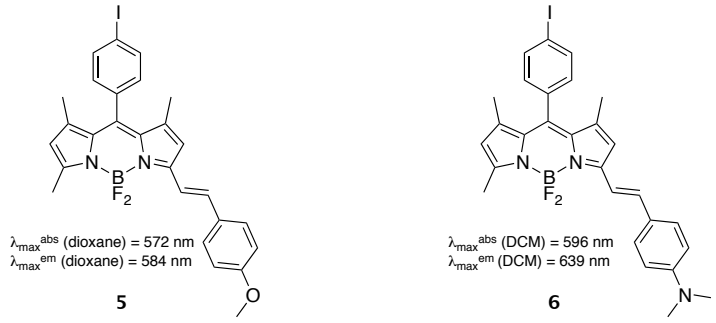

Figure 3.7. Structure and spectral properties of BODIPYs **5** and **6**.

Their synthesis (**Scheme 3.4**) was adapted from literature protocols.[24,25] The first step, in which 1 equivalent of the acyl chloride of iodobenzoic acid **3** is reacted with 2 equivalents of 2,4-dimethylpyrrole, was conducted in dichloromethane at room temperature. Then, after 22 hours, triethylamine and boron trifluoride diethyletherate were added. The yield of **4**, however, was unexpectedly very low. Burgess et al.[24] characterized some of the byproducts that are formed in this reaction (2-ketopyrrole **4a** and the corresponding boron complex **4b**, **Figure 3.8**) and suggested that the amount of these compounds becomes more prominent as the proportion of acyl chloride is increased. So the reaction conditions were changed until a 40% yield was reached using a molar ratio of 1:2.5 acyl chloride to pyrrole and by carrying out the reaction in a Schlenk tube in the dark, under strict inert atmosphere.

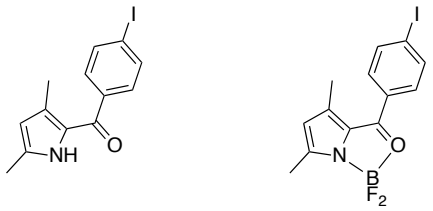

4a **4b**

Figure 3.8. Possible byproducts formed during the dipyrromethene core construction.[24]

Once the BODIPY core was formed, compound **4** was reacted, in turn, with p-anisaldehyde and 4-(dimethylamino)benzaldehyde to give chromophores **5** and **6** respectively, through the Knoevenagel condensation. As a first attempt, these reactions were conducted with the assistance of microwaves. The protocol is reported in the literature[22,26] and previously in the research group[16] similar BODIPYs were synthesized in higher yields using the microwave irradiation as compared to the traditional procedure at reflux. The reactions were carried out in toluene and in the presence of piperidine, acetic acid and 4 Å molecular sieves, with consecutive 10 minutes microwave irradiation steps (200 W) keeping the temperature at 130 °C. After each step the reaction mixture was cooled down and monitored by TLC. In the case of BODIPY **6**, the reaction with 4-(dimethylamino)benzaldehyde was stopped after seven steps, when no change from the previous step was observed. A certain amount of reagent **4** was still visible on the TLC, together with a green byproduct, but pushing the reaction by further increasing the temperature and the number of MW cycles led to the formation of other spots on the TLC and thus to partial degradation of the product. After purification, compound **6** was isolated in 18% yield. The p-anisaldehyde BODIPY **5** was found to be more fragile, with respect to **6**. In fact, to prevent the degradation of the dye, just one 4 minutes irradiation step was performed, keeping the power at 200 W and the temperature at 130 °C, to give the desired product in 15% yield after column chromatography.

Even if the reaction yields were comparable with those found in the literature,[25,27] the traditional reflux procedure was also tried for both reactions. p-Toluensulfonic acid was used instead of acetic acid and the mixture was refluxed in toluene for 3 hours,

again using 4 Å molecular sieves to trap the water since the small scale of the reaction (25 mg of compound **4**) did not allow for the use of the Dean-Stark apparatus. In this case, the amount of byproducts visible on TLC for both the dyes decreased and the yields increased to 41% for the dimethylamino derivative **6** and to 29% for the p-methoxy **5**, pointing out that the traditional procedure in this case was the more promising one. Scaling up the reaction was, unfortunately, not possible, since when increasing the amount of reagent the yield dropped down, and thus the reaction was repeated several times using maximum 30 mg in each reaction.

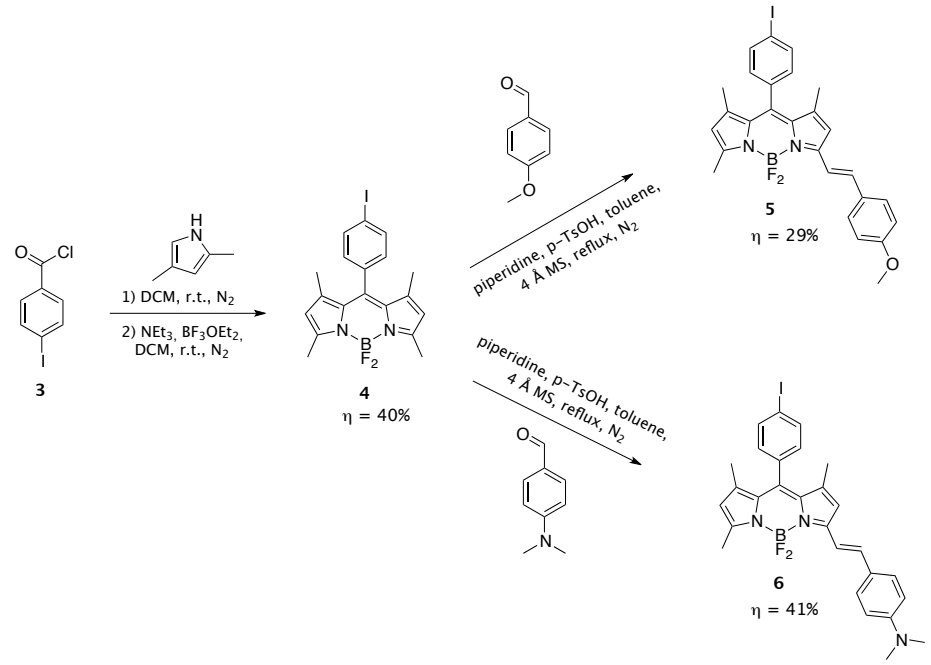

3

4
η = 40%

5
η = 29%

6
η = 41%

Scheme 3.4. Synthesis of BODIPYs **5** and **6**.

Concerning the scaffold, two calixarenes in different conformations were synthesized (**Scheme 3.5**). Starting from dipropoxycalix[4]arene **7**, the common diiodinated intermediate **8** was obtained. Adapting the classical literature protocol,[28] the reaction was performed with AgOTFA and I_2 in chloroform. After few hours a large amount of reagent was still present, thus the reaction time was prolonged and several additions of silver salt and I_2 were performed. The product, that was isolated in 55% yield after column chromatography, however, did not correspond to the desired compound **8**,

but, as confirmed by NMR, ESI-MS and even XRD analysis (**Figure 3.9**), to the oxidized calixarene **8a**.

Figure 3.9. Solid state molecular structure of **8a**

After trying another unsuccessful procedure[29] with $Cu(CH_3COO)_2$ and acetic acid in the presence of I_2, we repeated the first procedure using fewer equivalents of iodine and silver trifluoroacetate and decreasing the reaction time to 30 minutes and obtained the desired product in 39% yield.

At this stage the reaction of alkylation of the two phenolic oxygens of **8** allowed us to obtain the tetraaalkylated compounds in *cone* and *1,3-alternate* conformations according to the reaction conditions. *Cone* calixarene **9** was obtained performing the alkylation reaction with propyl iodide, using sodium hydride as base and DMF as solvent. Then the iodine atoms at the upper rim were replaced by two trimethylsilyl ethynyl groups through a Sonogashira reaction in 55% yield. Finally, the silyl protecting groups were removed with KF in DMF and the final calixarene **11** was obtained in 88% yield.

On the other hand, the use in the alkylation of **8** of Cs_2CO_3 in acetonitrile gave calixarene **15** in the *1,3-alternate* conformation, which was isolated after preparative TLC in 21% yield. The low yield and the need of chromatography, however, pushed us to follow another synthetic route in which, first, the iodine atoms on **8** are replaced by the ethynyl groups obtaining **12** in 55% yield, and, secondly, the conformation is changed through the alkylation at the lower rim. During the alkylation step, however, partial deprotection of the ethynyl groups of **13** was observed. The deprotection of **13**

was then completed by reaction with KF in DMF to give the final compound **14** in 70% yield for the two steps.

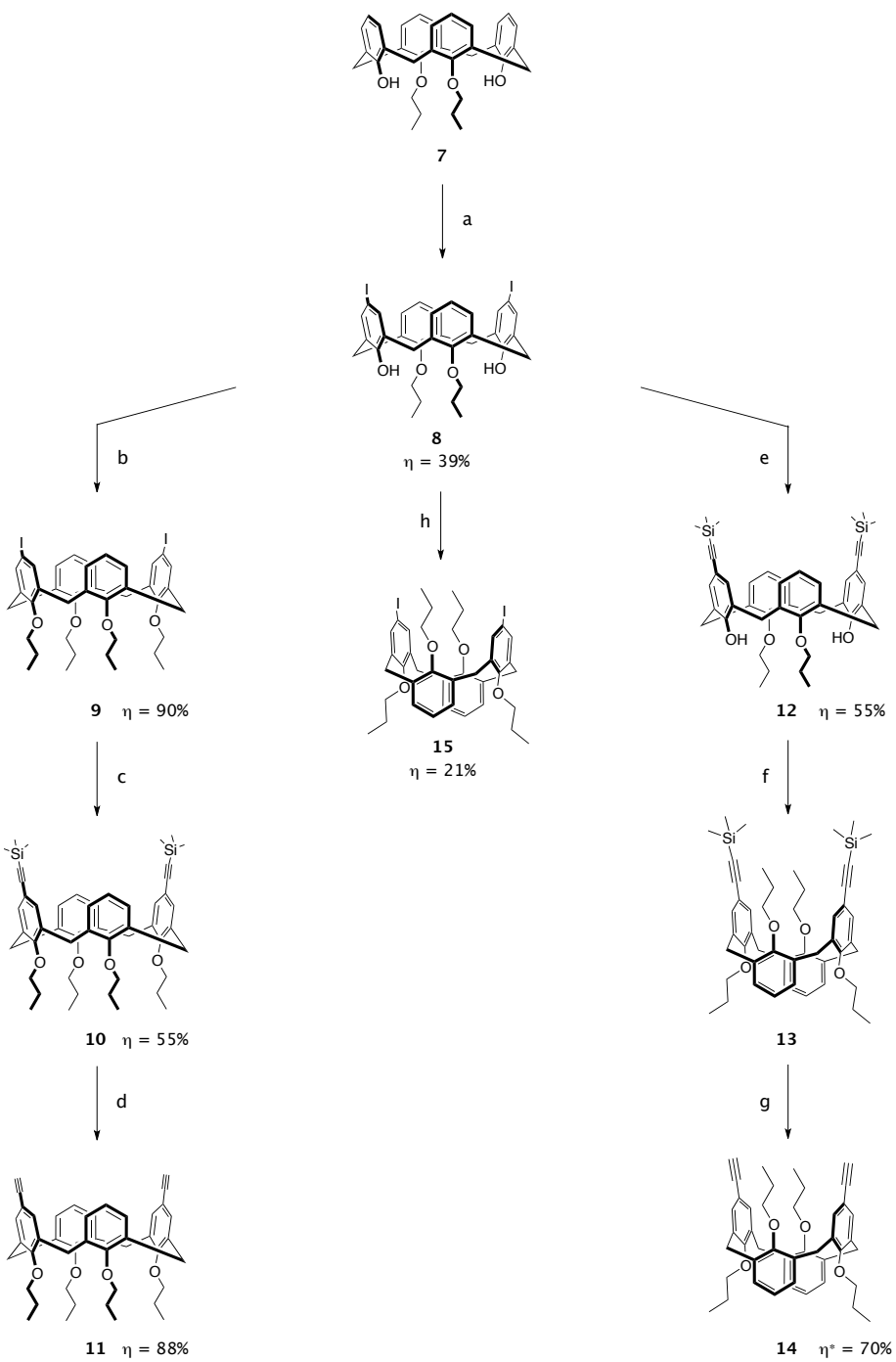

Scheme 3.5. Synthesis of calixarenes **11** and **14**: a) AgOTFA, I_2, $CHCl_3$, reflux; b) NaH, PrI, DMF, r.t.; c) TMSA, $Pd(PPh_3)_2Cl_2$, CuI, NEt_3, 65 °C, N_2; d) KF, DMF, 65 °C; e) TMSA, $Pd(PPh_3)_2Cl_2$, CuI, NEt_3, 70 °C, N_2; f) Cs_2CO_3, PrI, CH_3CN, reflux, N_2; g) KF,DMF, 65 °; h) Cs_2CO_3, PrI, CH_3CN, reflux, N_2. η^* is the total yield for the steps f and g.

Calixarenes **11** and **14** were then dissolved in a 1:1 mixture of dry THF and triethylamine and reacted, through the Sonogashira coupling, with an equimolar mixture of BODIPYs **5** and **6**, using CuI and $Pd(PPh_3)_2Cl_2$ as catalyst (**Scheme 3.6** and **Scheme 3.7**). After purification by column chromatography and preparative TLC plates, final compounds **1** and **2** were obtained in 27% and 43% yield, respectively. For the calixarene in the *cone* conformation (**1**) also small amounts of the two homobichromophoric compounds were isolated and characterized by ^{1}H NMR.

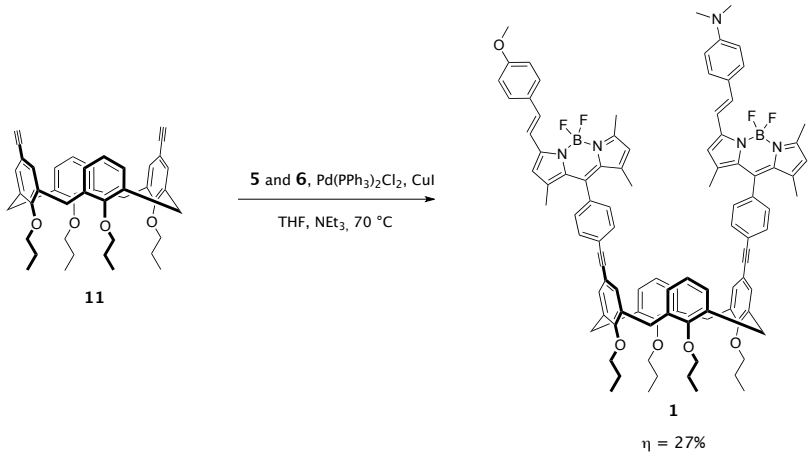

Scheme 3.6. Synthesis of **1**.

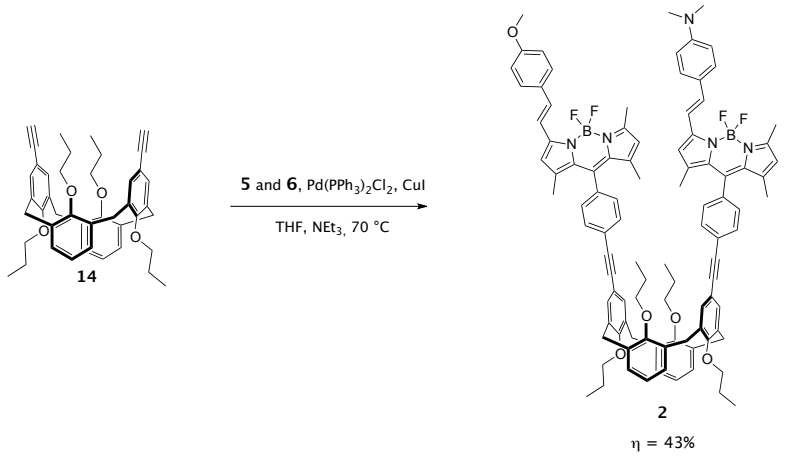

Scheme 3.7. Synthesis of **2**.

The two compounds were fully characterized by ^{1}H NMR and ^{13}C NMR spectroscopy and by High Resolution ESI-MS. NOESY spectra were useful to correctly assign all the signals in the ^{1}H NMR spectra, but no cross peaks between the signals of the two BODIPYs were found, ruling out a close proximity between the two dyes. The conformation adopted by calixarene **1** in solution was investigated by ^{1}H NMR spectroscopy. As explained in section 1.3.1, the *cone* calix[4]arene, substituted on the 1,3-distal positions, can adopt an open or a closed flattened conformation in solution, depending on the solvent, and the two conformations can be distinguished by ^{1}H NMR spectroscopy since the protons on the rings parallel to each other experience the shielding cone of the outward-oriented rings and thus resonate at higher fields. In the case of **1**, from the spectrum in acetone-d_6 (**Figure 3.10a**) it seems that the preferred conformation is the open flattened cone, as indicated by the resonance of the aromatic protons (singlet at 7.22 ppm for the protons ortho to the alkynyl groups, doublet at 6.64 ppm and triplet at 6.55 ppm for the protons of the unsubstituted aromatic rings). From the comparison between the ^{1}H-NMR spectra of **1** in acetone-d_6 and $CDCl_3$ (**Figure 3.10**), no significant differences in the chemical shifts of the aromatic protons of the unsubstitued rings were observed (6.35-6.26 ppm in CDCl3, 6.63-6.53 ppm in acetone-d_6), indicating that the preferred conformation is, again, the one minimizing the steric repulsion between the substituents at the upper rim. A spectrum in dmso-d_6 was also recorded and no changes at all in the chemical shift of the aromatic protons were observed with respect to the spectrum in acetone.

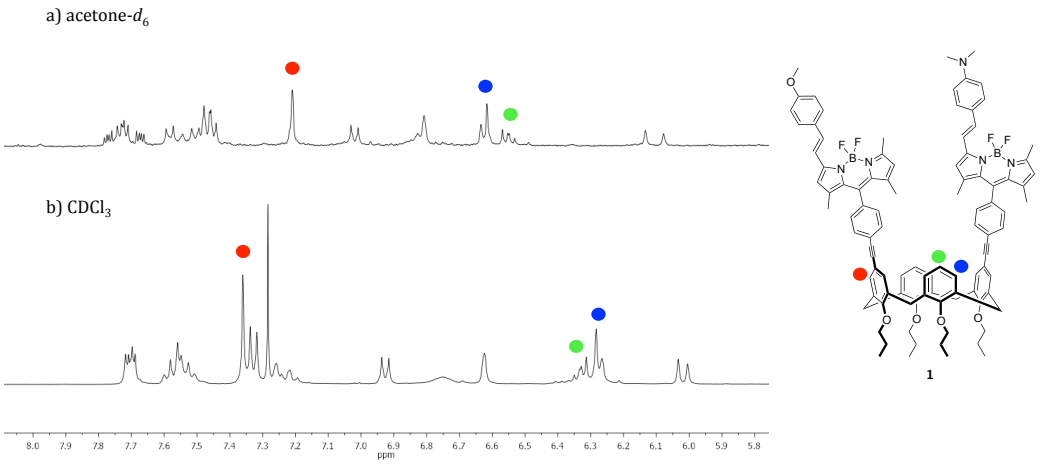

Figure 3.10. Comparison of the aromatic region of the ^{1}H NMR spectra of **1** (400 MHz) in a) acetone-d_6 and b) $CDCl_3$.

3.3.2 Spectroscopic studies

3.3.2.1 Steady-state absorption and fluorescence

As described above (section 3.1.1), the couple of chromophores was selected based on their spectroscopic features, in particular their quasi-degenerate excitations. BODIPYs **5** and **6** were used as references for a correct interpretation of the data gathered on bichromophoric calixarenes **1** and **2**. The main spectroscopic properties measured for **1**, **2**, **5** and **6** are reported in **Table 3.1**. Absorption and emission spectra in different solvents (toluene, dichloromethane and acetonitrile) of the two reference dyes are reported in **Figure 3.11**.

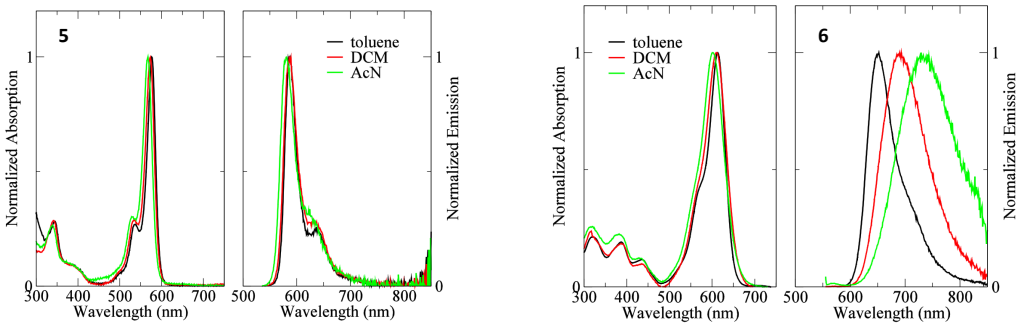

Figure 3.11. Absorption and emission spectra of **5** (on the left) and **6** (on the right) in different solvents.

Both reference compounds display narrow absorption bands in the green-orange region of the visible spectrum; other less intense transitions fall in the UV, below 450 nm. Solvent effects on the peak positions are marginal and result only in a little inhomogeneous broadening. Emission of **5** falls below 700 nm in all the investigated solvents and is almost specular to absorption with high quantum yields, approaching unity in apolar environments. On the contrary, **6** is strongly solvatofluorochromic, showing a displacement of the emission maximum of approximately 80 nm from toluene to acetonitrile. Its quantum yield is highly sensitive to solvent polarity (**Table 3.1**), dropping to less than 10% in polar media.

Concerning the bichromophoric calixarenes **1** and **2**, the spectra of both molecules (**Figure 3.12**) recall the characteristic features of the reference compounds, whose contributions can be easily recognized both in absorption and emission. Their quantum yields (**Table 3.1**) are almost independent on the excitation wavelengths and are lower for **2**, irrespective of the solvent considered.

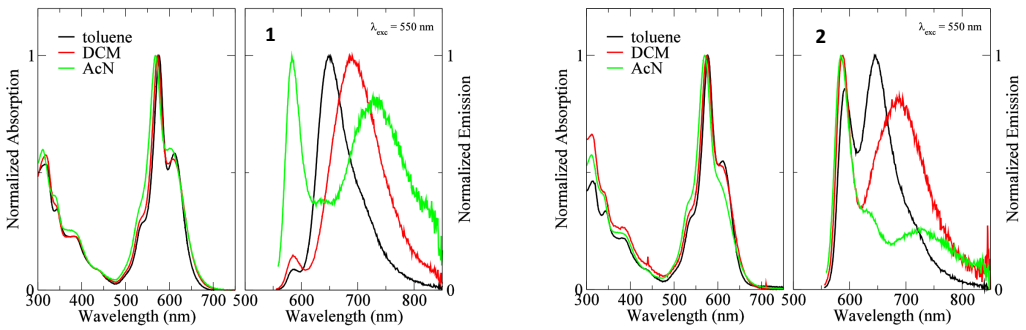

Figure 3.12. Absorption and emission spectra of **1** (on the left) and **2** (on the right) in different solvents.

Table 3.1. Main spectroscopic properties of **5**, **6**, **1** and **2** in toluene, dichloromethane and acetonitrile. Quantum yields were measured at 23 °C using Rhodamine 101 in ethanol as standard (λ_{exc} = 530 nm, Φ = 100%). Fluorescence lifetimes were measured using λ_{exc} = 563 nm. Absorption coefficients for **6**, **1** and **2** in acetonitrile are not reported due to solubility issues.

Solvent	Compound	λ_{abs}^{max} (nm)	λ_{em}^{max} (nm)	ε_{max} (10^4 M^{-1} cm^{-1})	Φ (%) [λ_{exc} (nm)]	τ (ns) [λ_{em} (nm)]
Toluene	**5**	576	587	13.5	100 [535]	3.62 [635]
	6	613	652	10.4	86 [570]	3.42 [650]
	1	576	588/649	14.4	76 [535] 77 [565]	0.20 (27%); 3.29 (73%) [580] 3.03 (82%); 4.42 (18%) [650] 3.32 [750]
	2	577	591/645	13.6	55 [535] 52 [550]	1.82 (63%); 4.55 (37%) [580] 1.86 (66%); 4.59 (34%) [650]
DCM	**5**	573	586	11.0	95 [534]	3.88 [635]
	6	609	693	7.75	73 [550]	3.30 [688]
	1	573	585/690	14.0	51 [534] 51 [550]	0.08 (34%); 3.38 (66%) [580] 3.18 [688] 3.27 [755]
	2	575	588/684	15.5	12 [534] 12 [550]	0.70 (82%); 3.43 (18%) [580] 0.64 (60%); 2.15 (40%) [690]
ACN	**5**	567	581	9.80	71 [530]	3.93 [630]
	6	601	729	-	7 [550]	0.77 [730]
	1	568	583/733	-	4 [530] 4 [550]	3.09 [583] 3.06 [600]
	2	570	584/730	-	3 [530] 3 [550]	3.84 (51%): 3.51 (49%) [583]

Comparing the two bichromophoric calixarenes in different conformation **1** and **2**, quasi-superimposable absorption bands are observed in toluene and dichloromethane, while in acetonitrile a slight decrease of the acceptor shoulder occurs for **2** (**Figure 3.13**). Comparison of the emission spectra of the bichromophores, however, reveals substantial differences in terms of ratio between the donor and the acceptor contributions (**Figure 3.13**). Specifically, while for the *cone* derivative **1** the main contribution comes from the acceptor, for the *1,3-alternate* isomer **2** the two contributions are comparable, at least in dichloromethane and toluene, since in acetonitrile the quantum yield of the acceptor is one order of magnitude lower than the donor's. This result could be read as an evidence of interactions between the dyes, consistently affected by the donor-acceptor distance.

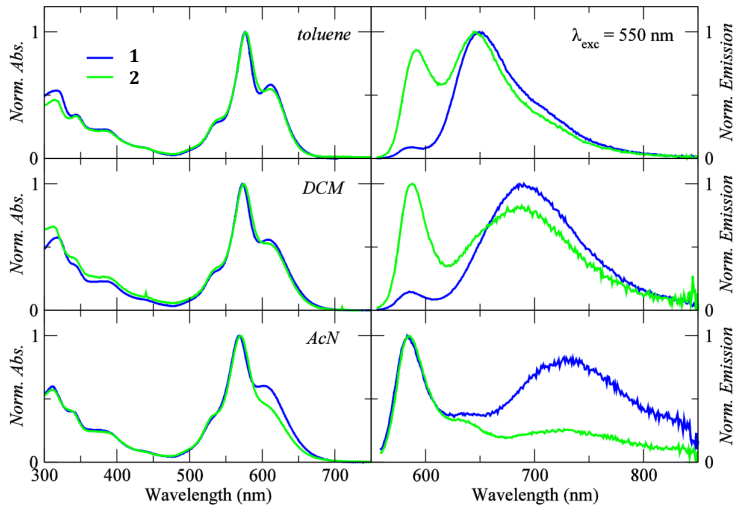

Figure 3.13. Comparison between absorption and emission spectra of **1** and **2**.

3.3.2.2 Energy transfer studies

In order to study the energy transfer between the two dyes anchored on the calixarene scaffold, the spectral overlap between BODIPYs **5** and **6** must be taken into account. Assuming that **5** acts as the energy donor (D) and **6** as the energy acceptor (A), we can see from **Figure 3.14** that the emission of **5** matches the absorption of **6**.

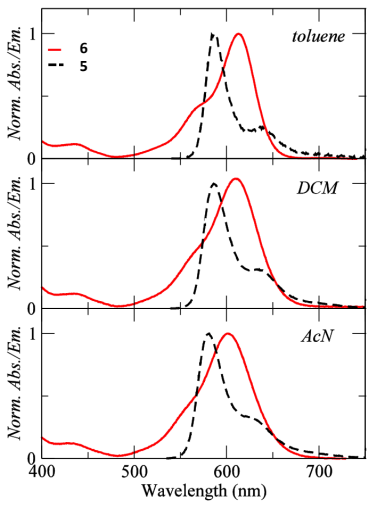

Figure 3.14. Spectral overlap between emission of **5** (dotted line) and absorption of **6** (continuous line) in different solvents.

The values of the overlap integrals *J* (defined in chapter 2) reported in **Table 3.2** confirm these qualitative findings. The Förster radii, calculated using

$$R_0^6 = 8.79 \cdot 10^{-5}\, k^2\, n^{-4}\, \phi_D\, J \qquad (13)$$

where *n* is the refractive index of the solvent, *k* the orientational factor (in our case we assumed k^2 = 2/3), ϕ_D the quantum yield of the isolated donor and J the overlap integral, were found to be higher than 100 Å, indicating that the energy transfer from **5** to **6** is active at long distance.

To take into account the possibility of a backtransfer from **6** to **5**, the overlaps between emission of **6** and absorption of **5** were also estimated (**Figure 3.15**).

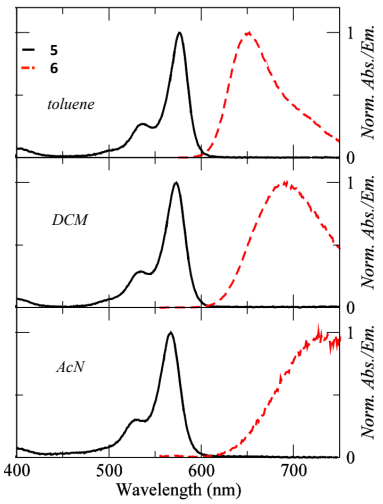

Figure 3.15. Spectral overlap between emission of **6** (dotted line) and absorption of **5** (continuous line).

It was found that the overlap integrals for the backtransfer (**Table 3.2**) are two orders of magnitude lower than for the direct transfer, pointing out that direct transfer is indeed the favored process. Förster radii for the backtransfer were calculated to be in between 40 and 50 Å in the three investigated solvents, significantly lower than those estimated for the direct transfer, but higher than the donor-acceptor distance in our dyads. This means that back energy transfer cannot be neglected in our case.

Table 3.2. Estimation of the overlap integrals *J* and Forster radii R_0.

Solvent	Emission	Absorption	J (M^{-1} cm^3 $(nm)^4$)	R_0 (Å)
Toluene	**5 (D)**	**6 (A)**	$3.02 \cdot 10^{17}$	123
	6 (A)	**5 (D)**	$1.03 \cdot 10^{15}$	47
DCM	**5 (D)**	**6 (A)**	$3.18 \cdot 10^{17}$	127
	6 (A)	**5 (D)**	$5.46 \cdot 10^{14}$	42
ACN	**5 (D)**	**6 (A)**	$2.47 \cdot 10^{17}$	121
	6 (A)	**5 (D)**	$7.61 \cdot 10^{15}$	46

To estimate the efficiency of the energy transfer two methods were used. The first considers the decrease in the donor emission when linked to the acceptor in bichromophoric calixarenes **1** and **2**. Looking at the *cone* derivative **1**, a huge quenching of the donor emission is observed, whereas for the *1,3-alternate* isomer **2** a less dramatic reduction occurs (**Table 3.3**). Using equation (6) (chapter 2) to calculate the transfer efficiency, values of more than 95% for **1** in all solvents and of about 70% and 80% in toluene and DCM, respectively, for **2** are found (**Table 3.3**). These values are reliable if backtransfer and other unquantifiable side processes are excluded.

Table 3.3. Estimation of the energy transfer efficiencies from quenching of the donor emission. Φ_D is the quantum yield of the isolated donor; $\Phi_{D(A)}$ is the quantum yield of the donor in the presence of the acceptor.

Solvent	Φ_D%	Compound	λ_{exc} (nm)	$\Phi_{D(A)}$%	Efficiency %
Toluene	100	**1**	535	5	95
			550	6	94
		2	535	30	70
			550	33	67
DCM	95	**1**	530	5	95
			550	5	94
		2	535	17	82
			550	20	79
ACN	71	**1**	530	2	97
			550	2	97
		2	530	3	96
			550	6	92

The second method for the determination of the energy transfer efficiencies is based on the comparison between the normalized absorption spectra of the bichromophoric calixarenes and their excitation spectra collected on the acceptor emission. **Figure 3.16** shows that for **1** the spectra match almost completely, suggesting nominally quantitative energy transfer in all the investigated solvents.

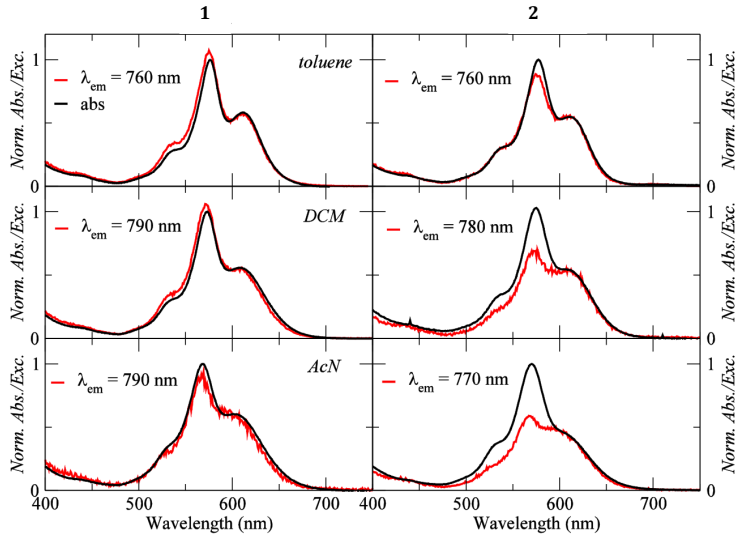

Figure 3.16. Comparison between the excitation spectra collected at the acceptor emission wavelength (red line) and the corresponding absorption spectra (black line) for compounds **1** (left) and **2** (right) in different solvents.

For **2**, instead, excitation spectra display lower intensity in the donor region with respect to the corresponding absorption. Efficiencies values estimated using equation (10), defined in chapter 2, are reported in **Table 3.4**. High values (> 95%) for **1** were found, in agreement with the results based on the donor quenching, while major discrepancies are observed for **2**, especially in acetonitrile and dichloromethane, where efficiencies of about 50% were found, compared with the > 80% of the former method.

Table 3.4. Estimation of the intramolecular energy transfer efficiency from the comparison of excitation and absorption spectra.

Solvent	Compound	Efficiency %
Toluene	**1**	100
	2	84
DCM	**1**	100
	2	52
ACN	**1**	93
	2	47

Finally, estimation of the transfer efficiencies via lifetimes measurements was not directly applicable due to the low residual fluorescence of the donor. Bi-exponential decays were observed for the donor in the dyads both in toluene and dichloromethane, indicating strong interchromophore interactions. On the other hand, the lifetimes of the acceptor in the dyads, where available, were only slightly different with respect to those of the isolated acceptor.

3.4 Concluding remarks

This chapter describes the synthesis of two calix[4]arene-based bichromophoric dyads for the study of quantum coherence energy transfer. With the aim to investigate if quantum coherence is possible also in small, flexible, artificial systems, two different BODIPYs were linked to two calixarenes in *cone* and *1,3-alternate* conformation. The two chosen dyes fulfill strict requirements that make them ideal candidates for the study of this phenomenon, that is they present quasi-degenerate excitation, narrow absorption and emission bands and their absorption falls in the red region of the visible spectrum. In order to give rise to coherent phenomena then, the two dyes must be kept at close distance, thus the BODIPYs were linked to the calixarenes through an alkynyl group. The heterobichromophoric calixarenes were isolated, together with a small amount of homobichromophoric systems. The two structures were therefore studied with steady-state spectroscopy and their principal features highlighted. The energy transfer efficiencies were calculated with two methods and the percentage compared. For the *cone* derivative the two methods are substantially in agreement, providing an almost quantitative energy transfer between the two dyes. For the *1,3-alternate* isomer, instead, discrepancies were observed. In particular, lower efficiencies were found, compared to the *cone* derivative, even if a comparable, if not higher, energy transfer is expected, giving the higher spatial proximity of the BODIPYs in the structure. Moreover, the efficiencies calculated in dichloromethane and acetonitrile drop from higher than the 80% found with the first method to around 50% with the second one. Finally, taking a look at the lifetimes, the biexponential decays

observed for the donor in the dyads seem to suggest the presence of strong interactions between the dyes. It can then be concluded that when strong coupling is present Förster theory becomes rather limited and is not able to successfully describe such systems. A new model therefore needs to be developed, capable of defining these systems appropriately. In addition, the two isomers will be studied by transient absorption spectroscopy, and in case of interesting results, by 2D-electronic spectroscopy as well, to have a look into the dynamics of the transfer and to get a complete understanding of the systems.

3.5 Experimental section

General information. All moisture sensitive reactions were carried out under a nitrogen or argon atmosphere, using previously oven-dried glassware. All dry solvents were prepared according to standard procedures, distilled before use and stored over 3 or 4 Å molecular sieves. All other reagents were commercial samples and used without further purification. Microwave reactions were carried out using a CEM Discovery System reactor. Analytical TLC were performed using prepared plates of silica gel (Merck 60 F-254 on aluminum) and then, according to the functional groups present on the molecules, revealed with UV light or using staining reagents. Merck silica gel 60 was used for flash chromatography (40-63 μm) and for preparative TLC plates (10-12 μm). ^{1}H NMR and ^{13}C NMR spectra were recorded on Bruker AV300 and Bruker AV400 spectrometers (observation of ^{1}H nucleus at 300 MHz and 400 MHz, respectively, and of ^{13}C nucleus at 75 MHz and 100 MHz, respectively) and partially deuterated solvents were used as internal standards to calculate the chemical shifts (δ values in ppm). All ^{13}C NMR spectra were performed with proton decoupling. Electrospray ionization (ESI) mass analysis were performed with a Waters single-quadrupole spectrometer in positive mode using MeOH or CH_3CN as solvents. High resolution mass spectra were recorded on a LTQ Orbitrap XL instrument in positive mode using MeOH or CH_3CN as solvents. Melting points were determined on an Electrothermal apparatus in closed capillaries. Absorption spectra were collected with

a Perkin-Elmer Lambda 250 spectrophotometer on freshly prepared solutions at room temperature. Emission measurements were performed on diluted solutions (concentration ~10^{-6} M) with a Fluoromax-3 Horiba Jobin-Yvon fluorometer. During the measurements the samples were thermostated at a temperature of 23 °C. All solvents were used as received: toluene for HPLC ≥ 99.9% purchased from Sigma Aldrich, dichloromethane (DCM) for HPLC from Baker and Acetonitrile (ACN), for HPLC from VWR Chemicals. For the estimation of emission quantum yields a diluted solution of Rhodamine 101 in ethanol (QY = 100%, λ_{exc} = 530 nm) was used as the standard. Fluorescence lifetimes were measured in a TCSPC configuration, equipping the Fluoromax-3 instrument with a Horiba FluoroHub controller. Selected pulsed nanoLEDs were used as the excitation source. Reconvolution fit of the decay profiles returned the lifetime values, that were judged by the χ^2 test (results were retained if χ^2 < 1.2).

25,27-dipropoxycalix[4]arene **7**,[30] 5,17-diiodo-25,27-dipropoxycalix[4]arene **8**,[31] 5,17-diiodo-25,26,27,28-tetrapropoxycalix[4]arene **9**,[32] 5,17-bis(trimethylsilylethynyl)-25,27-dipropoxycalix[4]arene **12**[31] were synthesized according to literature procedures.

4,4-difluoro-8-(4-iodo)phenyl-1,3,5,7-tetramethyl-4-bora-3a,4a-diaza-s-indacene (4): To a solution of *p*-iodobenzoic acid (1 g, 4.03 mmol) in dry DCM (20 mL) oxalyl chloride (1.8 mL, 20.16 mmol) together with few drops of dry DMF was added. The mixture was stirred at room temperature for 5 hours, after which the solvent was removed under reduced pressure. The acyl chloride **3** thus obtained was immediately redissolved in dry DCM (20 mL) in a Schlenk tube under nitrogen atmosphere and 2,4-dimethylpyrrole (1.25 mL, 12.10 mmol) was added. The solution was stirred at room temperature in the dark for 22 hours, then triethylamine (2.25 mL, 16.13 mmol) was added. After 20 minutes boron trifluoride diethyl etherate (3.0 mL, 24.19 mmol) was introduced and the reaction stirred overnight in the dark. The reaction was quenched by addition of 40 mL of a saturated solution of $NaHCO_3$. After stirring for 30 minutes the two layers were separated and the aqueous phase extracted twice with DCM. The

organic layers were reunited and washed 4 times with water, dried with Na_2SO_4 and evaporated under vacuum. The crude was purified by column chromatography (hexane/AcOEt 9:1) to give the product as a bright orange solid in 40% yield (726 mg, 1.61 mmol). ^{1}H NMR (400 MHz, $CDCl_3$) δ (ppm): 7.84 (d, *J* = 8.3 Hz, 2H, ArH), 7.04 (d, *J* = 8.3 Hz, 2H, ArH), 5.98 (s, 2H, CH), 2.54 (s, 6H, CH_3), 1.41 (s, 6H, CH_3). The compound showed the same physico-chemical properties as those reported in the literature.[33]

BODIPY 5:

To a solution of **4** (100 mg, 0.22 mmol) and 4-methoxybenzaldehyde (27 µL, 0.22 mmol) in dry toluene (5 mL), 4 Å molecular sieves (few beads), piperidine (64 µL, 0.67 mmol) and *p*-toluenesulfonic acid (127 mg, 0.67 mmol) were added and the mixture heated to reflux for 5 hours. The solvent was removed under reduced pressure and the residue purified by column chromatography (hexane/AcOEt 85:15 and then hexane/DCM 1:1) to obtain a purple solid in 29% yield (37 mg, 0.065 mmol).

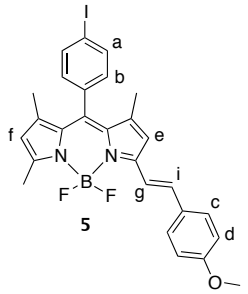

5

^{1}H NMR (400 MHz, $CDCl_3$) δ (ppm): 7.88 (d, *J* = 8.3 Hz, 2H, H_a), 7.57 (d, *J* = 8.8 Hz, 2H, H_c), 7.56 (d, *J* = 16.4 Hz, 1H, H_g), 7.24 (d, *J* = 16.4 Hz, 1H, H_i), 7.10 (d, *J* = 8.3 Hz, 2H, H_b), 6.93 (d, *J* = 8.8 Hz, H_d), 6.62 (s, 1H, H_e), 6.03 (s, 1H, H_f), 3.87 (s, 3H, OCH_3), 2,61 (s, 3H, CH_3), 1.49 (s, 3H, CH_3), 1.45 (s, 3H, CH_3). The compound showed the same physico-chemical properties as those reported in the literature.[25]

BODIPY 6:

To a solution of **4** (100 mg, 0.22 mmol) and 4-(dimethylamino)benzaldehyde (30 mg, 0.22 mmol) in dry toluene (5 mL), 4 Å molecular sieves (few beads), piperidine (64 µL, 0.67 mmol) and *p*-toluenesulfonic acid (127 mg, 0.67 mmol) were added and the mixture heated to reflux for 5 hours. The solvent was removed under reduced

pressure and the residue purified by column chromatography (hexane/DCM 1:1) to obtain a blue solid in 41% yield (48 mg, 0.092 mmol).

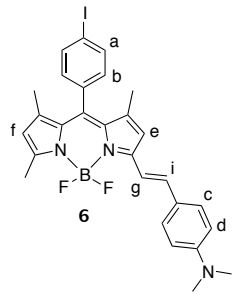

6

^{1}H NMR (400 MHz, $CDCl_3$) δ (ppm): 7.86 (d, *J* = 8.0 Hz, 2H, H_a), 7.53 (d, *J* = 8.6 Hz, 2H, H_c), 7.50 (d, *J* = 16.4 Hz, 1H, H_g), 7.24 (d, *J* = 16.2 Hz, 1H, H_i), 7.10 (d, *J* = 8.0 Hz, 2H, H_b), 6.71 (d, *J* = 8.6 Hz, 2H, H_d), 6.63 (s, 1H, H_e), 5.99 (s, 1H, H_f), 3.05 (s, 6H, $N(CH_3)_2$), 2.60 (s, 3H, CH_3), 1.49 (s, 3H, CH_3), 1.44 (s, 3H, CH_3). The compound showed the same physico-chemical properties as those reported in the literature.[27]

5,17-bis(trimethylsilylethynyl)-25,26,27,28-tetrapropoxycalix[4]arene (10):

In a Schlenk tube 5,17-diiodo-25,26,27,28-tetrapropoxycalix[4]arene **9** (100 mg, 0.12 mmol), $Pd(PPh_3)_2Cl_2$ (12.5 mg, 0.018 mmol) and CuI (3.4 mg, 0.018 mmol) were suspended in dry triethylamine (4 mL). After stirring for 15 minutes at room temperature, trimethylsilylacetilene (67 µL, 0.47 mmol) was added and the mixture heated to 65 °C for 3 days. The catalyst was filtered off and the solution concentrated under vacuum. The residue was purified by column chromatography (cyclohexane/toluene 9:1) to afford a white solid in 55% yield (51 mg, 0.065 mmol). ^{1}H NMR (400 MHz, $CDCl_3$) δ (ppm): 7.30 (s, 4H, ArH), 6.23 (t, *J* = 7.5 Hz, 2H, ArH), 6.15 (d, *J* = 7.4 Hz, 4H, ArH), 4.41 (d, *J* = 13.3 Hz, 4H, ArC*H*H_{ax}Ar), 4.04 (t, *J* = 8.1 Hz, 4H, OCH_2), 3.66 (t, *J* = 6.8 Hz, 4H, OCH_2), 3.13 (d, *J* = 13.4 Hz, 4H, ArCH*H*$_{eq}$Ar), 1.99-1.81 (m, 8H, OCH_2CH_2), 1.11 (t, *J* = 7.4 Hz, 6H, CH_3), 0.90 (t, *J* = 7.5 Hz, 6H, CH_3), 0.30 (s, 18H, $Si(CH_3)_3$). ^{13}C NMR (100 MHz, $CDCl_3$) δ (ppm): 158.7, 154.9, 137.1, 132.6, 132.4, 127.6, 122.2, 116.0, 105.9, 92.3, 76.5, 30.7, 23.5, 22.9, 10.8, 9.8. ESI-MS: m/z calcd for $C_{50}H_{64}O_4Si_2$ [(**10**+H)$^+$] 785.4, found 785.6 (40%); calcd for $C_{50}H_{64}O_4Si_2Na$ [(**10**+Na)$^+$] 807.4, found 807.6 (100%); calcd for $C_{50}H_{64}O_4Si_2K$ [(**10**+K)$^+$] 823.5, found 824.5 (65%).

5,17-diethynyl-25,26,27,28-tetrapropoxycalix[4]arene (11):

To a solution of **10** (230 mg, 0.29 mmol) in dry DMF (25 mL), KF (340 mg, 5.86 mmol) was added and the mixture heated to 65 °C for 6 hours. The reaction was quenched with 1M HCl (25 mL) and the white precipitate was filtered off to give **11** in 88% yield (166 mg, 0.065 mmol). ^{1}H NMR (300 MHz, $CDCl_3$) δ (ppm): 7.07 (s, 4H, ArH), 6.43-6.31 (m, 6H, ArH), 4.39 (d, *J* = 13.4 Hz, 4H, ArC*H*H_{ax}Ar), 3.94 (t, *J* = 7.8 Hz, 4H, OCH_2), 3.72 (t, *J* = 7.1 Hz, 4H, OCH_2), 3.11 (d, *J* = 13.4 Hz, 4H, ArC*H*H_{eq}Ar), 2.95 (s, 2H, C≡CH), 1.98-1.80 (m, 8H, OCH_2CH_2), 1.03 (t, *J* = 7.4 Hz, 6H, CH_3), 0.92 (t, *J* = 7.5 Hz, 6H, CH_3). ^{13}C NMR (75 MHz, $CDCl_3$) δ (ppm): 158.2, 155.6, 136.3, 133.3, 132.4, 127.9, 122.3, 115.1, 84.3, 75.5, 30.7, 23.3, 23.1, 10.5, 10.0. ESI-MS: m/z calcd for $C_{44}H_{48}O_4Na$ [(**11**+Na)$^+$] 663.8, found 664.1.

5,17-diethynyl-25,26,27,28-tetrapropoxycalix[4]arene, *1,3-alternate* (14):

To a suspension of calix[4]arene **12** (152 mg, 0.22 mmol) in CH_3CN (30 mL), Cs_2CO_3 (424 mg, 1.30 mmol) was added. After stirring for 30 minutes, 1-iodopropane (127 µL, 1.30 mmol) was added and the mixture heated to reflux for 24 hours. The solvent was evaporated under reduced pressure then the residue was partitioned between 1M HCl and DCM. The organic layer was washed again with 1M HCl, twice with water and then evaporated under vacuum. The mixture of 5,17-bis(trimethylsilylethynyl)-25,26,27,28-tetrapropoxycalix[4]arene, *1,3-alternate* **13** and 5,17-ethynyl-25,26,27,28-tetrapropoxycalix[4]arene, *1,3-alternate* **14** thus obtained was immediately dissolved in dry DMF (15 mL) and KF (160 mg, 2.75 mmol) was added. After 3 hours the reaction was quenched with 1M HCl, the precipitate filtered off and purified by column chromatography (hexane/DCM 6:4) to give a white solid in 70% yield (97 mg, 0.15 mmol). ^{1}H NMR (400 MHz, $CDCl_3$) δ (ppm): 7.22 (s, 4H, ArH), 7.01 (d, *J* = 7.5 Hz, 4H, ArH), 6.74 (t, *J* = 7.5 Hz, 2H, ArH), 3.67 (s, 8H, $ArCH_2Ar$), 3.56 (t, *J* = 7.2 Hz, 4H, OCH_2), 3.43 (t, *J* = 7.2 Hz, 4H, OCH_2), 2.94 (s, 2H, C≡CH), 1.63-1.45 (m, 8H, OCH_2CH_2), 0.94 (t, *J* = 7.5 Hz, 6H, CH_3), 0.83 (t, *J* = 7.5 Hz, 6H, CH_3). ^{13}C NMR (100 MHz, $CDCl_3$) δ (ppm): 157.3, 156.7, 133.8, 133.7, 133.4, 129.8, 121.7, 115.2, 84.2, 74.9, 73.0, 72.8, 36.9, 23.2, 23.0, 10.2. ESI-MS: m/z calcd for $C_{44}H_{48}O_4Na$ [(**14**+Na)$^+$] 663.8, found 664.1.

5,17-diiodo-25,26,27,28-tetrapropoxycalix[4]arene, *1,3-alternate* (15):

To a suspension of calix[4]arene **8** (61 mg, 0.080 mmol) in CH_3CN (10 mL), Cs_2CO_3 (156 mg, 0.48 mmol) was added. After stirring for 30 minutes, 1-iodopropane (47 µL, 0.48 mmol) was added and the mixture heated to reflux for 22 hours. The solvent was evaporated under reduced pressure then the residue was partitioned between 1M HCl and DCM. The organic layer was washed again with 1M HCl, twice with water and then evaporated under vacuum. The residue was purified by preparative TLC plates (hexane/AcOEt 9:1) to afford a white solid in 21% yield (14 mg, 0.017 mmol). ^{1}H NMR (400 MHz, $CDCl_3$) δ (ppm): 7.38 (s, 4H, ArH), 7.00 (d, *J* = 7.2 Hz, 4H, ArH), 6.72 (t, *J* = 7.6 Hz, 2H, ArH), 3.61 (s, 8H, $ArCH_2Ar$), 3.59 (t, *J* = 7.2 Hz, 4H, OCH_2), 3.47 (t, *J* = 7.2 Hz, 4H, OCH_2), 1.73-1.61 (m, 4H, OCH_2CH_2), 1.60-1.49 (m, 4H, OCH_2CH_2), 1.05 (t, *J* = 7.2 Hz, 6H, CH_3); 0.93 (t, *J* = 7.2 Hz, 6H, CH_3). ^{13}C NMR (100 MHz, $CDCl_3$) δ (ppm): 156.5, 138.5, 136.0, 133.0, 130.0, 121.7, 85.4, 73.2, 73.0, 36.4, 23.4, 10.7, 10.3. ESI-MS: m/z calcd for $C_{40}H_{46}O_4I_2Na$ [(**15**+Na)$^+$] 867.6, found 867.9.

Compound 1:

In a Schlenk tube were introduced calix[4]arene **11** (21.1 mg, 0.033 mmol), BODIPY **5** (19.6 mg, 0.034 mmol), BODIPY **6** (20 mg, 0.034 mmol), $Pd(PPh_3)_2Cl_2$ (3.5 mg, 0.0049 mmol) and CuI (1 mg, 0.0049 mmol) under argon atmosphere, then triethylamine (1 mL) and dry THF (1 mL) were added. The mixture was heated to 70 °C for 3 hours, then the solvent was evaporated under reduced pressure. The residue was purified by column chromatography (hexane/AcOEt 8:2) and preparative TLC plates (toluene/DCM 9:1) to afford compound **1** as a dark blue solid (13.7 mg, 0.0089 mmol, 27% yield).

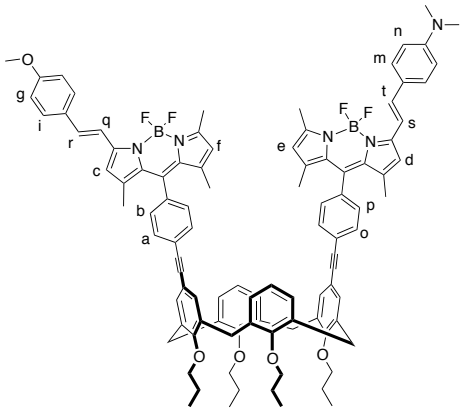

1

Mp: >300 °C. ^{1}H NMR (400 MHz, $CDCl_3$) δ (ppm): 7.74-7.65 (m, 4H, H_a and H_o), 7.62-7.48 (m, 6H, H_m, H_i, H_q and H_s), 7.36 (s, 4H, ArH_{calix}), 7.33 (d, *J* = 8.2 Hz, 4H, H_b and H_p), 7.28-7.17 (m, 2H, H_r and H_t), 6.93 (d, *J* = 8.8 Hz, 2H, H_g), 6.75 (br s, 2H, H_n), 6.62 (two isochronous singlets, 2H, H_c and H_d), 6.33 (t, *J* = 6.9 Hz, 2H, ArH_{calix}), 6.27 (d, *J* = 6.6 Hz, 4H, ArH_{calix}), 6.03 (s, 1H, H_e), 6.00 (s, 1H, H_f), 4.48 (d, *J* = 13.3 Hz, 4H, Ar*C*H_{ax}Ar), 4.09 (t, *J* = 7.6 Hz, 4H, OCH_2), 3.87 (s, 3H, OCH_3), 3.73 (t, *J* = 7.3 Hz, 4H, OCH_2), 3.21 (d, *J* = 13.4 Hz, 4H, Ar*C*H_{eq}Ar), 3.06 (s, 6H, $N(CH_3)_2$), 2.62 (s, 6H, 2xCH_3), 2.05-1.87 (m, 8H, $OCH_2C\mathit{H}_2$), 1.52 (s, 6H, 2xCH_3), 1.48 (s, 3H, CH_3), 1.47 (s, 3H, CH_3), 1.13 (t, *J* = 7.4 Hz, 6H, $OCH_2CH_2C\mathit{H}_3$), 0.96 (t, *J* = 7.5 Hz, 6H, $OCH_2CH_2C\mathit{H}_3$). ^{13}C NMR (100 MHz, $CDCl_3$) δ (ppm): 160.4, 158.7, 155.2, 154.8, 153.6, 142.4, 142.1, 139.2, 137.1, 136.3, 134.9, 134.7, 132.7, 132.3, 132.1, 132.0, 131.4, 131.0, 129.37, 129.30, 129.0, 128.6, 128.4, 127.7, 124.5, 124.4, 122.3, 121.1, 120.6, 117.8, 117.6, 116.9, 115.8, 115.7, 114.2, 91.5, 91.4, 87.56, 87.50, 77.2, 55.3, 30.8, 23.5, 23.1, 14.95, 14.90, 14.7, 14.6, 14.5, 10.7, 9.9. HR-MS: m/z calcd for $C_{99}H_{98}N_5O_5B_2F_4$ [(**1**+H)$^+$] 1534.76902, found 1534.76470.

Small amounts of the two homo-bichromophoric products were also isolated by chromatography for a partial characterization:

Compound 1a:

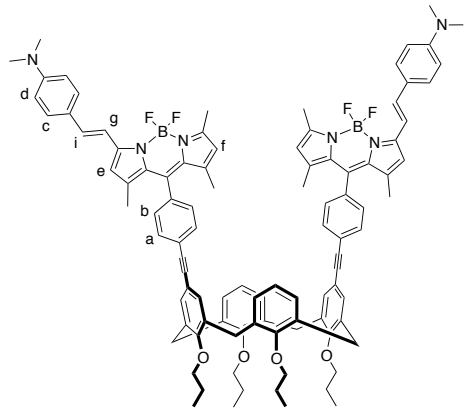

1a

^{1}H NMR (400 MHz, $CDCl_3$) δ (ppm): 7.70 (d, *J* = 8.1 Hz, 4H, H_a), 7.53 (d, *J* = 8.8, 4H, H_c), 7.51 (d, *J* = 16.2 Hz, 2H, H_g), 7.37 (s, 4H, ArH), 7.33 (d, *J* = 8.1 Hz, 4H, H_b), 7.25 (d, *J* = 16.1 Hz, 2H, H_i), 6.71 (d, *J* = 8.8 Hz, 4H, H_d), 6.63 (s, 2H, H_f), 6.32 (t, *J* = 7.5 Hz, 2H, ArH), 6.26 (d, *J* = 7.4 Hz, 4H, ArH), 6.00 (s, 2H, H_e), 4.48 (d, *J* = 13.3 Hz, 4H, Ar*CH*H_{ax}Ar), 4.09 (t, *J* = 7.7 Hz, 4H, OCH_2), 3.73 (t, *J* = 6.8 Hz, 4H, OCH_2), 3.21 (d, *J* = 13.3 Hz, 4H, Ar*CH*H_{eq}Ar), 3.05 (s, 6H, $N(CH_3)_2$), 2.62 (s, 6H, CH_3), 2.03-1.88 (m, 8H, OCH_2CH_2), 1.51 (s, 6H, CH_3), 1.47 (s, 6H, CH_3), 1.13 (t, *J* = 7.4 Hz, 6H, $OCH_2CH_2CH_3$), 0.95 (t, *J* = 7.5 Hz, 6H, $OCH_2CH_2CH_3$).

Compound 1b:

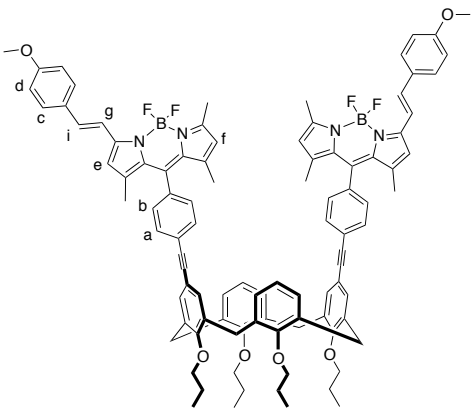

1b

^{1}H NMR (400 MHz, $CDCl_3$) δ (ppm): 7.71 (d, *J* = 8.1 Hz, 4H, H_a), 7.58 (d, *J* = 15.9 Hz, 2H, H_g), 7.57 (d, *J* = 8.7 Hz, 4H, H_c), 7.35 (s, 4H, ArH), 7.33 (d, *J* = 8.2 Hz, 4H, H_b), 7.23 (d, *J* = 16.1 Hz, 2H, H_i), 6.92 (d, *J* = 8.7 Hz, 4H H_d), 6.62 (s, 2H, H_f), 6.33 (t, *J* = 6.1 Hz, 2H, ArH), 6.28 (d, *J* = 6.7 Hz, 4H, ArH), 6.03 (s, 2H, H_e), 4.48 (d, *J* = 13.3 Hz, 4H, ArC*H*H_{ax}Ar), 4.08 (t, *J* = 7.9 Hz, 4H, OCH_2), 3.87 (s, 6H, OCH_3), 3.73 (t, *J* = 6.8 Hz, 4H, OCH_2), 3.21 (d, *J* = 13.4 Hz, 4H, ArC*H*H_{eq}Ar), 2.62 (s, 6H, CH_3), 2.04-1.89 (m, 8H, OCH_2CH_2), 1.52 (s, 6H, CH_3), 1.48 (s, 6H, CH_3), 1.13 (t, *J* = 7.4 Hz, 6H, $OCH_2CH_2CH_3$), 0.95 (t, *J* = 7.5 Hz, 6H, $OCH_2CH_2CH_3$).

Compound 2:

In a Schlenk tube were introduced calix[4]arene **14** (26.2 mg, 0.041 mmol), BODIPY **5** (24.3 mg, 0.043 mmol), BODIPY **6** (24.9 mg, 0.043 mmol), $Pd(PPh_3)_2Cl_2$ (4.3 mg, 0.0061 mmol) and CuI (1.2 mg, 0.0061 mmol) under argon atmosphere, then triethylamine (1 mL) and dry THF (1 mL) were added. The mixture was heated to 70 °C for 3 hours, then the solvent was evaporated under reduced pressure. The residue was purified by preparative TLC plates (toluene/DCM 9:1 and then hexane/DCM 8:2) to afford compound **2** as a dark blue solid (27.6 mg, 0.018 mmol, 43% yield).

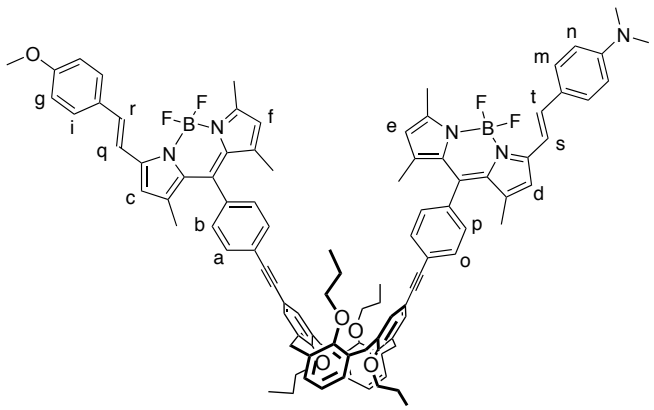

2

Mp: >300 °C. ^{1}H NMR (400 MHz, $CDCl_3$) δ (ppm): 7.65-7.59 (m, 4H, H_a and H_o), 7.56-7.47 (m, 6H, H_m, H_i, H_q and H_s), 7.31 (s, 4H, ArH), 7.29-7.25 (m, 4H, H_b and H_p), 7.23 (d, *J* = 16.0 Hz, 2H, H_r and H_t), 7.06 (d, *J* = 7.5 Hz, 4H, ArH_{calix}), 6.89 (d, *J* = 7.5 Hz, 2H, H_g), 6.83 (t, *J* = 7.5 Hz, 2H, ArH_{calix}), 6.69 (br s, 2H, H_n), 6.59 (two isochronous singlets, 2H,

H_c and H_d), 6.00 (s, 1H, H_f), 5.97 (s, 1H, H_e), 3.86 (s, 3H, OCH_3), 3.81 (s, 8H, $ArCH_2Ar$), 3.58 (t, *J* = 7.3 Hz, 4H, OCH_2), 3.36 (t, *J* = 6.7 Hz, 4H, OCH_2), 3.04 (s, 6H, $N(CH_3)_2$), 2.60 (s, 6H, 2xCH_3), 1.62-1.50 (m, 4H, OCH_2CH_2), 1.49 (s, 6H, 2xCH_3), 1.46 (s, 3H, CH_3), 1.45 (s, 3H, CH_3), 1.43-1.31 (m, 4H, OCH_2CH_2), 0.92 (t, *J* = 7.4 Hz, 6H, $OCH_2CH_2CH_3$), 0.76 (t, *J* = 7.4 Hz, 6H, $OCH_2CH_2CH_3$). ^{13}C NMR (100 MHz, $CDCl_3$) δ (ppm): 160.4, 157.5, 156.9, 154.7, 153.7, 142.6, 142.4, 141.9, 139.1, 136.5, 134.5, 134.3, 133.6, 133.3, 132.0, 131.9, 129.9, 129.3, 129.0, 128.5, 128.3, 124.8, 124.6, 122.0, 121.1, 120.5, 117.9, 117.7, 116.8, 116.09, 116.03, 114.2, 112.0, 91.5, 91.4, 87.1, 87.0, 72.4, 72.2, 55.3, 40.2, 37.8, 22.9, 22.8, 14.97, 14.91, 14.7, 14.6, 14.5, 10.1, 10.1. HR-MS m/z calcd for $C_{99}H_{98}N_5O_5B_2F_4$ [(**2**+H)$^+$] 1534.76902, found 1534.76512.

3.6 References

(1) Schrondinger, E.; English translation: Trimmer, J. D. The Present Situation in Quantum Mechanics: A Translation of Schordinger's "Cat Paradox" Paper. *Proc. Am. Philos. Soc.* **1980**, *124*, 323–338.

(2) Collini, E. Spectroscopic Signatures of Quantum-Coherent Energy Transfer. *Chem. Soc. Rev.* **2013**, *42* (12), 4932–4947.

(3) Ritz, T.; Adem, S.; Schulten, K. A Model for Photoreceptor-Based Magnetoreception in Birds. *Biophys. J.* **2000**, *78* (2), 707–718.

(4) Rodgers, C. T.; Hore, P. J. Chemical Magnetoreception in Birds: The Radical Pair Mechanism. *Proc. Natl. Acad. Sci.* **2009**, *106* (2), 353–360.

(5) Turin, L. A Spectroscopic Mechanism for Primary Olfactory Reception. *Chem. Senses* **1996**, *21* (6), 773–791.

(6) Franco, M. I.; Turin, L.; Mershin, A.; Skoulakis, E. M. C. Molecular Vibration-Sensing Component in Drosophila Melanogaster Olfaction. *Proc. Natl. Acad. Sci.* **2011**, *108* (9), 3797–3802.

(7) Brixner, T.; Stenger, J.; Vaswani, H. M.; Cho, M.; Blankenship, R. E.; Fleming, G. R. Two-Dimensional Spectroscopy of Electronic Couplings in Photosynthesis. *Nature* **2005**, *434* (7033), 625–628.

(8) Engel, G. S.; Calhoun, T. R.; Read, E. L.; Ahn, T. K.; Mančal, T.; Cheng, Y. C.; Blankenship,

R. E.; Fleming, G. R. Evidence for Wavelike Energy Transfer through Quantum Coherence in Photosynthetic Systems. *Nature* **2007**, *446* (7137), 782–786.

(9) Collini, E.; Wong, C. Y.; Wilk, K. E.; Curmi, P. M. G.; Brumer, P.; Scholes, G. D. Coherently Wired Light-Harvesting in Photosynthetic Marine Algae at Ambient Temperature. *Nature* **2010**, *463* (7281), 644–647.

(10) Panitchayangkoon, G.; Hayes, D.; Fransted, K. A.; Caram, J. R.; Harel, E.; Wen, J.; Blankenship, R. E.; Engel, G. S. Long-Lived Quantum Coherence in Photosynthetic Complexes at Physiological Temperature. *Proc. Natl. Acad. Sci.* **2010**, *107* (29), 12766–12770.

(11) Quantum Effects in Biology. In *Quantum Effects in Biology*; Engel, G. S., Plenio, M. B., Mohseni, M., Omar, Y., Eds.; Cambridge University Press: Cambridge, 2014; pp 350–395.

(12) Scholes, G. D. Quantum-Coherent Electronic Energy Transfer: Did Nature Think of It First? *J. Phys. Chem. Lett.* **2010**, *1* (1), 2–8.

(13) Hayes, D.; Griffin, G. B.; Engel, G. S. Engineering Coherence Among Excited States in Synthetic Heterodimer Systems. *Science.* **2013**, *340*, 1431–1434.

(14) Diehl, F. P.; Roos, C.; Duymaz, A.; Lunkenheimer, B.; Köhn, A.; Basché, T. Emergence of Coherence through Variation of Intermolecular Distances in a Series of Molecular Dimers. *J. Phys. Chem. Lett.* **2014**, *5* (2), 262–269.

(15) Butkus, V.; Alster, J.; Bašinskaite, E.; Augulis, R.; Neuhaus, P.; Valkunas, L.; Anderson, H. L.; Abramavicius, D.; Zigmantas, D. Discrimination of Diverse Coherences Allows Identification of Electronic Transitions of a Molecular Nanoring. *J. Phys. Chem. Lett.* **2017**, *8* (10), 2344–2349.

(16) Tosi, I. Model Systems for Artificial Photosynthesis: Calix[4]Arenes Functionalized with Chromophoric Units for Energy and Charge Transfer, Doctorate in Chemical Sciences - Cycle XXVII. Università di Parma, 2014.

(17) Ulrich, G.; Ziessel, R.; Harriman, A. The Chemistry of Fluorescent Bodipy Dyes: Versatility Unsurpassed. *Angew. Chemie - Int. Ed.* **2008**, *47* (7), 1184–1201.

(18) El-Khouly, M. E.; Fukuzumi, S.; D'Souza, F. Photosynthetic Antenna-Reaction Center Mimicry by Using Boron Dipyrromethene Sensitizers. *ChemPhysChem* **2014**, *15* (1), 30–47.

(19) Loudet, A.; Burgess, K. BODIPY Dyes and Their Derivatives: Syntheses and Spectroscopic

Properties. *Chem. Rev.* **2007**, *107* (11), 4891–4932.

(20) Wu, L.; Burgess, K. A New Synthesis of Symmetric Boraindacene (BODIPY) Dyes. *Chem. Commun.* **2008**, No. 40, 4933.

(21) Barton, O. G.; Schmidtmann, M.; Müller, A.; Mattay, J. Diaminotriazine Substituted 1,3-Alternate Calix[4]Arenes. *New J. Chem.* **2004**, *28* (11), 1335–1339.

(22) Baruah, M.; Qin, W.; Flors, C.; Hofkens, J.; Vallée, R. A. L.; Beljonne, D.; Van Der Auweraer, M.; De Borggraeve, W. M.; Boens, N. Solvent and pH Dependent Fluorescent Properties of a Dimethylaminostyryl Borondipyrromethene Dye in Solution. *J. Phys. Chem. A* **2006**, *110* (18), 5998–6009.

(23) Atilgan, S.; Ozdemir, T.; Akkaya, E. U. A Sensitive and Selective Ratiometric Near IR Fluorescent Probe for Zinc Ions Based on the Distyryl - Bodipy Fluorophore. *Org. Lett.* **2008**, *10* (18), 4065–4067.

(24) Chen, J.; Burghart, A.; Wan, C.-W.; Thai, L.; Ortiz, C.; Reibenspies, J.; Burgess, K. Synthesis and Spectroscopic Properties of 2-Ketopyrrole–BF2 Complexes: A New Class of Fluorescent Dye. *Tetrahedron Lett.* **2000**, *41* (14), 2303–2307.

(25) Bura, T.; Hablot, D.; Ziessel, R. Fluorescent Boron Dipyrromethene (Bodipy) Dyes Having Two and Four Vinyl Residues. *Tetrahedron Lett.* **2011**, *52* (18), 2370–2374.

(26) Lee, J. S.; Kang, N. Y.; Yun, K. K.; Samanta, A.; Feng, S.; Hyeong, K. K.; Vendrell, M.; Jung, H. P.; Chang, Y. T. Synthesis of a BODIPY Library and Its Application to the Development of Live Cell Glucagon Imaging Probe. *J. Am. Chem. Soc.* **2009**, *131* (29), 10077–10082.

(27) Ziessel, R.; Ulrich, G.; Harriman, A.; Alamiry, M. A. H.; Stewart, B.; Retailleau, P. Solid-State Gas Sensors Developed from Functional Difluoroboradiazaindacene Dyes. *Chem. - A Eur. J.* **2009**, *15* (6), 1359–1369.

(28) Barnett, J. R.; Andrews, L. J.; Keefer, R. M. Trifluoroacetyl Hypohalites as Aromatic Halogenating Agents. *J. Am. Chem. Soc.* **1972**, *94* (17), 6129–6134.

(29) Horiuchi, A. C.; Satoh, Y. J. A Convenient Procedure for Iodination of Electron-Rich Aromatic Compounds Using Iodine-Copper (II) Acetate. *Bull. Chem. Soc. Jpn.* **1984**, *57* (9), 2691–2692.

(30) Ugozzoli, F.; Casnati, A.; Pochini, A.; Ungaro, R.; Arnaud, F.; Fanni, S.; Schwing, M. J.; Egberink, R. J. M.; Jong, F. de; Reinhoudt, D. N. Synthesis, Complexation, and Membrane Transport Studies of 1,3-Alternate Calix[4]Arene-Crown-6 Conformers: A New Class of Cesium Selective Ionophores. *J. Am. Chem. Soc.* **1995**, *117* (10), 2767–

2777.

(31) He, X.; Yam, V. W. W. A Highly Selective Bifunctional Luminescence Probe for Potassium and Fluoride Ions. *Org. Lett.* **2011**, *13* (9), 2172–2175.

(32) Hennrich, G.; Murillo, M. T.; Prados, P.; Al-Saraierh, H.; El-Dali, A.; Thompson, D. W.; Collins, J.; Georghiou, P. E.; Teshome, A.; Asselberghs, I.; Clays, K. Alkynyl Expanded Donor-Acceptor Calixarenes: Geometry and Second-Order Nonlinear Optical Properties. *Chem. - A Eur. J.* **2007**, *13* (27), 7753–7761.

(33) Tahtaoui, C.; Thomas, C.; Rohmer, F.; Klotz, P.; Duportail, G.; Mély, Y.; Bonnet, D.; Hibert, M. Convenient Method to Access New 4,4-Dialkoxy- and 4,4-Diaryloxy-Diaza-s-Indacene Dyes: Synthesis and Spectroscopic Evaluation. *J. Org. Chem.* **2007**, *72* (1), 269–272.

CHAPTER 4

TOWARDS REVERSIBLE ENERGY TRANSFER TO LANTHANOID IONS MEDIATED BY CALIX[4]ARENES

The work presented in this chapter was carried out at the Department of Chemistry of Curtin University in Perth, Western Australia, during a period of six months.

4.1 Introduction

4.1.1 Lanthanoids

With atomic number ranging from 57 to 71, from lanthanum to lutetium, the fifteen metallic elements of period six in the periodic table are referred to as lanthanides. Following IUPAC nomenclature, however, the preferred designation is lanthanoids, abbreviated as Ln, where the suffix –oid indicates the similarity among a group of elements.[1] Together with Scandium and Yttrium, they are often called *rare earths*, despite the fact that they are not exceptionally rare. Each lanthanoid element is in fact more common in earth's crust than platinum, gold or silver,[2] and the rarest thulium is more abundant than iodine or bismuth. The term *rare earth* is probably dating back to prior World War II, when the availability of these elements was rather limited. Nowadays the availability of pure rare earths is greatly increased, thanks to the improved separation techniques, and the lanthanoids have become an intensively studied set of elements.

Their magnetic and spectroscopic properties make them ideal candidates for several basic and sophisticated applications. Lanthanoid compounds, in fact, play a considerable role in the current high-technology world, being major components, for instance, of electronic devices, optical and telecommunication systems, lasers, magnets, rechargeable batteries and contrast agents for magnetic resonance imaging.[3] Exemplary applications of visible emitters such as Eu^{3+}, Tb^{3+}, Sm^{3+} and Dy^{3+} can be found in light emitting devices (LEDs) and organic light emitting devices (OLEDs),[4,5] not to mention their role in solar energy conversion[6,7] and development of hybrid materials.[8–12] For lanthanoids complexes that display emission in the near-infrared region, the most attractive application is found in the biomedical area,[6,13–15] since near-infrared photons enable deep tissue penetration and are less affected by scattering.[16] The focus of research effort is therefore aimed towards the development of highly luminescent lanthanoid-containing molecular and polymeric compounds.

4.1.2 Properties of the lanthanoids

The chemical and physical behavior of the lanthanoids is mainly governed by the properties of the 4*f* orbitals and their electrons. Their typical electronic configuration is $[Xe]4f^n6s^2$, where lanthanum, cerium, gadolinium, and lutetium constitute an exception following the electronic configuration of $[Xe]4f^{n-1}5d^16s^2$. By removing three electrons the most stable and most common oxidation state of the lanthanoids is formed, *i.e.* the trivalent state in which the electronic configuration is of the general form $[Xe]4f^n$ (n = 0 - 14), with the exceptions of europium, cerium and ytterbium, which possess lower ionization energies for different oxidation states.[17] The 4*f* electrons are effectively shielded from the environment by the completely filled 5*s* and 5*p* orbitals and for this reason they are often termed as *inner core*[18]. As a result, the coordination properties of the lanthanide ions are deeply influenced: the ions are essentially spherical and the 4*f* orbitals are shielded from the ligands, taking no part in chemical bonding. In addition, in contrast to transition metals, the coordination geometries are determined by ligand steric factors as opposed to crystal field effects. Another phenomenon ascribed to the shielding of the 4*f* orbitals is the *lanthanide contraction*, which defines the decrease in the ionic radii of the lanthanoids with increasing atomic number.[19]

One of the properties that make trivalent lanthanoids ions and their complexes so attractive is their line-like emission, generally 100 – 300 cm^{-1} in width, corresponding to intra-4*f* transitions. These transitions are relatively unaffected by the nature of the ligand and the line emitting properties, which result in very pure colours, always occur at the same wavelength indipendently of crystal field effects. In addition, lanthanoid complexes are often characterized by long luminescence lifetimes.[20] Apart from lanthanum and lutetium, for which no *f-f* transition is possible, and gadolinium, for which luminescence is seldomly observed due to the large energy gap between the ground and the first excited state, all the other lanthanoids are luminescent and can

be separated into three groups based on the energy of the transition: UV emitters, visible emitters and near-infrared (NIR) emitters.

The energy levels of the 4*f* orbitals are not degenerate, as shown in **Figure 4.1** for Eu^{3+}, as a consequence of electronic repulsion, spin-orbit coupling and small influences of the ligand field. Among these, the strongest interaction is the electronic repulsion between the electrons, which causes the separation in terms in the order of 10^4 cm^{-1}. Spin-orbit coupling, that is the interaction between the magnetic moments of the electrons due to their spin and the magnetic moments due to their movement around the nucleus, causes a further splitting of the energy levels, in the order of 10^3 cm^{-1}, into the so-called J-states. In a coordination environment, then, the ligand field induces an additional splitting, not very pronounced, due to the inner core nature of the 4*f* electrons.

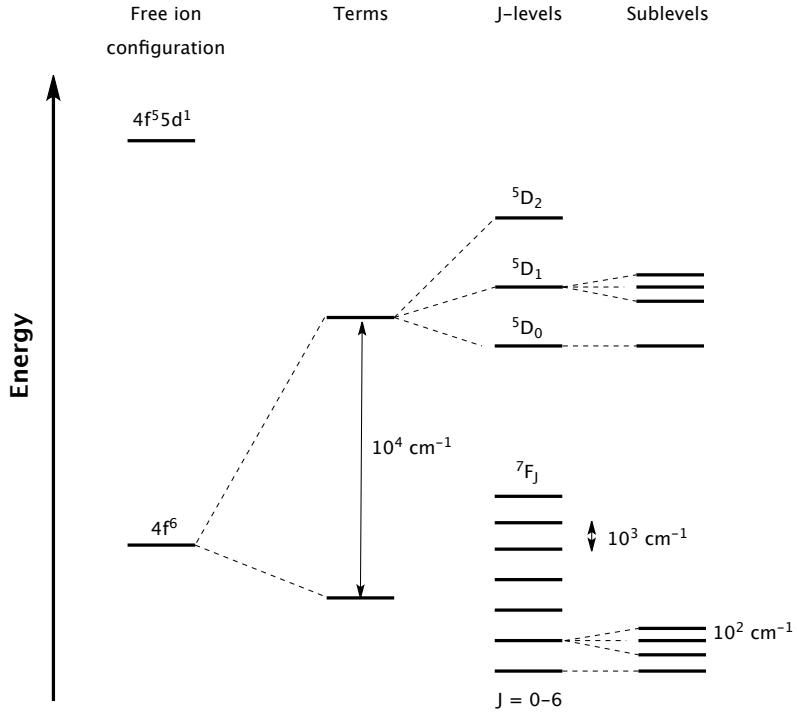

Figure 4.1. Splitting of the 4*f* energy states of Eu^{3+}.

In general, electronic transitions are governed by a set of selection rules. When studying the lanthanoids, two main rules need to be considered: the spin selection

rule and the Laporte selection rule. The first rule asserts that electronic transitions that involve a change in the spin multiplicity are forbidden. This can be relaxed through the spin-orbit coupling, common in species containing heavy atoms. The Laporte selection rule forbids transitions between levels of the same parity. Intrashell transitions, intra-*f* for example, are therefore forbidden. However, in an asymmetric environment these transitions become weakly allowed.

4.1.3 Antenna effect

As explained above, the 4*f*-4*f* transitions are spin and parity forbidden and, as a consequence, the absorption coefficients (ε) of the lanthanoid ions are rather low (tipically less than 10 M^{-1} cm^{-1}), making direct excitation of the metal a difficult and inefficient process. To overcome this disadvantage, lanthanoid luminescence can be photosensitized by a chromophore with greater capacity of absorbing light, through what was defined as the *antenna effect*.[21,22] This effect simply describes the absorption of the electromagnetic radiation, typically in the UV or the visible spectral region, by a sensitizing molecule, usually an organic chromophore, that is capable of transferring the energy to the lanthanoid excited state, resulting in metal-centered emission (**Figure 4.2**).

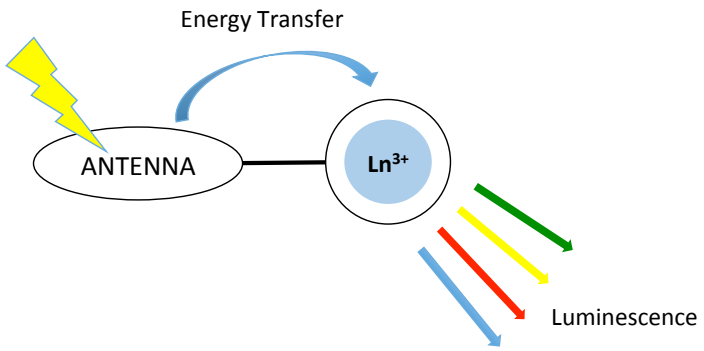

Figure 4.2. Schematic representation of the antenna effect.

More in detail, excitation of the chromophore involves the promotion of an electron to its singlet excited state. From there it can return to the ground state directly (radiatively *via* fluorescence or non-radiatively) or populate the triplet state of the

chromophore by an intersystem crossing mechanism (ISC). Intersystem crossing is a transition between two electronic states with different spin multiplicity, enhanced by the strong spin-orbit coupling induced by the heavy lanthanoid cation. From the triplet state, then, the system can return to the ground state (radiatively *via* phosphorescence or non-radiatively) or perform an energy transfer (ET) step to the excited lanthanoid level that can in turn relax to its ground state giving rise to the typical line-like emission or through a non-radiative pathway (**Figure 4.3**). The energy transfer step involved in the lanthanoid photosensitization is supposed to occur *via* a mixture of the Dexter and Förster mechanisms.[23,24]

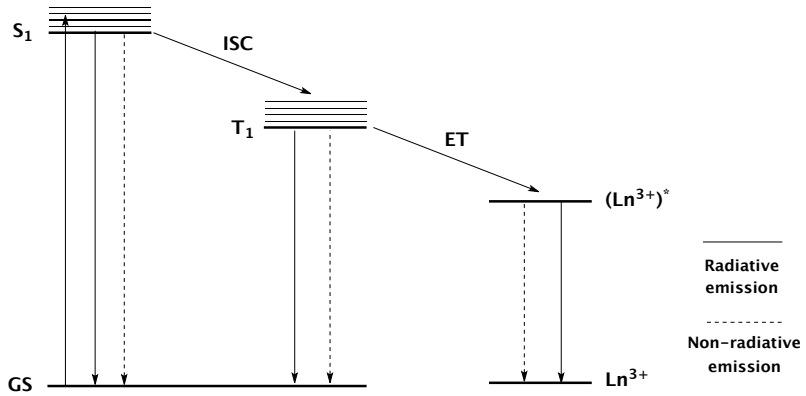

Figure 4.3. Electronic states diagram showing the main processes in the antenna effect.

The triplet state of the sensitizing ligand therefore plays a pivotal role in the antenna effect, even if it is not excluded that the energy transfer to the lanthanoid could take place from the singlet state as well.[25,26] In order to have efficient energy transfer, the antenna should then have triplet state energy levels matching the lanthanoid luminescent states. If, for instance, the energy of the triplet state is lower than the lanthanoid accepting state, the energy transfer will be very unlikely to happen. And if, on the contrary, the energy of the triplet state is too high compared to the lanthanoid emissive state, a rather inefficient transfer will follow. If, finally, the energy gap is too small, an energy back-transfer can occur from the lanthanoid to the ligand and the energy will be lost through the decay of the ligand from its triplet state. The optimal energy gap between the ligand triplet excited state and the emissive state of the

lanthanoid has been reported to be between 3000-3500 cm^{-1} for efficient and irreversible sensitization.[27,28]

Another important parameter to consider when optimizing the sensitization of the lanthanoids is the energy gap between the singlet and triplet excited states of the antenna. In fact, in order to have an efficient intersystem crossing, the energy difference should be greater than 5000 cm^{-1}.[28]

It is important to remember that the antenna should also have a high absorption coefficient and should be in close proximity to the lanthanoid ion, due to the distance dependence of the energy transfer process.

The energies of the singlet and triplet states of an organic molecule can be determined experimentally. One method consists in measuring the chromophore emission in a glassed solution at 77K. The low temperature, in fact, decreases the amount of non-radiative vibrational relaxation, enhancing the radiative emission from the triplet state. Another method involves the addition of Gd^{3+} to the solution, to improve the intersystem crossing by the heavy atom effect. In this case, the energy of the lowest excited state of the lanthanoid is around 30000 cm^{-1}, that is too high to be populated by the antenna effect, and the emission from the triplet state will therefore benefit. The energies of the singlet and the triplet states can be estimated as the highest energy of the emitted fluorescence and phosphorescence light, respectively.

The efficiency of the antenna effect is described by the overall quantum yield (ϕ_{Ln}^{L}), which accounts for the whole process, from absorption of the antenna to emission of the lanthanoid. ϕ_{Ln}^{L} is therefore dependent on the intersystem crossing quantum yield (ϕ_{ISC}), on the energy transfer quantum yield (ϕ_{ET}) and on the intrinsic quantum yield (ϕ_{Ln}^{Ln}) of the lanthanoid excited state and can be written as

$$\phi_{Ln}^{L} = \phi_{ISC} \cdot \phi_{ISC} \cdot \phi_{Ln}^{Ln} \qquad (14)$$

The product of ϕ_{ISC} and ϕ_{ET} gives the sensitization quantum yield (ϕ_{sens}) that is the efficiency of absorption to energy transfer:

$$\phi_{sens} = \phi_{ISC} \cdot \phi_{ET} \qquad (15)$$

ϕ_{Ln}^{Ln} describes the contribution of the lanthanoid luminescence compared to non-radiative decay, once the energy has been transferred to the lanthanoid and can be expressed as

$$\phi_{Ln}^{Ln} = \frac{k_r}{k_r + k_{nr}} \qquad (16)$$

where k_r is the rate constant of spontaneous emission and k_{nr} is the non-radiative rate constant. Similarly, the radiative lifetime (τ_R) describes the lifetime of a lanthanoid excited state in the absence of non-radiative decay pathways

$$\tau_R = \frac{1}{k_r} \qquad (17)$$

while the observed lifetime (τ_{obs}) is defined as the time taken for the lanthanoid excited state to reduce to 1/e of its original value

$$\tau_{obs} = \frac{1}{k_r + k_{nr}} \qquad (18)$$

ϕ_{ISC} and τ_{obs} can be determined experimentally; τ_R can also be measured or calculated from the emission spectrum. By rearranging equation (13) the sensitization efficiency can be determined as

$$\phi_{Ln}^{L} = \phi_{sens} \cdot \frac{\tau_{obs}}{\tau_R} \qquad (19)$$

4.1.4 Coordination chemistry of trivalent lanthanoid ions

As pointed out above, the most common oxidation state of the lanthanoids is the trivalent state. Due to the inner core nature of the 4*f* orbitals, which are not directly available for bonding, lanthanoids are generally assumed to form electrostatic bonds with the coordinated ligands, and thus their only property that contribute to the coordination chemistry is their ionic radius. As a result, the coordination number is dictated by how many ligands can be packed around the central metal ion; the larger the ion, the greater the surface area available for coordination. And as a consequence of the lanthanide contraction, the coordination sphere decreases with increasing atomic number. Lanthanoids possess a wide range of high coordination numbers, generally ranging from 7 to 12, with the most common being 8, 9 and 10. Of course the bulkier the ligand, the higher the surface area covered upon coordination.

Due to the electrostatic nature of the coordination bond, lanthanoids trivalent ions behave as hard acids and thus interact strongly with ligands bearing highly electronegative atoms, such as oxygen and fluorine, or negatively charged groups. Even if the coordination chemistry of lanthanoid ions with oxygen donors remains the most studied and discussed, also neutral nitrogen donors have gained increased interest.[29,30] Among the multitude of literature examples of ligands for lanthanoid ions, pre-organized macrocyclic compounds represent a fairly new field of investigation, since their complexes with lanthanoids have been mostly developed and studied in the last three decades.[31] Several examples of lanthanoid complexes with macrocyclic ligands such as crown ether, cryptands and spherands[17,32,33] are reported, as well as with phthalocyanines and porphyrins.[34,35] Among these, calixarenes represent a highly attractive family of macrocycles, due to the possibility they offer of inserting multiple binding units in a preorganized arrangement.

4.1.5 Calix[4]arene-based ligands for lanthanoids

Several examples of lanthanoid-calix[4]arene complexes are present throughout the literature,[36–41] with particular focus on their use as lanthanide extractants for nuclear waste remediation[42,43] and as MRI contrast agents.[44,45] The calix[4]arene is indeed a versatile platform, rich in oxygen donor atoms and readily accessible in significant scales, in which the lower and the upper rim can be separately and diversely functionalized, in order to modify the coordination characteristics of the ligand and to impart specific properties to the molecule. The nature, number and orientation of the pendant arms attached to the calixarene can be modified, with the aim to meet specific coordination requirements or afford a point of conjugation to other molecules or materials. In addition, the scaffold presents a sufficient flexibility to adapt its conformation to a potential metal guest.

Applications of lanthanoid-calix[4]arene complexes as luminescent compounds and materials have been recently reviewed.[41,46] The most common binding motifs are represented by the introduction on the lower rim of oxygen donors, such as acids,

esters and amides. One of the earliest examples of highly luminescent calix[4]arene-lanthanoid complexes, reported by Ungaro et al.,[47] features four diethylacetamide moieties at the lower rim of p-*tert*-butylcalix[4]arene (**I**, **Figure 4.4**). The sensitization of the lanthanoid occurred through excitation of the phenyl rings of the calixarene, while the diethylamide residues at the lower rim demonstrated a strong binding affinity towards the lanthanoid, together with a good capacity for the encapsulation of the metal that results efficiently shielded from the solvent. Its complex with Tb^{3+} exhibited a remarkably high luminescence quantum yield (Φ = 20%) and a long luminescent lifetime (τ =1.5 ms). Soon after, Sato and Shinkai[48] demonstrated that the triacetamide derivative could still stably retain the lanthanoid ion and exploited the fourth phenolic ring to introduce a different sensitizer (**II**, **Figure 4.4**). In this system, the energy transfer to the lanthanoid can occur both from the phenyl rings of the calixarene and from the phenacyl substituent, yielding good sensitization efficiency also in the case of europium (Φ = 6% for the complex Eu^{3+}/**II**).

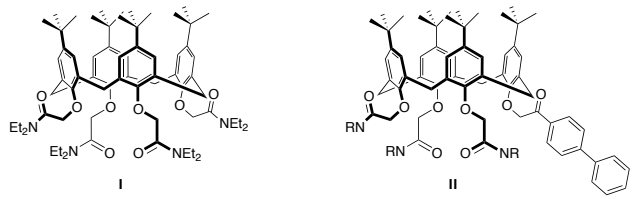

Figure 4.4. Examples of tetra-[47] and triacetamide[48] calix[4]arenes.

Several tetrasubstituted calix[4]arene were subsequently developed and their complexes with the lanthanoids investigated. A nice example is represented by the triscarboxylates **III** and **IV** reported in **Figure 4.5**, designed to form neutral complexes with the trivalent lanthanoids and further functionalized with an antenna moiety through an amide link.[28,49] The triphenylene antenna of calixarene **III** was found to have strong sensitizing ability towards Tb^{3+} and Eu^{3+}. Fluorescein derivative **IV** was designed for the sensitization of NIR emitters and yielded good lifetime values for the complexes with neodymium and erbium (τ = 1.23 μs for Nd^{3+}/**IV**, τ = 1.71 μs for Er^{3+}/**IV**).

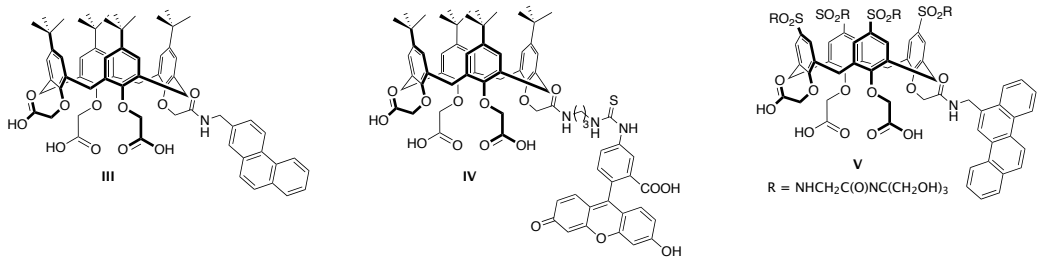

Figure 4.5. Examples of triacid calix[4]arenes functionalized with an antenna moiety.[3,50,51]

Water-soluble derivatives were prepared by functionalization of the upper rim with sulfonamide-linked polyalcohol residues as for calixarene **V** in **Figure 4.5**.[51] In this example a neutral complex with Eu^{3+} is formed, that exhibits strong lanthanide emission thanks to the functionalization with a chrysene moiety.

It may be meaningful to underline that larger calixarenes did not yield better performances in the energy transfer to the lanthanoid, compared to the tetramer derivatives; the only significant quantum yield (Φ = 20%) was obtained for the terbium complex of p-sulfonyl-calix[8]arene.[52]

4.2 Aim of the chapter

This chapter deals with the synthesis of calix[4]arene-based systems functionalized with binding ligands for lanthanoid ions and with suitable antennae for the lanthanoid sensitization. Shinkai[48] in fact demonstrated that the introduction on the calixarene scaffold of a proper sensitizing unit can increase the quantum yield of the complex and induce the energy-transfer luminescence on a wider variety of lanthanoid ions. In particular, he proposed that, depending on the lanthanoid ion, the sensitization could occur *via* two different pathways, as represented in **Figure 4.6**: from the calixarene phenyl rings through their $\pi\pi^*$ electronic transitions or from the additional antenna moiety possessing a lower triplet state.

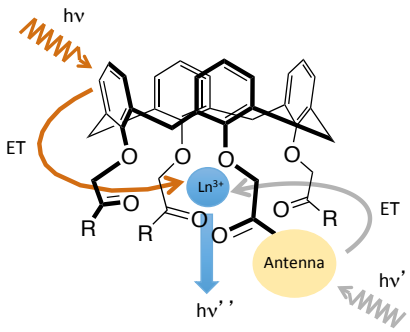

Figure 4.6. Lanthanoid emission sensitization process in a calix[4]arene-antenna system.

With this in mind, we report the synthesis of a small library of calix[4]arene/antenna ligands for lanthanoid ions (**Figure 4.7**). The idea is to gain a good efficiency in the sensitization of visible and NIR emitters, by exploring the potential of different antennae having an excited triplet state matching the lanthanoid 4*f** excited state. In particular, the use of redox reversible antennae, such as flavins, to activate or deactivate the emission of lanthanoid ions upon an external stimulus, will allow us to investigate the potential of on-off switching of lanthanoid luminescence. The calixarenes are functionalized at the lower rim with three or four amide groups, as binding sites for the lanthanoid, while the antenna is linked either on the fourth position of the lower rim or on the upper rim. By exploiting the two rims of the calixarene to anchor the antenna, in fact, it will be possible to investigate the role of the distance between the sensitizer and the lanthanoid ion on the sensitization efficiency. In addition, the anchoring of two antennae at the upper rim would allow us to examine if an increase in the number of sensitizing units leads to a higher efficiency.

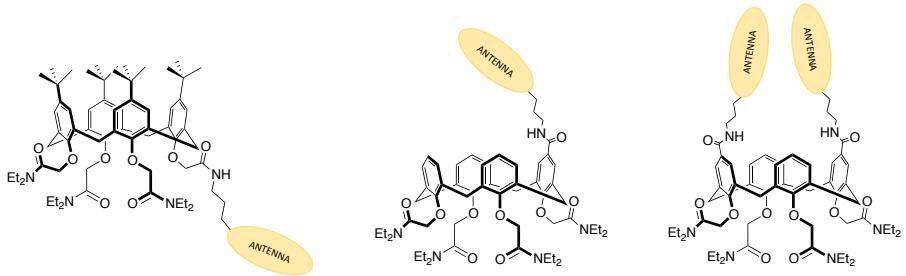

Figure 4.7. Schematic representation of the small library of calix[4]arene-antenna target molecules.

4.3 Results and discussion

4.3.1 Synthesis

4.3.1.1 Antenna chromophores

A suitable redox-reversible chromophore to be anchored to the calixarene scaffold was found in **NpFR1**[53] (**Figure 4.8**).

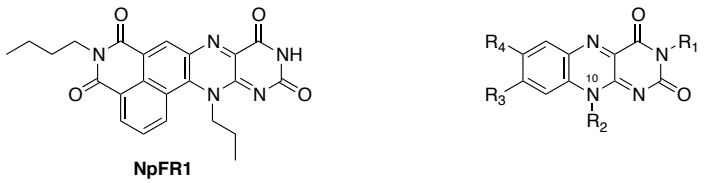

Figure 4.8. Naphthalimide-flavin redox sensor devised by New et al. in 2014[53] (on the left) and generic structure of flavin (on the right).

NpFR1 was designed and synthesized by New et al. in 2014 as a novel fluorescent redox sensor to study oxidative stress in adipocytes. It is based on the structure of flavins (**Figure 4.8**), molecules naturally found within cells, that play a pivotal role in sub-cellular redox processes and are usually fluorescent in oxidized form and non-fluorescent upon reduction.[54] **NpFR1** is different from naturally-occurring flavins for the naphthalimide fluorophore incorporated into the structure, and it presents a non-hydrogen atom at the N-10 position of the flavin, which is required to maintain reversibility of reduction.[55] **NpFR1** was found to be almost non-fluorescent in reduced form, with a 125-fold increase of fluorescence upon oxidation. It was therefore chosen as suitable antenna for the sensitization of lanthanoid ions for its peculiar redox properties and its known and rather straightforward preparation. In addition, the molecule allows several modifications on the structure that permit the introduction of suitable functions for the anchoring to a scaffold (**Figure 4.9**). For synthetic reasons we decided to insert the linker on N-10 and devised compound **23** (**Figure 4.10**).

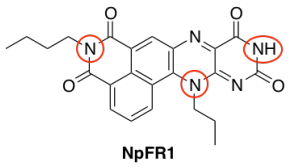

Figure 4.9. Positions for the introduction of modifications on **NpFR1**.

In order to have a comparison among different antennae, we also selected two simpler analogues of **NpFR1** to be anchored to the calixarenes (**25** and **26**, **Figure 4.10**) easily synthesized from intermediates in the synthesis of **23**.

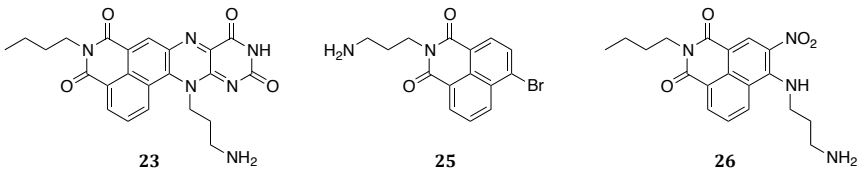

Figure 4.10. Selected chromophores **23**, **25**, **26** to be anchored to the calixarenes.

As reported in **Scheme 4.1**, the synthesis of the flavin-type antenna **23** started with the introduction of N-butylamine on 4-bromo-1,8-naphthalic anhydride **17** to give the alkylated naphthalimide **18** as yellow cristals in 58% yield. Successively, nitration of **18** using sodium nitrate and sulphuric acid as solvent afforded compound **19** in 72% yield. Constitutional isomer **19a** was also formed during the reaction and it was removed from the desired product with a simple recrystallization from EtOH: compound **19**, in fact, precipitated, while its isomer **19a** remained in the mother liquor. The linker, bearing a protected amino group for the anchoring to the calixarenes, was then introduced on **19**: the bromine atom was substituted with freshly prepared mono-Boc-protected diaminopropane **27** to give the bright yellow solid **20** in 63% yield. A portion of compound **20** was deprotected using 3 M HCl in ethyl acetate obtaining antenna **26** that was subsequently used in the reaction with calixarene **4** (see **Scheme 4.3**); the remaining part was subjected to reduction of the nitro group. The first attempt of reduction was made with sodium dithionite under reflux, but the reaction did not go to completion and the mixture was rather complex to purify. Reduction with $NH_2NH_2 \cdot H_2O$ in the

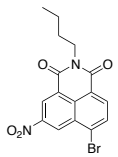

presence of Pd/C was then tried, but also in this case the desired product was not recovered. Eventually, the hydrogenation in presence of Pd/C was successful, affording product **21** in quantitative yield after filtration of the catalyst. Compound **21** was immediately reacted with alloxan monohydrate to give the flavin-type molecule **22**, purified by column chromatography, and obtained pure in 80% yield. Finally, the Boc group was removed with HCl in ethyl acetate to give the final product **23** as a dark yellow solid.

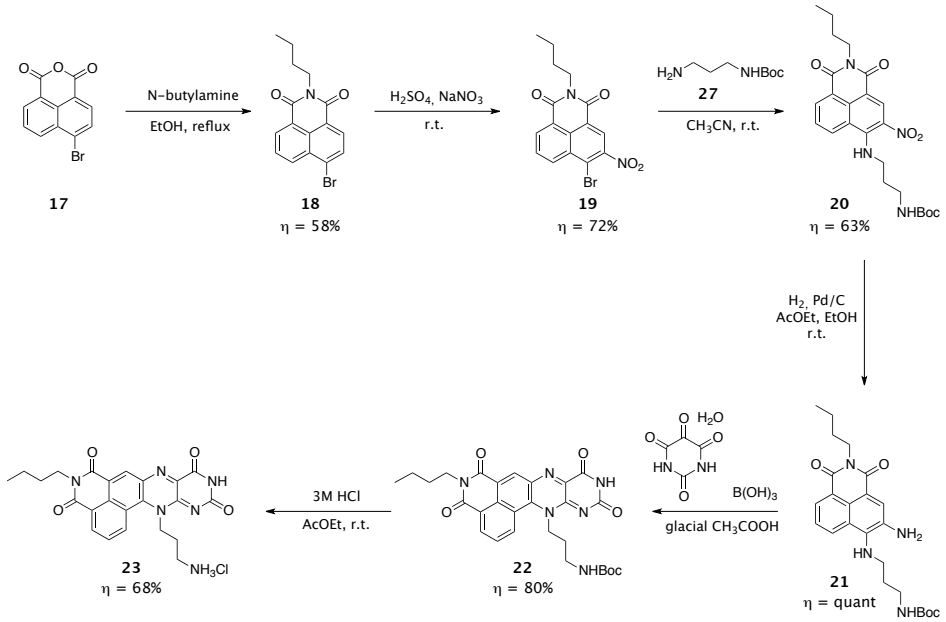

Scheme 4.1. Synthetic pathway for the synthesis of **23**.

To synthesize the third chromophore (**25**), anhydride **17** was reacted with mono-Boc-protected diaminopropane **27**, obtaining **24** in discrete yield. The Boc group was then removed in the same conditions seen above, to give **25** in 91% yield (**Scheme 4.2**).

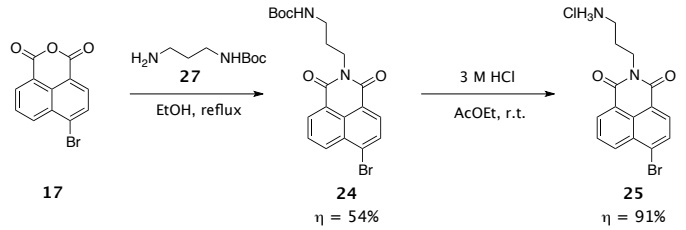

Scheme 4.2. Synthetic pathway for the synthesis of **25**.

4.3.1.2 Calixarenes with the antenna at the lower rim

The synthetic pathway to introduce three amide moieties and one antenna at the lower rim of calix[4]arene is reported in **Scheme 4.3**:

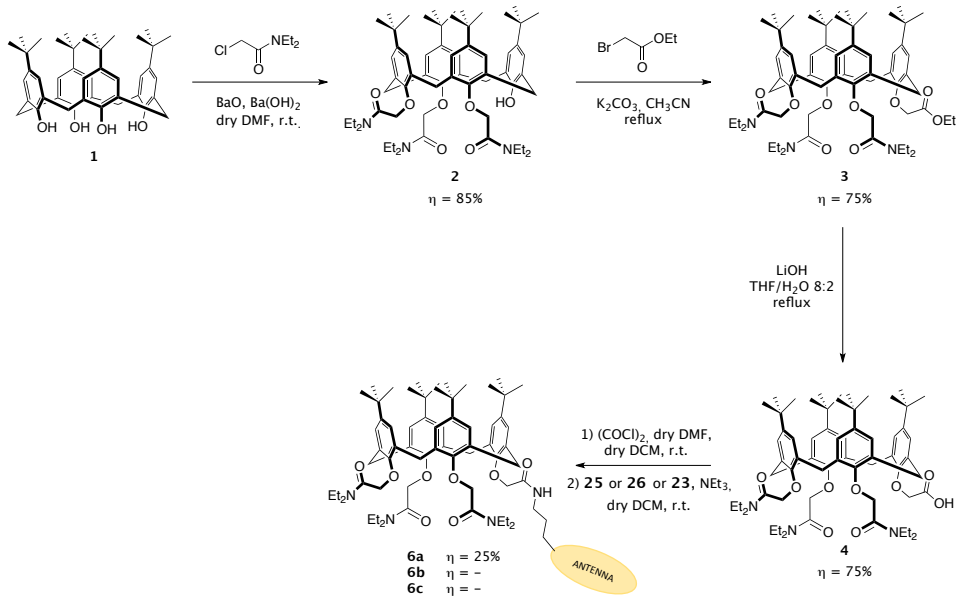

Scheme 4.3. Reaction pathway for the synthesis of the lower rim-functionalized calix[4]arenes.

The first step was adapted from literature protocol:[56] after reaction of p-*tert*-butylcalix[4]arene **1** with BaO, $Ba(OH)_2 \cdot 8H_2O$ and 2-chloro-N,N-diethylacetamide in DMF, compound **2** was isolated through precipitation from 1 M HCl, dissolved in DCM, washed with water and obtained pure in 85% yield without the need of further purification. To alkylate the free phenolic position of **2** with ethyl bromoacetate, different reaction conditions were tried. The classic procedure that employs NaH as a

base in DMF did not give good results, probably because of the tendency of the amide groups at the lower rim of the calixarene to strongly bind alkali ions,[57,58] and thus was abandoned. The second attempt used potassium *tert*-butoxide instead of NaH, in acetone; in this case the product was obtained but it was rather impure and, given the difficulty of column purification of this type of compounds, was discarded. The best results were then achieved with potassium carbonate in acetonitrile at reflux. Compound **3** was obtained in 75% yield after simple trituration in petroleum spirits. Hydrolysis of the ethyl ester **3** was performed using LiOH in a 4:1 mixture of THF/water to give the final compound **4** in 75% yield, without the need of further purification. Compound **4** was then transformed in acyl chloride by using oxalyl chloride in dry DCM with DMF as catalyst, and one of the antennae (**23**, **25**, or **26**) was added using NEt_3 as a base in dry DCM. The reaction with **25** afforded the desired product **6a** in 25% yield after a tricky purification by column chromatography and preparative TLC, due to the tendency of the compound to streak on silica and alumina. Ligand **6a** was fully characterized by 1D and 2D ^{1}H and ^{13}C NMR spectroscopy and by ESI-MS spectrometry. The ^{1}H NMR spectrum of **6a** in $CDCl_3$ (**Figure 4.11**, top) showed the signals of the OCH_2 and of the calixarene bridge all reunited around 4.5 ppm, and the amide NH signal at high values of chemical shift (11.77 ppm). These results were consistent with the formation of a complex with sodium or potassium cations.[59] Several acid washes were thus performed, in order to obtain the free ligand. The comparison between the ^{1}H NMR spectra of **6a** before and after the acid wash is shown in **Figure 4.11**: after the wash the signals of the OCH_2 and of the calixarene bridge become more differentiated and shifted towards 5 ppm, and the amide NH signal results upfield shifted (9.36 ppm).

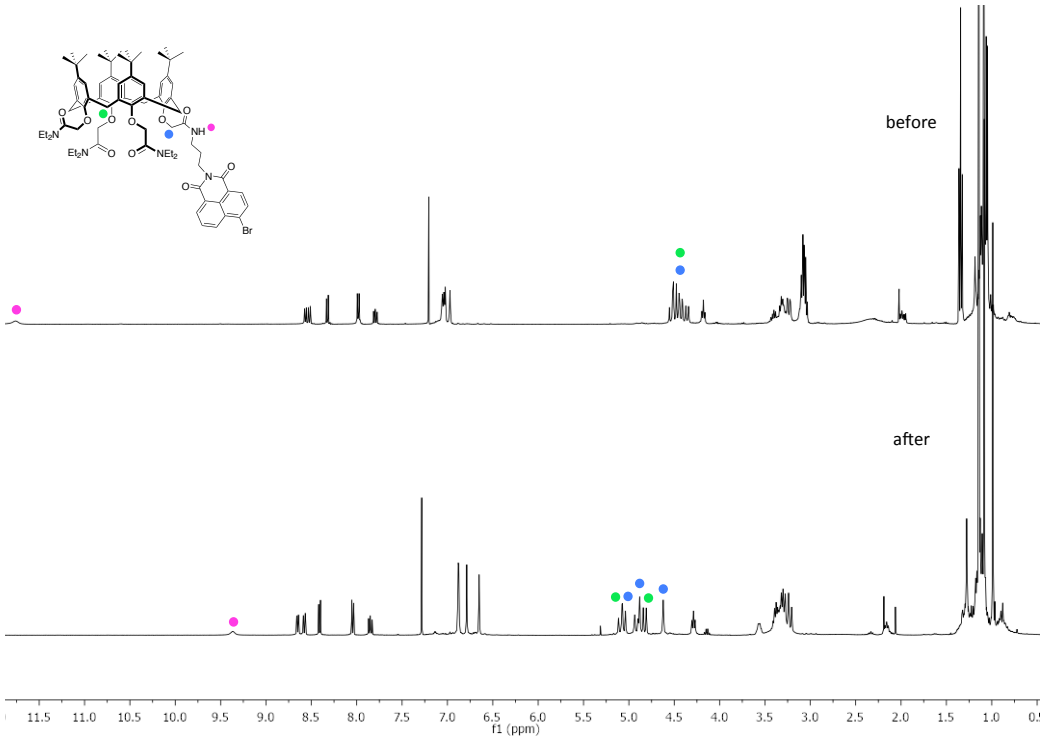

Figure 4.11. Comparison of the ^{1}H NMR spectra ($CDCl_3$, 400 MHz) of **6a** before (top) and after (bottom) the acid wash.

The conjugation reaction between calixarene **4** and antenna **26** was carried out in a 1:1 mixture of dry DCM and dry DMF to help the dissolution of the chromophore. As for **6a**, the purification was long and rather complex but this time the product was not recovered clean. Evidences of the formation of the desired compound **6b** were given by ^{1}H NMR and ESI-MS, but the low amount of isolated product did not allow to proceed further with the purification.

Regarding the reaction of calixarene **4** with **23**, instead, no evidence of the formation of the desired product **6c** was found. The reaction was carried out several times in different conditions but changing the solvent, the temperature and the base did not allow for the isolation of the product even after several attempts of purification of the crude by column chromatography and preparative TLC.

4.3.1.3 Calixarenes with the antenna at the upper rim

The synthetic pathway to functionalize a calix[4]arene with four amide groups at the lower rim and one antenna at the upper rim is reported in **Scheme 4.4**.

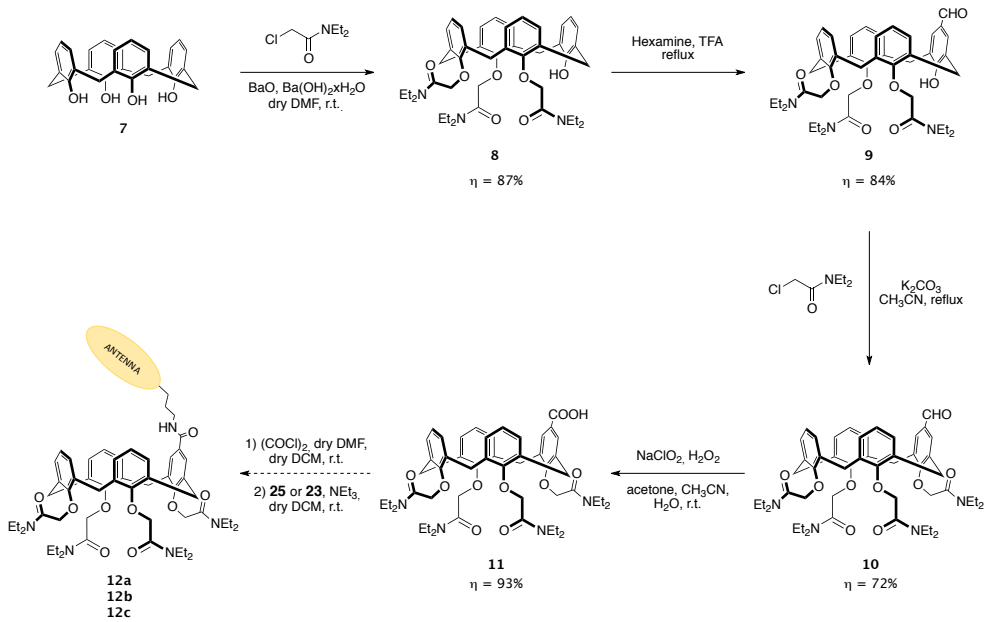

Scheme 4.4. Reaction pathway for the synthesis of the calixarenes with the antenna at the upper rim.

Starting from tetrahydroxycalix[4]arene **7**, three diethylacetamide chains were introduced at the lower rim using the same conditions seen for **2**, obtaining compound **8** in 87% yield without the need of column purification. The greater reactivity of the phenyl ring bearing the hydroxyl group, compared to the alkylated ones, was then exploited to selectively introduce only one formyl moiety on the calixarene. Reaction of **8** with tin (IV) chloride and dichloromethyl methyl ether in dry DCM, however, proceeded very slowly; after purification, a large amount of the starting material was recovered and the isolated product was not clean. Hexamethylenetetramine and TFA under reflux were then used on compound **8** and the monoformylated calix[4]arene **9** was obtained in 84% yield. Compound **9** was then alkylated on the last OH group with 2-chloro-*N*,*N*-diethylacetamide using K_2CO_3 in acetonitrile, to obtain pure product **10** in 72% yield after sonication in a 1:1 petroleum spirits/diethyl ether mixture. The oxidation of the formyl group was achieved by reacting **10** with sodium chlorite and

hydrogen peroxide as scavenger for hypochlorous acid.[60] The reaction proceeded very slowly, 4 days and several additions of oxidants were necessary to obtain the disappearance of the starting material, but in the end monocarboxylic calixarene **11** was obtained in 93% yield and acceptable purity. Reactions of **11** with antennae **25** and **23** to get the final ligands **12a** and **12c**, were tried, but unfortunately, also in this case, no evidence of the formation of the desired products was found. Other reaction conditions will need to be tested in order to obtain the desired calixarene-antenna systems. Reaction with antenna **26** is still to be tried.

The same synthetic pathway as for **11** was followed to obtain the disubstituted calixarene **16** (**Scheme 4.5**). The dialkylation reaction was carried out using K_2CO_3 and KI in acetonitrile and product **13** was obtained in 66% yield after trituration in diethyl ether. For the formylation reaction, hexamethylenetetramine in TFA was used and the pure compound **14** was isolated after column chromatography in 95% yield. The two free phenolic positions were then alkylated with 2-chloro-*N,N*-diethylacetamide using Na_2CO_3 and NaI in acetonitrile and the excess of the alkylating agent was removed by trituration in a 1:1 mixture of petroleum spirits/diethyl ether. The aldehyde oxidation was carried out using $NaClO_2$ with hydrogen peroxide and the final calixarene **16** isolated in 94% yield. The conjugation reaction of compound **16** with antennae **23**, **25** and **26** is foreseen but not yet performed.

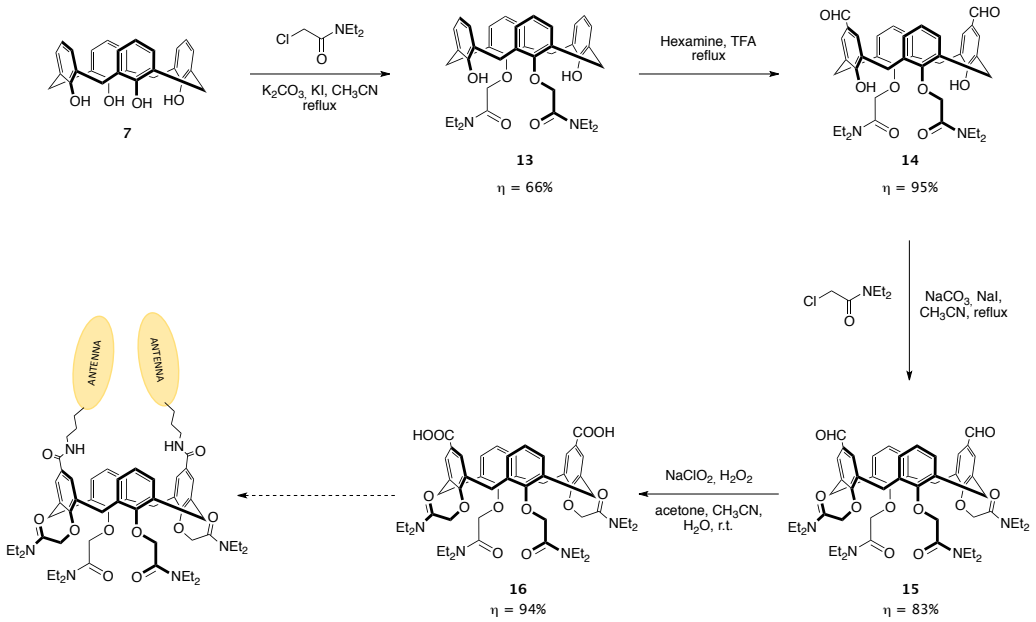

Scheme 4.5. Reaction scheme for the synthesis of diacid calixarene **16**.

4.3.2 Spectroscopic studies

Due to the unfortunate results of the conjugation reactions, only the antenna ligand **6a** could be studied so far. The system itself is complex, due to the presence of two moieties that can act as antenna, as explained in section 4.2. Therefore, calixarene **4** and chromophore **25**, which was deprotonated before measuring all the spectra, were studied, together with **6a**, and used as references. The absorption spectra in DCM of these species are reported in **Figure 4.12**. The absorption profile of **6a** matches the spectroscopic features of **4** and **25**, which display their absorption bands centered at around 280 nm and 350 nm, assigned to $\pi\pi^*$ transitions centered on the phenyl rings of the calixarene and on the naphthalimide ring respectively. The absorption of a solution of ligand **6a** and an excess of Gd^{3+} salt is also reported as a purple line, which presents a small red-shift, compared to the ligand alone, consistent with the formation of a complex between **6a** and the lanthanoid.[61]

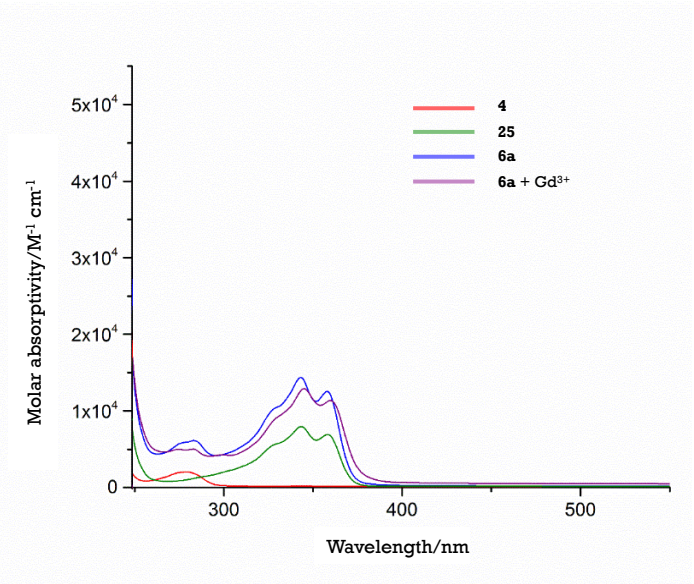

Figure 4.12. Absorption spectra of **4**, **25**, **6a** and **6a** with an excess of Gd^{3+} in DCM.

4.3.2.1 Triplet state measurements

In order to understand the key photophysical properties of the lanthanoid complexes, it is essential to determine where the triplet state of the ligand lies. The energies of the triplet states of **6a**, **4** and **25** were therefore determined from the emission spectra of the compounds in a frozen methanol matrix at 77 K and compared with the ones at 77 K in the presence of Gd^{3+}. The results for **4** and **25** are reported in **Figure 4.13**, in which both excitation and emission spectra are displayed. The emission spectrum of calixarene **4** in frozen methanol presents a broad structureless band spanning the 350 nm to 500 nm spectral region. After addition of an excess of Gd^{3+} the emission profile is exactly the same. The measured lifetime of this band was found to be 65 µs, thus the band was attributed to emission from the triplet state of the calixarene. This finding is in agreement with the fluorescence spectrum of **4** at room temperature, that shows the emission from the singlet state centered at 300 nm. The energy value of the triplet state was calculated from the 0-0 transition, indicated by the asterisk in **Figure 4.13**, and was found to be 25316 cm^{-1}, very similar to the values reported in the literature for calixarenes.[28,61,62]

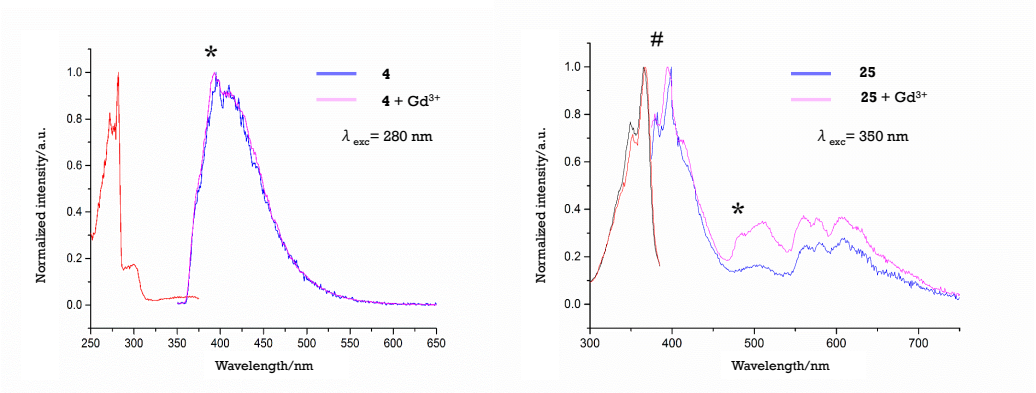

Figure 4.13. Normalized excitation and emission spectra of **4** (λ_{em} = 400 nm; λ_{exc} = 280) and **25** (λ_{em} = 412; λ_{exc} = 350 nm) in methanol at 77 K. The # symbol indicates the 0-0 transition for the singlet excited state; the * symbol indicates the 0-0 transition for the triplet excited state.

The emission spectrum at 77 K of **25** (**Figure 4.13**, right) displays three different bands, centered around 400 nm, 500 nm and 600 nm. The main band, spanning the visible spectral region from 390 nm to 450 nm, was attributed to emission from the singlet of the antenna. After the addition of Gd^{3+}, in fact, this band remains unchanged. On the contrary, the band centered at 500 nm is slightly increased in intensity and was thus attributed to emission from the triplet state, which is enhanced due to the improvement in the efficiency of the ISC as a consequence of the presence of the heavy Gd^{3+} ion. The measured lifetimes confirmed the assignment, yielding a value of 9 µs for the triplet state; lifetime of the singlet state instead could not be measured. The band centered at 600 nm was attributed to the formation of an aggregated state.[63,64] Emission spectra registered at different concentrations (**Figure 4.14**), in fact, showed increased intensity of the band at 600 nm when raising the concentration, whereas the one at 500 nm decreased greatly, probably quenched by aggregation.

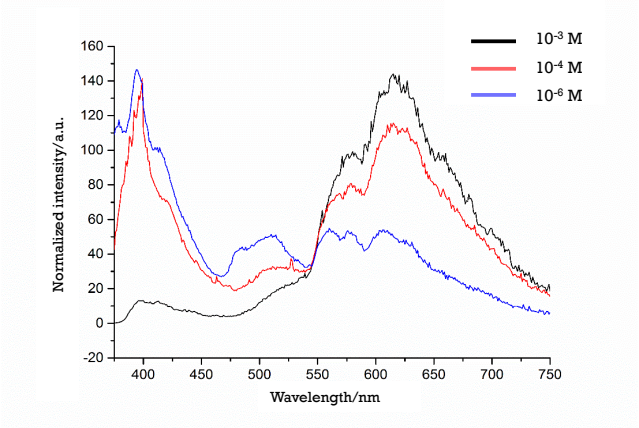

Figure 4.14. Emission spectra (λ_{exc} = 350 nm, MeOH, 77 K) of **25** + Gd^{3+} at different concentrations.

The singlet and triplet state energies of **25** were estimated from the lowest wavelength of each emission band, as shown by the asterisk and the hash mark in **Figure 4.13**, and found to be 26247 cm^{-1} and 20704 cm^{-1}.

Emission spectra of ligand **6a** (**Figure 4.15**) at 77 K were recorded using two different excitation wavelengths, 280 nm for the excitation of the phenyl rings of the calixarene, and 350 nm to selectively excite the antenna chromophore. The emission profiles are basically given by the sum of the emission of the calixarene and the antenna alone.

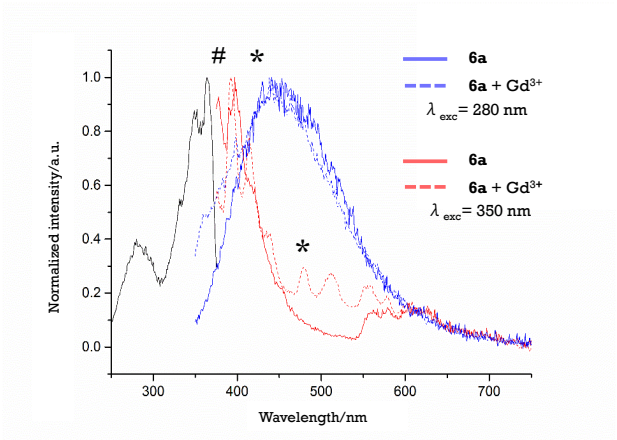

Figure 4.15. Normalized excitation (λ_{em} = 425 nm) and emission spectra (λ_{exc} = 280, 350 nm) of **6a** in methanol at 77 K. The # symbol indicates the 0-0 transition for the singlet excited state; the * symbol indicates the 0-0 transition for the triplet excited state.

By exciting at 280 nm, in fact, the emission profile of the ligand is again given by a broad structureless band spanning the 400 nm to 600 nm spectral region, which is not changed by the addition of Gd^{3+}. The only difference lies in the small red-shift of the band that yields a triplet state energy of 23364 cm^{-1}. Lifetime value at 400 nm is consistent with the lifetime of calixarene **4** triplet state and was found to be 67 μs. Excitation at 350 nm, on the other hand, results in a structured band at 400 nm assigned to the singlet of the antenna, and in the aggregation band at 600 nm. The addition of Gd^{3+} promotes the band at 480 nm, which was therefore assigned to the triplet state of the antenna, whose energy is 20878 cm^{-1}. Lifetime of the triplet state was found to be 500 μs. Emission from ligand **6a** was measured at different concentrations (10^{-3} M, 10^{-4} M, 10^{-5} M, 10^{-6} M) and again the intensity of the aggregation band was found to increase when raising the concentration. Triplet state energy of the aggregated form was estimated to lie around 18000 cm^{-1}.
Emission spectra of **4**, **25** and **6a** at 77 K were measured also in DCM and the values of the triplet states energies were comparable to those calculated in methanol.

After determining the triplet state energies of **4**, **25** and **6a**, calix[4]arene/Ln^{3+} complexes were prepared by adding stoichiometric amounts of the nitrate salts of Tb^{3+}, Eu^{3+} and Yb^{3+} to 10^{-4} M methanol solutions of **4** and **6a**. A graphical representation of the triplet states energies, together with the accepting lanthanoid states, is reported in **Figure 4.16**.

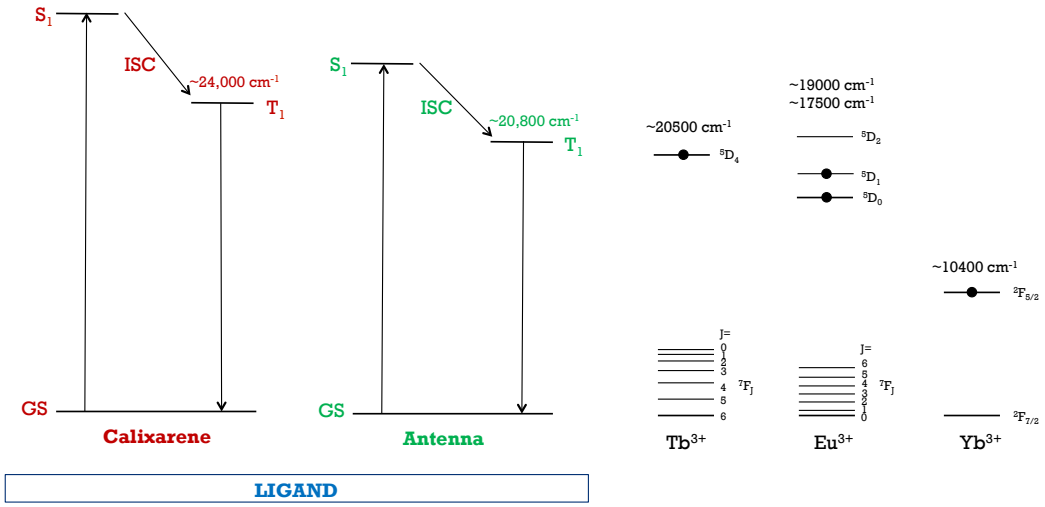

Figure 4.16. Electronic states energies of ligand **6a** and Tb^{3+}, Eu^{3+} and Yb^{3+} ions. Filled circle denotes the emissive states of the lanthanoid with the corresponding energies reported in black.

4.3.2.2 Terbium sensitization

Emission spectra of **4**/Tb^{3+} and **6a**/Tb^{3+} were measured in methanol at room temperature. As foreseeable from the calculated values of the triplet state energies, calixarene **4** is able to efficiently sensitize Tb^{3+} ion (**Figure 4.17**), *via* antenna effect, with an observed lifetime value for the complex of 1.5 ms, in agreement with the findings by Ungaro et al.[62]

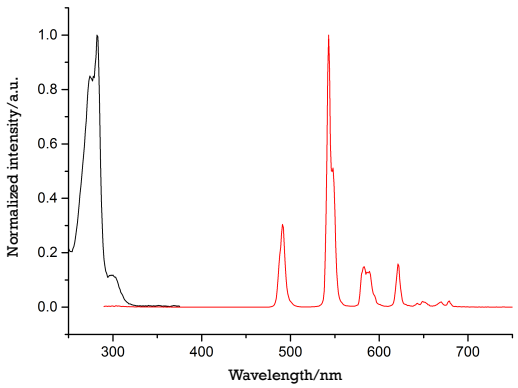

Figure 4.17. Normalized excitation (λ_{em} = 540 nm) and emission spectra (λ_{exc} = 280 nm) of the complex **4**/Tb^{3+} at 298 K.

As for ligand **6a**, when exciting at 280 nm, sensitization is still efficient (green trace in **Figure 4.18)**, for it occurs from the triplet state of the calixarene; the lifetime of the complex was measured to be 1.0 ms, lower compared to the calixarene alone probably because of quenching from the triplet state of the antenna. When exciting at 350 nm, on the other hand, no sensitization occurs, and the emission spectrum of the complex **6a**/Tb^{3+} is mostly given by emission from the antenna. Excitation spectrum measured at λ_{em} = 400 nm (black trace in **Figure 4.18**), in fact, matches the absorption profile of the antenna. The energy gap between the triplet state of the antenna and the accepting state of Tb^{3+} (ΔE ~300 cm^{-1}) is indeed too small to allow for an efficient energy transfer to happen.

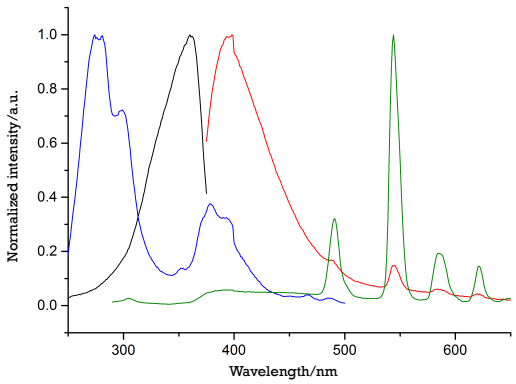

Figure 4.18. Normalized excitation (blue trace, λ_{em} = 540 nm; black trace, λ_{em} = 400 nm) and emission spectra (green trace, λ_{exc} = 280 nm; red trace, λ_{exc} = 350 nm) of the complex **6a**/Tb^{3+} at 298 K.

4.3.2.3 Europium sensitization

Emission spectra of the Eu^{3+} complexes with **4** (**Figure 4.19**) and **6a** (**Figure 4.20**) were measured in methanol, both at room temperature and at 77 K. In the case of **4**/Eu^{3+} typical emission of Eu^{3+} in the visible spectral region was observed. Sensitization was not efficient though as can be seen from **Figure 4.19**: the excitation spectrum measured at room temperature presents the line-like band at 400 nm relative to direct excitation of Eu^{3+}; at 77 K Eu^{3+} emission is clearly masked by the broad emission of the

calixarene, at both excitation wavelengths. The excited state lifetimes at 298 K and 77 K were fitted as biexponential with values of τ = 562 μs (60%), 1.443 μs (40%) and τ = 450 μs (31%), 1.302 μs (69%) respectively. The low sensitization from the calixarene could be ascribed to the formation of charge transfer levels responsible for the deactivation of Eu^{3+} emission *via* a non-radiative process and hence for the quenching of the luminescence emission.[48,61]

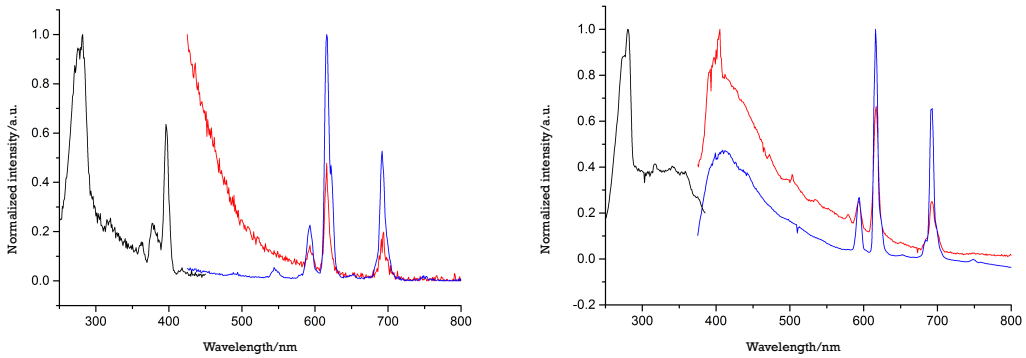

Figure 4.19. Normalized excitation (λ_{em} = 612 nm) and emission spectra (blue trace, λ_{exc} = 280 nm; red trace, λ_{exc} = 350 nm) of the complex **4**/Eu^{3+} at 298 K (on the left) and 77 K (on the right).

In the case of **6a**/Eu^{3+}, triplet state emission is occurring in conjunction with europium emission, demonstrating a not efficient energy transfer from the ligand to the lanthanoid. The excitation spectrum at room temperature shows contribution to europium emission from both calixarene and antenna, whereas at 77 K energy transfer to Eu^{3+} seems to occur only from the antenna. The small energy gap between the triplet state of the antenna and the Eu^{3+} accepting states (ΔE ~1800 cm^{-1} for $^5D_1$, ΔE ~3000 cm^{-1} for $^5D_1$), which is even smaller if we consider the triplet state of the aggregation band (ΔE ~500 cm^{-1}), in fact, allows for energy back-transfer from the lanthanoid to the ligand to happen. At 77 K this phenomenon is slowed down and we see low sensitization from the antenna.

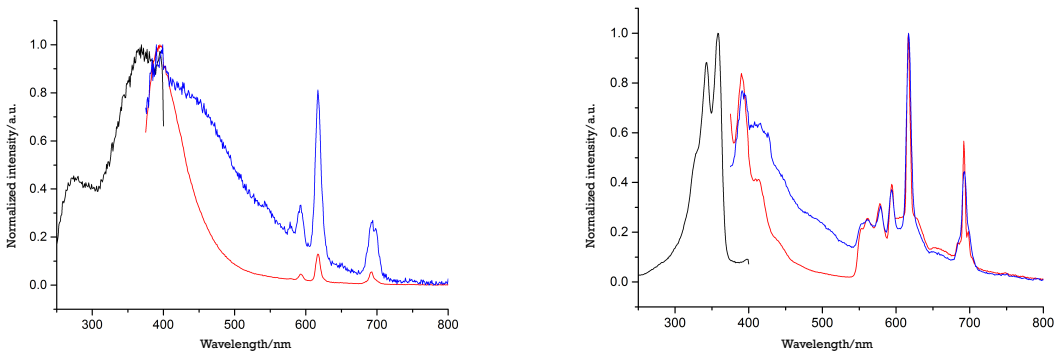

Figure 4.20. Normalized excitation (λ_{em} = 612 nm) and emission spectra (blue trace, λ_{exc} = 280 nm and red trace, λ_{exc} = 350 nm) of the complex **6a**/Eu^{3+} at 298 K (on the left) and 77 K (on the right).

For Eu^{3+} complexes it can be concluded then the introduction of a naphthalimide antenna does not improve the sensitization of the lanthanoid compared to the calixarene alone. Quantum yields could not be measured due to the overlap of the lanthanoid and the ligand emission.

4.3.2.4 Ytterbium sensitization

4/Yb^{3+} and **6a**/Yb^{3+} complexes luminescence was studied at room temperature and at 77 K. Ytterbium emission in the spectral region from 950 nm to 1050 nm was observed for both complexes (**Figure 4.21** and **Figure 4.22**). Ytterbium excited state lies way below the triplet energy level of the ligands, with a gap of about 14000 cm^{-1} for the calixarene and 10000 cm^{-1} for the antenna, far in both cases from the optimal gap for efficient sensitization. In spite of the relevant difference, however, observable emission from the Yb^{3+} species is still detected. In the case of Yb^{3+}, in fact, energy transfer may also occur through a metal-to-ligand charge transfer state,[65–67] that is the energy is travelling from the excited triplet state of the antenna to an energy sublevel of the lanthanoid associated with the reduced Yb^{2+} state. The energy of the ligand-to-metal charge transfer state depends on the ligand coordinated to the metal, but it is typically reported in the region of 19000 cm^{-1},[68] thus resulting in a lower energy gap to the triplet state of the antenna. For **4**/Yb^{3+} the excited state lifetime at 298 K was fit to

a monoexponential function giving a value of τ = 8.75 μs, whereas at 77 K values of τ = 86 μs (30%), 263 μs (70%) best fitted to biexponential decay were found.

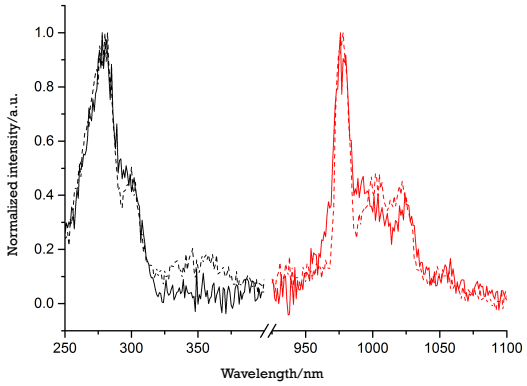

Figure 4.21. Normalized excitation (λ_{em} = 978 nm) and emission spectra of **4**/Yb^{3+}. Full curve: 298 K; dashed curve: 77 K.

As for **6a**/Yb^{3+}, sensitization seems to occur from both the calixarene and the antenna, but, unfortunately, due to the low intensity of the emission bands, quantum yields could not be measured. Also in this case the excited state lifetime at 298 K was fit to a monoexponential function giving a value of τ = 7.51 μs, whereas at 77 K values of τ = 8.7 μs (38%) and 49.99 μs (64%) best fitted to biexponential decay were found.

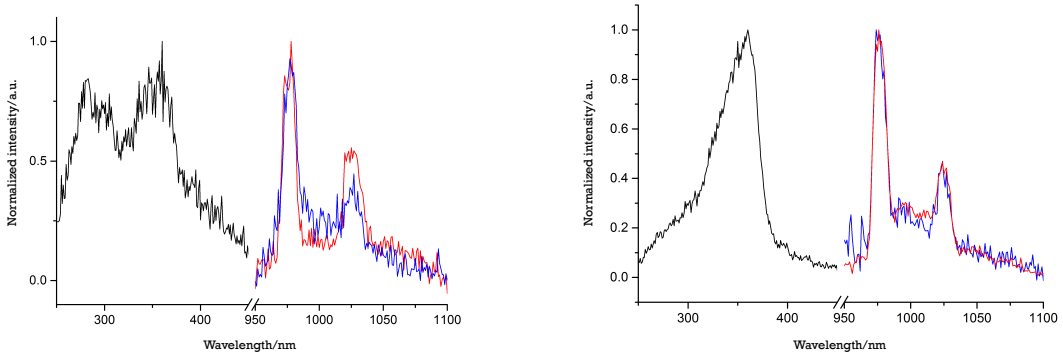

Figure 4.22. Normalized excitation (λ_{em} = 978 nm) and emission spectra (blue trace, λ_{exc} = 280 nm; red trace, λ_{exc} = 350 nm) of the complex **6a**/Yb^{3+} at 298 K (on the left) and 77 K (on the right).

A summary of the observed lifetime values for the complexes at different temperature is reported in **Table 4.1**.

Table 4.1. Observed excited state lifetimes for Tb^{3+}, Eu^{3+} and Yb^{3+} complexes.

	τ_{obs} (μs)	
	298 K	77 K
4/Tb^{3+}	1500	-
6a/Tb^{3+}	1000	-
4/Eu^{3+}	562 (60%); 1443 (40%)	450 (31%); 1302 (69%)
6a/Eu^{3+}	-	410 (4%); 6.8 (94%)
4/Yb^{3+}	8.75	86 (30%); 263 (70%)
6a/Yb^{3+}	7.51	8.7 (36%); 49.99 (64%)

4.4 Concluding remarks

This chapter describes the preliminary work on the synthesis of calix[4]arene-antenna systems for the sensitization of lanthanoid ions. In order to investigate the role of a few factors (*i.e.* the type and number of antennae and the distance between the antenna and the lanthanoid) in the energy transfer process from the antenna to the lanthanoid, a small library of calix[4]arenes functionalized with a binding site for the lanthanoid and one or two antenna chromophore has been designed. Three different antenna chromophores (**23**, **25** and **26**), absorbing in the UV and visible spectral region and functionalized with an amine-terminating spacer for linkage to the calixarene were obtained. Three different calixarenic scaffolds (**4**, **11** and **16**), functionalized with three amide groups at the lower rim for the complexation of the lanthanoid and with one or two carboxylic acid functions as anchoring points for the antenna, were successfully synthesized in high yields. Unfortunately, so far, only one conjugation reaction between antenna and calixarene afforded the desired antenna ligand (the naphthalimide lower rim-functionalized calixarene **6a**). **6a** was studied, together with calixarene **4** and antenna **25** precursors, to identify the triplet states of the system and

investigate the sensitization of Tb^{3+}, Eu^{3+} and Yb^{3+} in solution. Complex **4**/Tb^{3+} was found to be rather emissive with a luminescent lifetime of 1.5 ms, in agreement with the literature data. The antenna, on the other hand, was not able to sensitize terbium, as expected from the measurement of the triplet state energy. Concerning Eu^{3+} and Yb^{3+}, emission from the lanthanoid was observed for all the complexes, indicating sensitization of the lanthanoid by both calixarene **4** and ligand **6a**, with good excited state lifetime values. In all cases, however, emission of the ligand was detected, indicating a not efficient energy transfer to the lanthanoid. By comparison of calixarene **4** and ligand **6a**, it can be concluded that introducing a naphthalimide-type antenna at the lower rim of the calixarene, did not improve the sensitization performances towards Eu^{3+} and Yb^{3+} compared to the calixarene alone. These results should not be seen as discouraging after all, since the project aims to develop several systems with different triplet state energies, to be compared towards diverse lanthanoid ions.

4.5 Experimental section

General information. All moisture sensitive reactions were carried out under a nitrogen or argon atmosphere, using previously oven-dried glassware. All dry solvents were prepared according to standard procedures, distilled before use and stored over 3 or 4 Å molecular sieves. All other reagents were commercial samples and used without further purification. Analytical TLC were performed using prepared plates of silica gel (Merck 60 F-254 on aluminum) and then, according to the functional groups present on the molecules, revealed with UV light or using staining reagents: $FeCl_3$ (1% in H_2O/CH_3OH 1:1), ninhydrin (5% in EtOH) and Brady's reagent. Merck silica gel 60 (40-63 µm) was used for flash chromatography. Preparative TLC were performed using prepared plates of silica gel (Merck 60 F-254 10-12 µm on glass support). Purification of solid compounds was carried out with a Reveleris® X2 flash chromatography system and 40 µm Silica cartridges. ^1H NMR and ^{13}C NMR spectra were recorded on Bruker AV300 and Bruker AV400 spectrometers (observation of ^1H nucleus at 300 MHz and

400 MHz, respectively, and of ^{13}C nucleus at 75 MHz and 100 MHz, respectively) and partially deuterated solvents were used as internal standards to calculate the chemical shifts (δ values in ppm). All ^{13}C NMR spectra were performed with proton decoupling. Electrospray ionization (ESI) mass analysis were performed with a Waters single-quadrupole spectrometer in positive mode using MeOH or CH_3CN as solvents. Melting points were determined on an Electrothermal apparatus in closed capillaries. Absorption spectra were recorded at room temperature using a Perkin Elmer Lambda 35 UV/Vis spectrometer. Uncorrected steady-state emission and excitation spectra were recorded using an Edinburgh FLSP980-stm spectrometer equipped with a 450 W xenon arc lamp, double excitation and emission monochromators, a Peltier cooled Hamamatsu R928P photomultiplier (185–850 nm) and a Hamamatsu R5509-42 photomultiplier for detection of NIR radiation (800-1400 nm). Emission and excitation spectra were corrected for source intensity (lamp and grating) and emission spectral response (detector and grating) by a calibration curve supplied with the instrument. Excited-state decays (τ) for the lanthanides were recorded using a microsecond flashlamp. The goodness of fit was assessed by minimizing the reduced χ^2 function and by visual inspection of the weighted residuals. Experimental uncertainties are estimated to be ±8% for lifetime determinations. Solutions for triplet state measurements were prepared by addition of an excess of the nitrate salt of Gd^{3+} to the compound solution in MeOH and subsequent filtration. To record the luminescence spectra at 77 K, the samples were placed in quartz tubes (2 mm diameter) and inserted in a special quartz Dewar filled with liquid nitrogen. All the solvents used in the preparation of the solutions for the photophysical investigations were of spectrometric grade.

25,27-Bis{[(diethylamino)carbonyl]methoxy}-26,28-dihydroxycalix[4]arene **13**,[69] 5,17-diformyl-25,27-bis{[(diethylamino)carbonyl]methoxy}-26,28-dihydroxycalix[4]arene **14**,[69] 5,17-diformyl-25,26,27,28-tetrakis{[(diethylamino)carbonyl]methoxy}calix[4]arene **15**,[70] (3-Aminopropyl)-

carbamic acid tert-butyl ester **27**,[71] Tert-butyl-[3-(6-bromo-1,3-dioxo-1H-benz[de] isoquinolin-2(3H)-yl)propyl]carbamate **24**,[72] 2-(3-aminopropyl)-6-bromo-1*H*-Benz[*de*] isoquinoline-1,3(2*H*)-dione hydrochloride **25**,[73] 6-Bromo-2-butyl-1H-benzo[de]isoquinoline-1,3(2H)-dione **18**,[74] 6-Bromo-2-butyl-5-nitro-1H-benzo[de]isoquinoline-1,3(2H)-dione **19**[75] were synthesized according to literature procedures.

5,11,17,23-Tetra-*tert*-butyl-25,26,27-tris{[(diethylamino)carbonyl]methoxy}-28-hydroxycalix[4]arene (2):

To a slurry of BaO (0.71 g, 4.63 mmol) and $Ba(OH)_2 \cdot 8H_2O$ (3.41 g, 10.79 mmol) in dry DMF (60 mL), p-*tert*-butylcalix[4]arene **1** (2 g, 3.08 mmol) was added and the mixture stirred at room temperature for 1 h, under an inert atmosphere. A solution of 2-chloro-*N,N*-diethylacetamide (4.2 mL, 30.84 mmol) in dry DMF (20 mL) was then added dropwise, and the mixture stirred overnight. The reaction was quenched by addition of 1M HCl (150 mL) and the white precipitate filtered, dissolved in DCM (100 mL) and washed with water (100 mL). The organic phase was evaporated under reduced pressure and the product obtained as a white powder (3.89 g, 3.94 mmol, 85%). ^{1}H NMR (400 MHz, $CDCl_3$): δ (ppm) = 6.97 (s, 2H, ArH), 6.91 (s, 2H, ArH), 6.72 (d, *J* = 2.6 Hz, 2H, ArH), 6.70 (d, *J* = 2.5 Hz, 2H, ArH), 5.14 (s, 2H, OCH_2), 5.10 (d, *J* = 13.0 Hz, 2H, ArCH_{ax}HAr), 5.07 (d, *J* = 14.0 Hz, 2H, OC*H*H), 4.58 (d, *J* = 14.0 Hz, 2H, OCH*H*), 4.54 (d, *J* = 13.1 Hz, 2H, ArCH_{ax}HAr), 3.51-3.32 (m, 12H, NCH_2), 3.27 (d, *J* = 13.0 Hz, 2H, ArCH_{eq}HAr), 3.22 (d, *J* = 13.2 Hz, 2H, ArCH_{eq}HAr), 1.29-1.10 (m, 18H, NCH_2CH_3), 1.23 [s, 9H, $C(CH_3)_3$], 1.21 [s, 9H, $C(CH_3)_3$], 1.09 [s, 18H, $C(CH_3)_3$]. The compound showed the same physico-chemical properties as those reported in the literature.[56]

5,11,17,23-Tetra-*tert*-butyl-25,26,27-tris{[(diethylamino)carbonyl]methoxy}-28-(ethoxycarbonyl)methoxycalix[4]arene (3):

To a solution of compound **2** (1 g, 1.01 mmol) in acetonitrile (40 mL), K_2CO_3 (0.21 g, 1.52 mmol) and ethyl bromoacetate (0.22 mL, 2.02 mmol) were added. The mixture was refluxed overnight and then the solvent evaporated at reduced pressure. The residue was dissolved in 1M HCl (30 mL), extracted in DCM (2x20 mL) and the

combined organic layers were then evaporated in vacuo. The compound was purified by trituration in petroleum spirits to give a white solid (0.82 g, 0.762 mmol, 75%). Mp: dec > 220°C. ^{1}H NMR (400 MHz, $CDCl_3$): δ (ppm) = 7.10 (s, 4H, ArH), 6.71 (d, *J* = 2.5 Hz, 2H, ArH), 6.61 (d, *J* = 2.5 Hz, 2H, ArH), 5.37 (d, *J* = 12.7 Hz, 2H, ArCH_{ax}HAr), 5.16 (s, 2H, OCH_2), 4.90 (d, *J* = 13.8 Hz, 2H, OC*H*H), 4.71 (d, *J* = 12.8 Hz, 2H, ArCH_{ax}HAr), 4.64 (d, *J* = 13.6 Hz, 2H, OC*H*H), 4.62 (s, 4H, OCH_2), 3.50-3.30 (m, 12H, NCH_2), 3.26 (d, *J* = 12.8 Hz, 2H, ArCH_{eq}HAr), 3.23 (d, *J* = 12.6 Hz, 2H, ArCH_{eq}HAr), 1.29 [s, 18H, $C(CH_3)_3$], 1.22-1.11 (m, 18H, NCH_2CH_3), 0.89 [s, 18H, $C(CH_3)_3$]. ^{13}C NMR (100 MHz, $CDCl_3$) δ (ppm): 171.3, 169.4, 169.2, 168.8, 154.2, 154.1, 153.8, 153.4, 144.7, 144.5, 144.4, 144.2, 133.9, 133.8, 133.6, 133.3, 133.2,125.4, 125.3, 125.2, 125.1, 72.1, 71.8, 71.5, 70.9, 59.9, 41.0, 40.8, 39.9, 39.8, 33.83 , 33.80 , 33.76 , 33.74, 32.2, 32.1, 31.7, 31.6, 31.5,31.4, 31.3, 14.4, 14.2, 13.2, 13.1. ESI-MS: m/z calcd for $C_{66}H_{95}N_3O_9Na$ [(**3**+Na)$^+$] 1096.7, found 1097.3.

5,11,17,23-Tetra-*tert*-butyl-25,26,27-tris{[(diethylamino)carbonyl]methoxy}-28-carboxymethoxycalix[4]arene (4):

Compound **3** (0.72 g, 0.67 mmol) was dissolved in a mixture of THF (48 mL) and water (12 mL) and LiOH (0.032 g, 1.34 mmol) was added. The resulting mixture was refluxed and stirred for 8 hours. The pH was adjusted to 4 with aq 1M HCl and the product extracted with DCM. The organic layer was evaporated to give the desired compound (0.53 g, 0.505 mmol, 75%). Mp: dec > 230 °C. ^{1}H NMR (400 MHz, $CDCl_3$): δ (ppm) = 7.12 (s, 4H, ArH), 6.73 (d, *J* = 2.5 Hz, 2H, ArH), 6.63 (d, *J* = 2.5 Hz, 2H, ArH), 5.39 (d, *J* = 12.7 Hz, 2H, ArCH_{ax}HAr), 5.18 (s, 2H, OCH_2), 4.92 (d, *J* = 13.7 Hz, 2H, OC*H*H), 4.73 (d, *J* = 12.8 Hz, 2H, ArCH_{ax}HAr), 4.66 (d, *J* = 13.6 Hz, 2H, OC*H*H), 4.64 (s, 4H, OCH_2), 3.54-3.30 (m, 12H, NCH_2), 3.26 (d, *J* = 12.8 Hz, 2H, ArCH_{eq}HAr), 3.23 (d, *J* = 12.9 Hz, 2H, ArCH_{eq}HAr), 1.29 [s, 18H, $C(CH_3)_3$], 1.22-1.11 (m, 18H, NCH_2CH_3), 0.91 [s, 18H, $C(CH_3)_3$]. ^{13}C NMR (100 MHz, $CDCl_3$): δ (ppm) = 170.3, 169.9, 167.9, 152.1, 151.4, 146.9, 145.4, 145.2, 135.3, 134.5, 133.0, 132.4, 125.7, 125.6, 125.5, 125.0, 73.5, 72.7, 71.8, 41.3, 40.9, 40.4, 40.0, 34.1, 34.0, 33.7, 31.6, 31.5, 31.5, 31.2, 31.0, 14.3, 14.0, 13.0. ESI-MS: calcd for

$C_{64}H_{91}N_3O_9Na$ [(**4**+Na)$^+$] 1068.7, found 1069.2 (90%); calcd for $C_{64}H_{91}N_3O_9K$ [(**4**+K)$^+$] 1084.6, found 1085.2 (100%).

Compound 6a:

$(COCl)_2$ (99 µL, 1.15 mmol) and dry DMF (30 µL) were added to a solution of calixarene **4** (100 mg, 0.096 mmol) in dry DCM (15 mL), and the mixture was stirred at r.t. for 7 hours. After removing the solvent under reduced pressure, the acyl chloride thus obtained was redissolved in dry DCM (10 mL) and added to a stirred solution of **25** (35 mg, 0.11 mmol) and triethylamine (160 µL, 1.15 mmol) in dry DCM (5 mL). The reaction was allowed to proceed for 17 h, then the mixture was washed twice with 1M HCl and evaporated to dryness under reduced pressure. The yellowish residue was purified by column chromatography (AcOEt to AcOEt/MeOH 8:2) and preparative TLC (AcOEt/MeOH + 1% NEt_3) to give a beige solid (32 mg, 0.024 mmol, 25%).

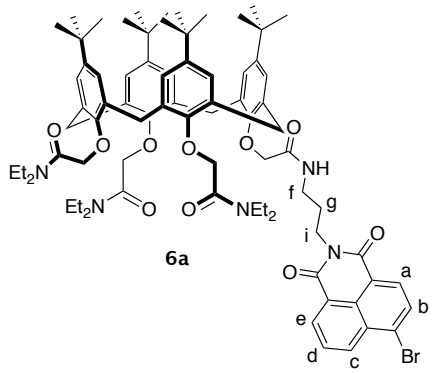

6a

^{1}H NMR (400 MHz, $CDCl_3$): δ (ppm) = 8.65 (dd, *J* = 7.3, 1.1 Hz, 1H, H_e), 8.58 (dd, *J* = 8.5, 1.1 Hz, 1H, H_c), 8.41 (d, *J* = 7.9 Hz, 1H, H_a), 8.04 (d, *J* = 7.9 Hz, 1H, H_b), 7.85 (dd, *J* = 8.5, 7.3 Hz, 1H, H_d), 6.88 (br s, 4H, ArH), 6.79 (s, 2H, ArH), 6.65 (s, 2H, ArH), 5.10 (d, *J* = 15.1 Hz, 2H, OC*H*H), 5.05 (d, *J* = 12.7 Hz, 2H, ArCH_{ax}HAr), 4.92 (d, *J* = 15.0 Hz, 2H, OCH*H*), 4.88 (s, 2H, OCH_2), 4.82 (d, *J* = 13.1 Hz, 2H, ArCH_{ax}HAr), 4.62 (s, 2H, OCH_2), 4.29 (t, *J* = 7.2 Hz, 2H, H_i), 3.57 (br s, 2H, H_f), 3.50-3.10 (m, 20H, NCH_2CH$_3$ and 4xArCHH_{eq}Ar), 2.16 (br s, 2H, H_g); 1.20-1.05 (m, 45H, 3xC$(CH_3)_3$ and NCH$_2$CH_3), 0.99 [s, 9H, C$(CH_3)_3$]. ^{13}C NMR (100 MHz, $CDCl_3$): δ (ppm) = 168.9, 153.1, 145.3, 133.8, 133.7, 133.3, 132.6, 131.9, 131.1, 131.0, 129.0, 128.0, 125.68, 125.61, 125.4, 125.3, 74.2, 71.8, 71.5, 63.5,

53.1, 41.1, 40.9, 40.2, 38.4, 37.5, 33.87, 33.84, 31.9, 31.5, 31.39, 31.31, 29.6, 28.4, 14.1, 14.0, 13.0, 8.2. ESI-MS: m/z calcd for $C_{79}H_{102}N_5O_{10}BrNa$ [(**6a**+Na)$^+$] 1382.7, found 1383.1.

25,26,27-Tris{[(diethylamino)carbonyl]methoxy}-28-hydroxycalix[4]arene (8):

To a slurry of BaO (1.08 g, 7.07 mmol) and $Ba(OH)_2{\cdot}8H_2O$ (5.20 g, 16.49 mmol) in dry DMF (60 mL), 25,26,27,28-tetrahydroxycalix[4]arene **7** (2 g, 4.71 mmol) was added and the mixture stirred at room temperature for 1 hour, under an inert atmosphere. A solution of 2-chloro-*N,N*-diethylacetamide (6.5 mL, 47.12 mmol) in dry DMF (30 mL) was then added dropwise, and the mixture stirred for 17 hours, after which 1M HCl (120 mL) was added. The white precipitate was filtered, dissolved in DCM (100 mL) and washed with water (100 mL). The organic phase was evaporated under reduced pressure and the product obtained as a white powder (3.12 g, 4.09 mmol, 87%). Mp: 195-197 °C. ^{1}H NMR (400 MHz, $CDCl_3$): δ (ppm) = 6.99 (d, *J* = 7.5 Hz, 2H, ArH), 6.94 (d, *J* = 7.5 Hz, 2H, ArH), 6.81 (t, *J* = 7.5 Hz, 1H, ArH), 6.67-6.51 (m, 7H, ArH), 5.17 (s, 2H, OCH_2), 5.14 (d, *J* = 13.3 Hz, 2H, ArCH_{ax}HAr), 4.99 (d, *J* = 13.8 Hz, 2H, OC*H*H), 4.57 (two isochronous doublets, *J* = 14.0 Hz, 4H, ArCH_{ax}HAr and OCH*H*), 3.55-3.37 (m, 12H, NCH_2), 3.32 (d, *J* = 13.2 Hz, 2H, ArCH_{eq}HAr), 3.29 (d, *J* = 13.5 Hz, 2H, ArCH_{eq}HAr), 1.34-1.08 (m, 18H, NCH_2CH_3). ^{13}C NMR (100 MHz, $CDCl_3$): δ (ppm) = 169.2, 167.8, 156.6, 155.3, 153.3, 135.3, 134.2, 133.7, 129.0, 128.9, 128.5, 128.2, 128.1, 123.5, 122.6, 118.2, 72.5, 70.9, 53.5, 41.2, 41.0, 40.1, 40.0, 32.0, 31.3, 31.2, 14.3, 14.2, 13.1, 13.0. ESI-MS: m/z calcd for $C_{46}H_{57}N_3O_7Na$ [(**8**+Na)$^+$] 786.9, found 786.7.

5-Formyl-25,26,27-tris{[(diethylamino)carbonyl]methoxy}-28-hydroxycalix[4]arene (9):

A solution of calixarene **8** (1.035 g, 1.36 mmol) and hexamethylenetetramine (1.14 g, 8.13 mmol) in trifluoroacetic acid (80 mL) was stirred overnight under reflux. 1M HCl (100 mL) and DCM (100 mL) were added to the flask and the mixture stirred at room temperature for 1 hour. The two phases were separated, the aqueous layer extracted with DCM and the organic phases reunited and washed with 1M HCl and then water. The solvent was evaporated at reduced pressure and the yellowish solid (0.90 g, 1.14

mmol, 84%) used in the next step without further purification. ^{1}H NMR (400 MHz, $CDCl_3$): δ (ppm) = 9.73 (s, 1H, CHO), 7.46 (s, 2H, ArH), 6.93 (d, *J* = 7.5 Hz, 2H, ArH), 6.79-6.69 (m, 5H, ArH), 6.68-6.60 (m, 2H, ArH), 5.17 (d, *J* = 13.3 Hz, 2H, ArC*H*$_{ax}$HAr), 5.14 (s, 2H, OCH_2), 5.10 (d, *J* = 14.1 Hz, 2H, OC*H*H), 4.62 (d, *J* = 13.5 Hz, 2H, ArC*H*$_{ax}$HAr), 4.58 (d, *J* = 14.2 Hz, 2H, OCH*H*), 3.59-3.21 (m, 16H, NCH_2 and $ArCH_2Ar$), 1.32-1.09 (m, 18H, NCH_2CH_3). ^{13}C NMR (100 MHz, $CDCl_3$): δ (ppm) = 191.7, 170.1, 168.1, 159.8, 159.1, 158.7, 155.8, 154.7, 135.0, 134.0, 132.5, 131.1, 129.3, 129.2, 129.1, 128.4, 127.7, 124.3, 123.5, 72.3, 70.6, 42.2, 41.2, 41.1, 40.5, 31.5, 31.0, 14.1, 13.9, 12.8, 12.82. ESI-MS: m/z calcd for $C_{47}H_{57}N_3O_8Na$ [(**9**+Na)$^+$] 814.4, found 814.9 (100%); calcd for $C_{47}H_{57}N_3O_8K$ [(**9**+K)$^+$] 830.4, found 830.9 (75%).

5-Formyl-25,26,27,28-tetrakis{[(diethylamino)carbonyl]methoxy}calix[4]arene (10):

To a suspension of calixarene **9** (0.1 g, 0.14 mmol) and K_2CO_3 (0.16 g, 1.13 mmol) in CH_3CN (12 mL), 2-chloro-*N,N*-diethylacetamide (92 µL, 0.63 mmol) was added and the mixture stirred overnight under reflux. The solvent was evaporated under vacuo and the residue partitioned between DCM and 1M HCl. The organic phase was washed twice with water and then dried under reduced pressure. A 1:1 mixture of diethyl ether and petroleum spirits was added to the flask and sonicated for 10' at room temperature. The whitish solid was filtered off to give the desired product in 72% yield (0.095 g, 0.10 mmol). Mp: 180-182 °C. ^{1}H NMR (400 MHz, $CDCl_3$): δ (ppm) = 9.67 (s, 1H, CHO), 7.19 (s, 2H, ArH), 6.78-6.44 (m, 9H, ArH), 5.31 (d, *J* = 13.4 Hz, 2H, ArC*H*$_{ax}$HAr), 5.21 (d, *J* = 13.5 Hz, 2H, ArCH*H*$_{ax}$Ar), 5.11 (s, 2H, OCH_2), 4.95 (d, *J* = 14.4 Hz, 2H, OC*H*H), 4.93 (s, 2H, OCH_2), 4.85 (d, *J* = 14.7 Hz, 2H, OCH*H*), 3.46-3.24 (m, 20H, NCH_2 and $ArCH_2Ar$), 1.25-1.01 (m, 24H, NCH_2CH_3). ^{13}C NMR (100 MHz, $CDCl_3$): δ (ppm) = 191.7, 168.6, 168.5, 168.1, 162.1, 156.1, 136.1, 134.9, 134.8, 134.1, 131.1, 130.5, 129.0, 128.6, 128.5, 122.9, 122.7, 71.7, 71.6, 41.2, 40.9, 40.2, 40.1, 31.9, 31.7, 14.2, 13.1. ESI-MS: m/z calcd for $C_{53}H_{68}N_4O_9Na$ [(**10**+Na)$^+$] 927.5, found 928.0.

5-Carboxy-25,26,27,28-tetrakis{[(diethylamino)carbonyl]methoxy}calix[4]arene (11):

To a solution of calixarene **10** (180 mg, 0.20 mmol) in a 1:1 mixture of chloroform and acetonitrile (6 mL), a 30% solution of hydrogen peroxide (68 µL, 0.60 mmol) and

sodium phosphate monobasic buffer (pH = 4,3) were added. A solution of sodium chlorite (36 mg, 0.40 mmol) in water (3 mL) was then added dropwise. After stirring the mixture overnight at room temperature, hydrogen peroxide (68 µL, 0.60 mmol) and sodium chlorite (36 mg, 0.40 mmol) were added together with 30 µL of 32% HCl to lower the pH, and the mixture was stirred overnight. The reaction was quenched by evaporating the organic solvents and then adding 1M HCl to the residue. The aqueous layer was extracted with DCM and the organic phase dried under reduced pressure to afford the desired compound without further purification (172 mg, 0.187 mmol, 93%). ^{1}H NMR (400 MHz, $CDCl_3$): δ (ppm) = 7.55 (s, 2H, ArH), 6.82-6.64 (m, 3H, ArH), 6.70-6.57 (m, 6H, ArH), 5.24 (d, *J* = 13.5 Hz, 2H, ArCHH_{ax}Ar), 5.18 (d, *J* = 13.5 Hz, 2H, ArCHH_{ax}Ar), 5.16 (s, 2H, OCH_2), 5.03 (s, 2H, OCH_2), 4.96-4.87 (m, 4H, OCH_2), 3.43-3.24 (m, 20H, NCH_2 and 2xArCHH_{eq}Ar), 1.25-1.04 (m, 24H, NCH_2CH_3). ^{13}C NMR (100 MHz, $CDCl_3$): δ (ppm) = 170.3, 168.8, 168.5, 168.4, 161.3, 156.4, 156.0, 135.4, 135.1, 134.8, 134.5, 133.9, 130.9, 128.7, 128.5, 123.1, 122.8, 122.5, 77.2, 71.7, 71.4, 41.0, 40.1, 31.8, 31.7, 14.2, 13.0. ESI-MS: m/z calcd for $C_{53}H_{68}N_4O_{10}Na$ [(**11**+Na)$^+$] 943.5, found 944.2.

5,17-Dicarboxy-25,26,27,28-tetrakis{[(diethylamino)carbonyl]methoxy}calix[4]arene (16):

To a solution of calixarene **15** (100 mg, 0.11 mmol) in a 1:1 mixture of chloroform and acetonitrile (4 mL), a 30% solution of hydrogen peroxide (49 µL, 0.44 mmol) and sodium phosphate monobasic buffer (pH = 4,3) were added. A solution of sodium chlorite (29 mg, 0.33 mmol) in water (2 mL) was then added dropwise. After stirring the mixture overnight at room temperature, hydrogen peroxide (49 µL, 0.44 mmol) and sodium chlorite (29 mg, 0.33 mmol) were added together with 30 µL of 32% HCl to lower the pH, and the mixture was stirred overnight. The day after half equivalents of hydrogen peroxide and sodium chlorite were added and the mixture stirred overnight. The reaction was quenched by evaporating the organic solvents and then adding 1M HCl to the residue. The aqueous layer was extracted with DCM and the organic phase dried under reduced pressure to afford the desired compound without further purification (99 mg, 0.103 mmol, 94%). ^{1}H NMR (400 MHz, $CDCl_3$): δ (ppm) = 12.90 (br

s, 2H, COOH), 7.16 (d, *J* = 7.4 Hz, 4H, ArH), 7.01 (t, *J* = 7.4 Hz, 2H, ArH), 6.84 (s, 4H, ArH), 5.24 (d, *J* = 13.8 Hz, 4H, ArC*H*H_{ax}Ar), 5.11 (s, 4H, OCH_2), 4.71 (s, 4H, OCH_2), 3.46-3.28 (m, 16H, NCH_2), 3.26 (d, *J* = 14.2 Hz, 4H, ArCH*H*$_{eq}$Ar), 1.26-0.98 (m, 24H, NCH_2CH_3). ^{13}C NMR (100 MHz, $CDCl_3$): δ (ppm) = 171.9, 169.2, 167.4, 160.2, 156.9, 135.9, 133.6, 130.1, 129.7, 123.6, 123.0, 71.7, 70.9, 41.1, 40.9, 40.3, 39.9, 31.7, 14.3, 13.0. ESI-MS: m/z calcd for $C_{54}H_{68}N_4O_{12}Na$ [(**15**+Na)$^+$] 987.5, found 988.0.

***Tert*-butyl-(3-((2-butyl-5-nitro-1,3-dioxo-2,3-dihydro-1*H*-benzo[*de*]isoquinolin-6-yl)amino)propyl)carbamate (20):**

To a suspension of **19** (843 mg, 2.24 mmol) in acetonitrile (90 mL) (3-Aminopropyl)-carbamic acid tert-butyl ester **24** (1.17 g, 6.71 mmol) was added and the mixture stirred under nitrogen for 1 hour before removing the solvent at reduced pressure. The crude product was recrystallised from EtOH to give an orange solid (658 mg, 1.40 mmol, 63%).

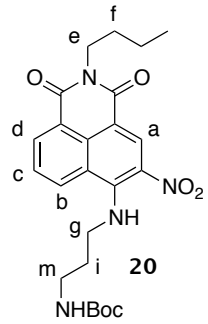

Mp: 133-134 °C. ^{1}H NMR (400 MHz, $CDCl_3$): δ (ppm) = 9.30 (s, 1H, H_a), 8.70 (dd, *J* = 7.5, 1.1 Hz, 1H, H_d), 8.67 (dd, *J* = 8.7, 1.2 Hz, 1H, H_b), 7.71 (dd, *J* = 8.6, 7.4 Hz, 1H, H_c), 4.66 (br s, 1H, NHBoc), 4.18 (t, *J* = 7.4 Hz, 2H, H_e), 4.01 (t, *J* = 6.9 Hz, 2H, H_g), 3.35 (q, *J* = 6.4 Hz, 2H, H_m), 2.05 (quin, *J* = 6.6 Hz, 2H, H_i), 1.77-1.68 (m, 2H, H_f), 1.51-1.41 (m, 2H, CH_2CH_3), 1.41 [s, 9H, $C(CH_3)_3$], 1.00 (t, *J* = 7.4 Hz, 3H, CH_2CH_3). ^{13}C NMR (100 MHz, $CDCl_3$): δ (ppm) = 163.7, 162.6, 156.1, 150.6, 133.8, 133.1, 132.5, 130.3, 129.7, 125.5, 123.4, 123.3, 111.4, 48.1, 40.3, 37.7, 32.3, 30.1, 28.3, 20.3, 13.8. ESI-MS: m/z calcd for $C_{24}H_{30}N_4O_6Na$ [(**20**+Na)$^+$] 493.2, found 493.4.

***Tert*-butyl-(3-((5-amino-2-butyl-1,3-dioxo-2,3-dihydro-1*H*-benzo[*de*]isoquinolin-6-yl)amino)propyl)carbamate (21):**

To a solution of **20** (102 mg, 0.217 mmol) in a 4:1 mixture of AcOEt/EtOH (5 mL), Pd/C (20 mg) was added and the suspension stirred for 24 hours under an atmosphere of hydrogen, after which it was filtered on celite and the filtrate evaporated under vacuum. The product was used in the next step immediately without further purification (93 mg, 0.211 mmol, quantitative).

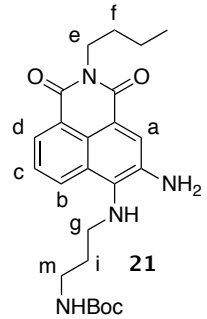

Mp: 156-157 °C. ^{1}H NMR (400 MHz, $CDCl_3$): δ (ppm) = 8.38 (d, *J* = 7.1 Hz, 1H, H_d), 8.36 (d, *J* = 6.6, Hz, 1H, H_b), 8.11 (s, 1H, H_a), 7.63 (dd, *J* = 7.3, 7.4 Hz, 1H, H_c), 4.80 (br s, 1H, NHBoc), 4.17 (t, *J* = 7.4 Hz, 2H, H_e), 3.46-3.39 (m, 2H, H_m), 3.29 (t, *J* = 6.6 Hz, 2H, H_g), 1.84 (quin, *J* = 6.2 Hz, 2H, H_i), 1.78-1.66 (m, 2H, H_f), 1.52 [s, 9H, $C(CH_3)_3$], 1.50-1.41 (m, 2H, CH_2CH_3), 0.99 (t, *J* = 7.4 Hz, 3H, CH_2CH_3). ^{13}C NMR (100 MHz, $CDCl_3$): δ (ppm) = 164.8, 164.2, 137.7, 127.6, 127.3, 126.1, 123.9, 123.04, 122.79, 79.82, 43.67, 40.06, 37.35, 31.95, 30.28, 28.47, 28.43, 20.41, 20.29, 13.88, 13.76. ESI-MS: m/z calcd for $C_{24}H_{32}N_4O_4$ [(**21**+H)$^+$] 441.5, found 441.5.

Compound 22:

To a suspension of **21** (621 mg, 1.41 mmol) in glacial acetic acid (30 mL), alloxan monohydrate (248 mg, 1.55 mmol) and boric acid (113 mg, 1.83 mmol) were added. After stirring for 3 hours at room temperature, the suspension was filtered and washed with water. The filtrate was extracted twice with DCM and the solvent evaporated under vacuum. The two solids were reunited and purified by column chromatography (DCM to DCM/MeOH 9:1) to give a yellow solid in 80% yield (617 mg, 1.13 mmol).

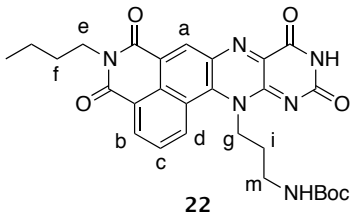

22

Mp: 183-184 °C. ^{1}H NMR (400 MHz, $CDCl_3$): δ (ppm) = 9.25 (s, 1H, H_a), 9.08 (d, *J* = 8.8 Hz, 1H, H_b), 8.92 (d, *J* = 7.3, Hz, 1H, H_d), 8.70 (br s, 1H, CONHCO), 8.11 (dd, *J* = 8.8, 7.4 Hz, 1H, H_c), 5.01 (br s, 1H, NHBoc), 4.98 (br s, 2H, H_g), 4.22 (t, *J* = 7.7 Hz, 2H, H_e), 3.50 (t, *J* = 6.5 Hz, 2H, H_m), 2.73 (br s, 2H, H_i), 1.80 (quin, *J* = 7.6 Hz, 2H, H_f), 1.50-1.41 (m, 2H, CH_2CH_3), 1.47 [s, 9H, $C(CH_3)_3$], 1.02 (t, *J* = 7.4 Hz, 3H, CH_2CH_3). ^{13}C NMR (100 MHz, $CDCl_3$): δ (ppm) = 163.0, 161.8, 158.7, 156.5, 154.9, 152.6, 137.7, 136.7, 134.6, 134.4, 134.2, 132.0, 131.7, 128.2, 124.3, 122.0, 121.5, 52.1, 42.1, 40.7, 30.0, 28.4, 27.9, 20.36, 13.7, 11.2. ESI-MS: m/z calcd for $C_{28}H_{30}N_6O_6Na$ [(**22**+Na)$^+$] 569.2, found 569.4.

Compound 23:

Compound **22** (800 mg, 1.46 mmol) was suspended in AcOEt (10 mL), 3M HCl was added (4 mL) and the mixture was stirred at 60°C for 3 hours, after which the solvent was evaporated under vacuum. The product (592 mg, 1.23 mmol, 84%) did not require further purification.

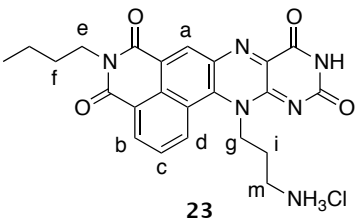

23

Mp: dec > 285 °C. ^{1}H NMR (400 MHz, dmso-*d6*): δ (ppm) = 11.75 (s, 1H, CONHCO), 8.89 (d, *J* = 8.8 Hz, 1H, H_b), 8.78 (d, *J* = 8.0 Hz, 1H, H_d), 8.76 (s, 1H, H_a), 8.13 (t, *J* = 8.0 Hz, 1H, H_c), 8.00 (br s, 3H, NH_3^+), 4.78 (t, *J* = 7.4 Hz, 2H, H_g), 4.08 (t, *J* = 7.4 Hz, 2H, H_e), 3.17-2.99 (m, 2H, H_m), 2.60 (br s, 2H, H_i), 1.65 (quin, *J* = 7.5 Hz, 2H, H_f), 1.38 (quin, *J* = 7.4 Hz, 2H, CH_2CH_3), 0.94 (t, *J* = 7.4 Hz, 3H, CH_2CH_3). ^{13}C NMR (100 MHz, dmso-*d6*): δ (ppm) = 163.5, 162.4, 160.0, 155.9, 153.5, 139.5, 137.2, 133.8, 133.4, 133.2, 132.8, 130.8, 128.6, 123.7, 121.9, 120.9, 50.6, 37.0, 29.9, 25.4, 20.2, 14.1. ESI-MS: m/z calcd for $C_{23}H_{22}N_3O_4Cl$ [(**23**-Cl)$^+$] 447.2, found 447.4.

6-((3-aminopropyl)amino)-2-butyl-5-nitro-1*H*-benzo[*de*]isoquinoline-1,3(2*H*)-dione hydrochloride (26):

Compound **20** (300 mg, 0.64 mmol) was suspended in AcOEt (5 mL), 3M HCl was added (2 mL) and the mixture was stirred at 60°C for 3 hours, after which the solvent was evaporated under vacuum. The product (250 mg, 0.62 mmol, quantitative) did not require further purification.

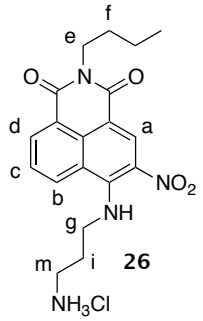

Mp: dec > 244 °C. ^{1}H NMR (400 MHz, dmso-*d6*): δ (ppm) = 9.16 (br s, 1H, NH), 8.97 (d, *J* = 8.4 Hz, 1H, H_d), 8.82 (s, 1H, H_a), 8.59 (d, *J* = 7.4, Hz, 1H, H_b), 7.85 (br s, 4H, H_c and NH_3^+), 4.03 (t, *J* = 6.2 Hz, 2H, H_e), 3.66 (br s, 2H, H_g), 2.86 (br s, 2H, H_m), 2.07 (quin, *J* = 6.7 Hz, 2H, H_i), 1.60 (quin, *J* = 7.5 Hz, 2H, H_f), 1.34 (sex, *J* = 7.6 Hz, 2H, CH_2CH_3), 0.92 (t, *J* = 7.3 Hz, 3H, CH_2CH_3). ^{13}C NMR (100 MHz, dmso-*d6*): δ (ppm) = 163.5, 162.5, 133.4, 132.8, 131.1, 130.4, 129.6, 129.5, 126.9, 126.8, 124.0, 122.8, 46.2, 39.4, 36.8, 30.1, 27.8, 20.2, 14.2. ESI-MS: m/z calcd for $C_{19}H_{23}N_4O_4Cl$ [(**26**-Cl)$^+$] 371.2, found 371.4.

4.6 References

(1) International Union of Pure and Applied Chemistry. *Nomenclature of Inorganic Chemistry: IUPAC Recomendations*; Connelly, N. G., Damhus, T., Hartshorn, R. M., T., H. A., Eds.; RSC Publishing, 2005.

(2) Castor, S. B.; Hedrick, J. B. *Rare Earth Elements*, 7th ed.; Society for mining, metallurgy, and exploration, Littleton, Colorado, 2006.

(3) Bünzli, J. C. G.; Eliseeva, S. V. Photophysics of Lanthanoid Coordination Compounds. *Compr. Inorg. Chem. II* **2013**, *8*, 339–398.

(4) Weiss, C. J.; Marks, T. J. Organo-f-Element Catalysts for Efficient and Highly Selective Hydroalkoxylation and Hydrothiolation. *Dalt. Trans.* **2010**, *39* (29), 6576–6588.

(5) De Bettencourt-Dias, A. Lanthanide-Based Emitting Materials in Light-Emitting Diodes. *J. Chem. Soc. Dalt. Trans.* **2007**, No. 22, 2229–2241.

(6) Bünzli, J. C. G.; Eliseeva, S. V. Lanthanide NIR Luminescence for Telecommunications, Bioanalyses and Solar Energy Conversion. *J. Rare Earths* **2010**, *28* (6), 824–842.

(7) Van Der Ende, B. M.; Aarts, L.; Meijerink, A. Lanthanide Ions as Spectral Converters for Solar Cells. *Phys. Chem. Chem. Phys.* **2009**, *11* (47), 11081–11095.

(8) Binnemans, K. Lanthanide-Based Luminescent Hybrid Materials. *Chem. Rev.* **2009**, *109*, 4283–4374.

(9) Feng, J.; Zhang, H. Hybrid Materials Based on Lanthanide Organic Complexes: A Review. *Chem. Soc. Rev.* **2013**, *42* (1), 387–410.

(10) Stanley, J. M.; Holliday, B. J. Luminescent Lanthanide-Containing Metallopolymers. *Coord. Chem. Rev.* **2012**, *256* (15–16), 1520–1530.

(11) Ennis, B. W.; Muzzioli, S.; Reid, B. L.; D'Alessio, D. M.; Stagni, S.; Brown, D. H.; Ogden, M. I.; Massi, M. Recyclable Calix[4]Arene-Lanthanoid Luminescent Hybrid Materials with Color-Tuning and Color-Switching Properties. *Dalt. Trans.* **2013**, *42* (19), 6894–6901.

(12) Driscoll, C. R.; Reid, B. L.; McIldowie, M. J.; Muzzioli, S.; Nealon, G. L.; Skelton, B. W.; Stagni, S.; Brown, D. H.; Massi, M.; Ogden, M. I. A "Plug-and-Play" Approach to the Preparation of Transparent Luminescent Hybrid Materials Based on Poly(Methyl Methacrylate), a Calix[4]Arene Cross-Linking Agent, and Terbium Ions. *Chem. Commun.* **2011**, *47* (13), 3876–3878.

(13) Faulkner, S.; Pope, S. J. A.; Burton-Pye, B. P. Lanthanide Complexes for Luminescence

Imaging Applications. *Appl. Spectrosc. Rev.* **2005**, *40* (1), 1–31.

(14) Eliseeva, S. V.; Bünzli, J. C. G. Lanthanide Luminescence for Functional Materials and Bio-Sciences. *Chem. Soc. Rev.* **2010**, *39* (1), 189–227.

(15) Amoroso, A. J.; Pope, S. J. A. Using Lanthanide Ions in Molecular Bioimaging. *Chem. Soc. Rev.* **2015**, *44* (14), 4723–4742.

(16) Frangioni, J. V. In Vivo Near-Infrared Fluorescence Imaging. *Curr. Opin. Chem. Biol.* **2003**, *7* (5), 626–634.

(17) Leonard, J. P.; Nolan, C. B.; Stomeo, F.; Gunnlaugsson, T. Photochemistry and Photophysics of Coordination Compounds II; Balzani, V., Campagna, S., Eds.; Springer Berlin Heidelberg: Berlin, Heidelberg, 2007; pp 1–43.

(18) de Bettencourt-Dias, A. Lanthanides: Electronic Structure. *Encycl. Inorg. Bioinorg. Chem.* **2012**.

(19) Cotton, S. *Lanthanide and Actinide Chemistry and Spectroscopy*; John Wiley & Sons, Ltd., 2006.

(20) Bünzli, J. C. G.; Eliseeva, S. V. Intriguing Aspects of Lanthanide Luminescence. *Chem. Sci.* **2013**, *4* (5), 1939–1949.

(21) Sabbatini, N.; Perathoner, S.; Balzani, V.; Alpha, B.; Lehn, J.-M. Antenna Effect in Eu3+ and Tb3+ Cryptates. In *Supramolecular Photochemistry*; Balzani, V., Ed.; Springer Netherlands: Dordrecht, 1987; pp 187–206.

(22) Lehn, J.-M. Antenna Effect. *Angew. Chemie Int. Ed. English* **1990**, *29*, 1304–1319.

(23) de Bettencourt-Dias, A. Lumin. Lanthan. Ions Coord. Compd. Nanomater. In *Lumin. Lanthan. Ions Coord. Compd. Nanomater.*; de Bettencourt-Dias, A., Ed.; John Wiley & Sons, Ltd., 2014; pp 1–48.

(24) Bünzli, J. C. G.; Eliseeva, S. V. *Photophysics of Lanthanoid Coordination Compounds*; 2013; Vol. 8.

(25) Kleinerman, M. Energy Migration in Lanthanide Chelates. *J. Chem. Phys.* **1969**, *51* (6), 2370–2381.

(26) Lazarides, T.; Alamiry, M. A. H.; Adams, H.; Pope, S. J. A.; Faulkner, S.; Weinstein, J. A.; Ward, M. D. Anthracene as a Sensitiser for Near-Infrared Luminescence in Complexes of Nd(III), Er(III) and Yb(III): An Unexpected Sensitisation Mechanism Based on Electron Transfer. *J. Chem. Soc. Dalt. Trans.* **2007**, No. 15, 1484–1491.

(27) Latva, M.; Takalo, H.; Mukkala, V.-M.; Matachescu, C.; Rodríguez-Ubis, J. C.; Kankare, J.

Correlation between the Lowest Triplet State Energy Level of the Ligand and Lanthanide(III) Luminescence Quantum Yield. *J. Lumin.* **1997**, *75* (2), 149–169.

(28) Steemers, F. J.; Verboom, W.; Reinhoudt, D. N.; van der Tol, E. B.; Verhoeven, J. W. New Sensitizer-Modified Calix[4]Arenes Enabling Near-UV Excitation of Complexed Luminescent Lanthanide Ions. *J. Am. Chem. Soc.* **1995**, *117* (37), 9408–9414.

(29) Giraud, M.; Andreiadis, E. S.; Fisyuk, A. S.; Demadrille, R.; Pécaut, J.; Imbert, D.; Mazzanti, M. Efficient Sensitization of Lanthanide Luminescence by Tetrazole-Based Polydentate Ligands. *Inorg. Chem.* **2008**, *47* (10), 3952–3954.

(30) De Bettencourt-Dias, A.; Barber, P. S.; Viswanathan, S. Aromatic N-Donor Ligands as Chelators and Sensitizers of Lanthanide Ion Emission. *Coord. Chem. Rev.* **2014**, *273–274*, 165–200.

(31) Sastri, V. S.; Bünzli, J.-C.; Rao, V. R.; Rayudu, G. V. S.; Perumareddi, J. R. Chapter 4 - Lanthanide and Macrocyclic Complexes. **2003**, 259–374.

(32) Sabbatini, N.; Guardigli, M.; Lehn, J.-M. Luminescent Lanthanide Complexes as Photochemical Supramolecular Devices. *Coord. Chem. Rev.* **1993**, *123* (1), 201–228.

(33) Bünzli, J.-C. G.; Piguet, C. Taking Advantage of Luminescent Lanthanide Ions. *Chem. Soc. Rev.* **2005**, *34* (12), 1048.

(34) Buchler, J. W.; Kihn-Botulinski, M.; de Cian, A.; Fischer, J.; Weiss, R.; Paulus, H. Cerium(IV) Bis(Octaethylporphyrinate) and Dicerium(III) Tris(Octaethylporphyrinate): Parents of a New Family of Lanthanoid Double-Decker and Triple-Decker Molecules. *J. Am. Chem. Soc.* **1986**, *108* (13), 3652–3659.

(35) Atsushi, S. Efficient Chirality Transcription Utilizing a Cerium(IV) Double Decker Porphyrin: A Prototype for Development of a Molecular Memory System. *J. Chem. Soc. Perkin Trans. I* **1999**, 3259–3264.

(36) Baldini, L.; Sansone, F.; Casnati, A.; Ungaro, R. Calixarenes in Molecular Recognition. In *Supramolecular Chemistry*; American Cancer Society, 2012.

(37) Georgiev, E. M.; Roundhill, D. M. An Assessment of Calixarene Amides as Potential Magnetic Resonance Imaging Enhancement Agents for Gadolinium(III). *Inorganica Chim. Acta* **1997**, *258* (1), 93–96.

(38) Lincheneau, C.; Quinlan, E.; Kitchen, J. A.; McCabe, T.; Matthews, S. E.; Gunnlaugsson, T. Delayed Lanthanide Luminescent Tb(III) Complexes Formed from Lower Rim Amide Functionalised Calix[4]Arenes. *Supramolecular Chemistry*. Taylor & Francis 2013, pp

869–880.

(39) Ogden, M. I.; Skelton, B. W.; White, A. H. Synthesis and Structural Studies of a Lanthanide Complex of a Calix[4]Arene Tris-Amide. *Comptes Rendus Chim.* **2005**, *8* (2), 181–187.

(40) Casnati, a; Sansone, F.; Sartori, a; Prodi, L.; Montalti, M.; Zaccheroni, N.; Ugozzoli, F.; Ungaro, R. Quinoline-Containing Calixarene Fluoroionophores: A Combined NMR, Photophysical and Modeling Study. *European J. Org. Chem.* **2003**, No. 8, 1475–1485.

(41) Massi, M.; Ogden, M. I. Luminescent Lanthanoid Calixarene Complexes and Materials. *Materials (Basel).* **2017**, *10* (12).

(42) Matthews, S. E.; Parzuchowski, P.; Garcia-Carrera, A.; Grüttner, C.; Dozol, J. F.; Böhmer, V. Extraction of Lanthanides and Actinides by a Magnetically Assisted Chemical Separation Technique Based on CMPO-Calix[4]Arenes. *Chem. Commun.* **2001**, *3* (5), 417–418.

(43) Barboso, S.; Garcia-Carrera, A.; Matthews, S. E.; Arnaud-Neu F.; Böhmer, V.; Dozol, J.-F.; Rouquette, H.; Schwing-Weill, M.-J. Calix[4]Arenes with CMPO Functions at the Narrow Rim. Synthesis and Extraction Properties. *J. Chem. Soc. Perkin Trans. II* **1999**, *4*, 719.

(44) Schühle, D. T.; Schatz, J.; Laurent, S.; Vander Elst, L.; Muller, R. N.; Stuart, M. C. A.; Peters, J. A. Calix[4]Arenes as Molecular Platforms for Magnetic Resonance Imaging (MRI) Contrast Agents. *Chem. - A Eur. J.* **2009**, *15* (13), 3290–3296.

(45) Aime, S.; Barge, A.; Botta, M.; Casnati, A.; Fragai, M.; Luchinat, C.; Ungaro, R. A Calix[4]Arene GdIII Complex Endowed with High Stability, Relaxivity, and Binding Affinity to Serum Albumin. *Angew. Chemie - Int. Ed.* **2001**, *40* (24), 4737–4739.

(46) Wang, Y.; Wang, L. Application and Luminescent Properties of the Complexes of Lanthanide Ions Based on Calixarene Derivatives. *Prog. Chem.* **2010**, *22*, 427–432.

(47) Sabbatini, N.; Guardigli, M.; Mecati, A.; Balzani, V.; Ungaro, R.; Ghidini, E.; Casnati, A.; Pochini, A. Encapsulation of Lanthanide Ions in Calixarene Receptors. A Strongly Luminescent Terbium(3+) Complex. *J. Chem. Soc. Chem. Commun.* **1990**, No. 12, 878–879.

(48) Sato, N.; Shinkai, S. Energy-Transfer Luminescence of Lanthanide Ions Encapsulated in Sensitizer-Modified Calix[41arenes. *J. Chem. Soc.-Perkin Trans. 2* **1993**, 621–624.

(49) Oude Wolbers, M. P.; Van Veggel, F. C. J. M.; Peters, F. G. A.; Van Beelen, E. S. E.; Hofstraat, J. W.; Geurts, F. A. J.; Reinhoudt, D. N. Sensitized Near-Infrared Emission

from Nd3+ and Er3+ Complexes of Fluorescein-Bearing Calix[4]Arene Cages. *Chem. - A Eur. J.* **1998**, *4* (5), 772–780.

(50) Eliseeva, S. V.; Bünzli, J.-C. G. Rare Earths: Jewels for Functional Materials of the Future. *New J. Chem.* **2011**, *35* (6), 1165.

(51) Steemers, F. J.; Meuris, H. G.; Verboom, W.; Reinhoudt, D. N.; Van der Tol, E. B.; Verhoeven, J. W. Water-Soluble Neutral Calix[4]Arene-Lanthanide Complexes: Synthesis and Luminescence Properties. *J. Org. Chem.* **1997**, *62* (13), 4229–4235.

(52) Sato, N.; Yoshida, I.; Shinkai, S. Energy-Transfer Luminescence of Lanthanide Ions Complexed with Water-Soluble Calix[n]Arenes. *Chem. Lett.* **1993**, *22* (7), 1261–1264.

(53) Yeow, J.; Kaur, A.; Anscomb, M. D.; New, E. J. A Novel Flavin Derivative Reveals the Impact of Glucose on Oxidative Stress in Adipocytes. *Chem. Commun.* **2014**, *50* (60), 8181–8184.

(54) Visser, A.; Ghisla, S.; Massey, V.; Muller, F.; Veeger, C. Fluorescence Properties of Reduced Flavins and Flavoproteins. *Eur. J. Biochem.* **1979**, *101* (1), 13–21.

(55) Grodowski, M. S.; Veyret, B.; Weiss, K. Photochemistry of Flavins. II. Photophysical Properties of Alloxazines Ans Isoalloxazines. *Photochem. Photobiol.* **1977**, *26* (4), 341–352.

(56) Ogden, M. I.; Skelton, B. W.; White, A. H. Syntheses, Structural Studies and Solution Properties of Iron Complexes of Some Amide-Substituted Calixarenes. *J. Chem. Soc. Dalt. Trans.* **2001**, No. 20, 3073–3077.

(57) Arduini, A.; Ghidini, E.; Pochini, A.; Ungaro, R.; Andreetti, G. D.; Calestani, G.; Ugozzoli, F. P-t-Butylcalix[4]Arene Tetra-Acetamide: A New Strong Receptor for Alkali Cations. *J. Incl. Phenom.* **1988**, *6* (2), 119–134.

(58) Creaven, B. S.; Donlon, D. F.; McGinley, J. Coordination Chemistry of Calix[4]Arene Derivatives with Lower Rim Functionalisation and Their Applications. *Coord. Chem. Rev.* **2009**, *253* (7–8), 893–962.

(59) Arduini, A.; Ghidini, E.; Pochini, A.; Ungaro, R.; Andreetti, G. D.; Calestani, G.; Ugozzoli, F. P-t-Butylcalix[4]Arene Tetra-Acetamide: A New Strong Receptor for Alkali Cations [1]. *J. Incl. Phenom.* **1988**, *6* (2), 119–134.

(60) Dalcanale, E.; Montanari, F. Selective Oxidation of Aldehydes to Carboxylic Acids with Sodium Chlorite-Hydrogen Peroxide. *J. Org. Chem.* **1986**, *51* (4), 567–569.

(61) D'Alessio, D.; Muzzioli, S.; Skelton, B. W.; Stagni, S.; Massi, M.; Ogden, M. I.

Luminescent Lanthanoid Complexes of a Tetrazole-Functionalised Calix[4]Arene. *Dalt. Trans.* **2012**, *41* (16), 4736.

(62) Sabbatini, N.; Guardigli, M.; Mecati, A.; Balzani, V.; Ungaro, R.; Ghidini, E.; Casnati, A.; Pochini, A. Lanthanide Ions in Calixarene Receptors. *Chem. Commun.* **1990**, *1990* (12), 878–879.

(63) Pantos, G. D. *Naphthalenediimide and Its Congeners*; Monographs in Supramolecular Chemistry; The Royal Society of Chemistry, 2017.

(64) Lasitha, P.; Prasad, E. Orange Red Emitting Naphthalene Diimide Derivative Containing Dendritic Wedges:Aggregation Induced Emission (AIE) and Detection of Picric Acid (PA). *RSC Adv.* **2015**, *5* (52), 41420–41427.

(65) Reid, B. L.; Stagni, S.; Malicka, J. M.; Cocchi, M.; Sobolev, A. N.; Skelton, B. W.; Moore, E. G.; Hanan, G. S.; Ogden, M. I.; Massi, M. Lanthanoid/Alkali Metal b-Triketonate Assemblies: A Robust Platform for Efficient NIR Emitters. *Chem. Eur. J.* **2015**, *21*, 18354–18363.

(66) Horrocks, W. D.; Bolender, J. P.; Smith, W. D.; Supkowski, R. M.; Park, U. V; Pennsyl, V. Photosensitized Near Infrared Luminescence of Ytterbium (III) in Proteins and Complexes Occurs via an Internal Redox Process. *J. Am. Chem. Soc.* **1997**, *119*, 5972–5973.

(67) Pushkarev, A. P.; Ilichev, V. A.; Balashova, T. V.; Vorozhtsov, D. L.; Burin, M. E.; Kuzyaev, D. M.; Fukin, G. K.; Andreev, B. A.; Kryzhkov, D. I.; Yablonskiy, A. N.; Bochkarev, M. N. Lanthanide Complexes with Substituted Naphtholate Ligands: Extraordinary Bright near Infrared Luminescence of Ytterbium. *Russ. Chem. Bull. Int. Ed.* **2013**, *62* (2), 392–397.

(68) Liu, G. K.; Jensen, M. P.; Almond, P. M. Systematic Behavior of Charge-Transfer Transitions and Energy Level Variation in Soft Donor Complexes of the Trivalent Lanthanides. **2006**, *110* (6), 0–7.

(69) Arnaud-neu, Ó.; Barboso, S.; Casnati, A.; Pinalli, A.; Cedex, S. Synthesis and Binding Properties of Calix[4]Arene Diamide Dicarboxylic Acids. *New J. Chem.* **2000**, *94*, 967–972.

(70) Casnati, A.; Sartori, A.; Pirondini, L.; Bonetti, F.; Pelizzi, N.; Sansone, F.; Ugozzoli, F.; Ungaro, R. Calix[4]Arene Anion Receptors Bearing 2,2,2-Trifluoroethanol Groups at the Upper Rim. *Supramol. Chem.* **2006**, *18* (3), 199–218.

(71) Amirbekyan, K.; Duchemin, N.; Benedetti, E.; Joseph, R.; Colon, A.; Markarian, S. A.;

Bethge, L.; Vonhoff, S.; Klussmann, S.; Cossy, J.; Vasseur, J. J.; Arseniyadis, S.; Smietana, M. Design, Synthesis, and Binding Affinity Evaluation of Hoechst 33258 Derivatives for the Development of Sequence-Specific DNA-Based Asymmetric Catalysts. *ACS Catal.* **2016**, *6* (5), 3096–3105.

(72) Langdon-Jones, E. E.; Symonds, N. O.; Yates, S. E.; Hayes, A. J.; Lloyd, D.; Williams, R.; Coles, S. J.; Horton, P. N.; Pope, S. J. A. Fluorescent Rhenium-Naphthalimide Conjugates as Cellular Imaging Agents. *Inorg. Chem.* **2014**, *53* (7), 3788–3797.

(73) Wu, J.; Yi, T.; Zou, Y.; Xia, Q.; Shu, T.; Liu, F.; Yang, Y.; Li, F.; Chen, Z.; Zhou, Z.; et al. Gelation Induced Reversible Syneresis via Structural Evolution. *J. Mater. Chem.* **2009**, *19* (23), 3971.

(74) Zhang, Z.; Chen, Y.; Xu, D.; Yang, L.; Liu, A. A New 1,8-Naphthalimide-Based Colorimetric and "Turn-on" Fluorescent Hg2+ Sensor. *Spectrochim. Acta - Part A Mol. Biomol. Spectrosc.* **2013**, *105*, 8–13.

(75) Zeng, X.; Zhang, X.; Zhu, B.; Jia, H.; Li, Y. A Highly Selective Wavelength-Ratiometric and Colorimetric Probe for Cysteine. *Dye. Pigment.* **2012**, *94* (1), 10–15.

APPENDIX

List of abbreviations

The following list reports the significance of various abbreviations and acronyms used throughout the thesis. Other nonstandard acronyms and abbreviated names for compounds or experimental techniques which are not in the list have been directly reported in the previous chapters.

AcOEt: Ethyl Acetate

Ar: Aromatic

Boc: tert-Butyloxycarbonyl

BODIPY: DIPYrromethene BOron Difluoride

COSY: Homonuclear COrellation Spectroscopy

DCM: Dichloromethane

DMF: Dimethylformammide

DMSO: Dymethyl sulfoxide

ESI-MS: Electron Spray Ionization – Mass Spectroscopy

EtOH: Ethanol

HOMO: Highest Occupied Molecular Obrital

LUMO: Lowest Unoccupied Molecular Orbital

MeOH: Methanol

Mp: Melting Point

NEt_3: Triethylamine

NMR: Nuclear Magnetic Resonance

NOESY: Nuclear Overhauser Effect/Enhancement Spectroscopy

ROESY: Rotating frame Nuclear Overhauser Spectroscopy

TFA: Trifluoroacetic acid

THF: Tetrahydrofuran

TLC: Thin Layer Chromatography

UV-vis: Ultraviolet-visible spectroscopy

Nomenclature of calix[4]arenes

In this thesis the simplified nomenclature proposed by Gutsche is used to name calix[4]arene compounds. The position on the macrocycle are numbered as indicated in the following figure. The hydroxyl substituent defines the *ipso* position: subsequently the *ortho*, *meta* and *para* positions on the aromatic rings are identified without ambiguity.

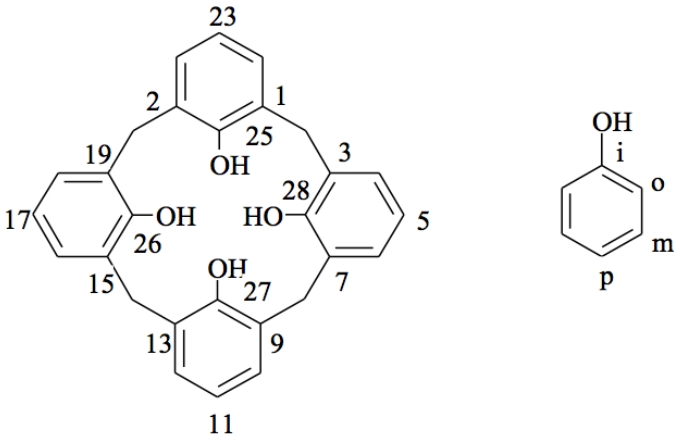

Conventional nomenclature devised by Gutsche.

Acknowledgements

Here we are… Three years have passed, pretty quickly I have to say, but for sure they were full of experiences, lessons, fun, changes, growth and also stressful moments. Actually my journey in lab 192 began a while ago, with my master thesis in 2014 with Prof. Sansone, and was followed by another year of challenging research with Prof. Casnati, to end with my PhD under the supervision of Prof. Laura Baldini. For the things that you taught me I, not only want to, but need to thank you! The three of you have been there during my whole chemistry carrier, you welcomed me when I was a master student and gave me the possibility to continue my education in your lab, being always supportive and open, and for this I will always be thankful. Thank you Laura for letting me work at my conditions, trusting my choices and giving me all the advices I needed at the right moment, and also for helping me even when I was 14000 km away from home. About this, I want to thank my Aussie supervisors, Prof. Mauro Mocerino and Prof. Max Massi for welcoming me in their labs, introducing me to the fascinating world of lanthanoids and giving me the opportunity to carry out my research always assisted by their excellent advices. The Australian experience was probably one of the best of my life, and for sure part of the merit is of my wonderful aussie labmates and friends. Annina, not at all easy to sum everything up in few words, but thank you for being my labmate, my friend, my confidante, my music/photo/art partner during these six months, and for still being in my life. Thank you, Chiaretta, because you were the first one there to explain to me how things work down under and for being part of my Italian family abroad. Laura, you have been the best teacher I could hope for, thank you for all the help you gave me, also once I was back in Italy. Nursh and Shifaza, thank you for the way you welcomed me in your life. Thank you Boony for the chitchats in the lab (and the ones we had here in Italy); thanks to Dan for being an amazing labmate; to Chao for giving me the opportunity of exploring sides of my character that I wasn't aware of (not sure this is actually a positive thing) and also because in the end you were a funny desk- and labmate; to Stouty just for being the craziest guy I have ever met. And thanks to Simon, Calum, Pete, Rhys, Nick, Jason (you're here too), Lauren, Mauro, Matt, Wei, Harry, James and Johannes for making my period abroad more joyful, and of course thank you all for the coffees and the beers!

Going back to Italy, thanks to Prof. Francesca Terenziani and Brunella Bardi for the spectroscopic measurements and the help in understanding the data.

About the guys of lab 192, I don't even know where to begin; probably begin from the start is a good idea… Marta, you have been the first person I met in lab 192, and my first chemistry guide. You have been of paramount importance (paramount is my new favorite English word and I'm really proud of it) in my chemistry journey, teaching me

how to work in a lab and showing me how to do things correctly, but here I feel the need to thank you for being my friend, above all the rest. Ila, I already told you this, but I want to refrain it so that it can settle properly in your mind: you and Marta have been my sources of inspiration, you two with your hard work and passion, with your advices and your intellect inspired me to do this PhD; thanks Ila for always being there. Grazie a Ste, aka Foxy, col quale bisticcio sempre, ma che qualche volta mi dà la sensazione di essere quasi amici. Grazie alla Gullo, appena arrivata, o perlomeno a me che vegeto in questo lab da troppo tempo sembra così, ma che mi ha subito conquistato; spero continuerai a far rispettare le regole in questo lab anche quando non ci sarò più e a portare un po' di brio nelle giornate poco gioiose. Grazie alla Bea, che ho scoperto un po' tardi, ma che fa ora parte delle persone che mi sopportano e spero ne farà parte ancora per un po'. Thanks to Andrea, Davide S., Rix, all my undergrad students (Ggiggi, Greta, Ali, Marco, Simo, Fede e Davide) and the people who somehow have been part of the lab (Ste B., Vale, Dani, Lizzie, Sergio, Lola, Tiz, Ire…) for the laughs and the aperitivi.

Thanks to my other half, for always being at my side, for putting up with me even when I was unbearable, for giving me good advices that I rarely followed, for all the little things that make our relationship the best I could hope for.

Grazie a voi, mamma e papà per tutte le possibilità che mi avete dato, per avermi sostenuto lungo tutti questi anni di studio che sono, forse, finalmente finiti e perché continuate a sostenermi, comunque e per sempre.

And last thanks to my uni mates and to my lifelong friends for enriching my life.

With love,
Fede